Novel techniques for coastal monitoring

A case study near Monster-Ter Heijde

TU Delft

Delft University of Technology

Novel techniques for coastal monitoring

A case study near Monster-Ter Heijde

Geomatics Synthesis Project 2008

28 October 2008

M. Bitenc
M.R. Bloemsma
K. Duijnmayer
K. Lin
S. Pizziol
M.A.G. Saleh
J. Stam
E. Widiastuti
Y. Yin

MSc Geomatics
Delft University of Technology

Preface

The Geomatics Synthesis Project is part of the second year of TU Delft's master programme in Geomatics. This year, the project focuses on integrated coastal surveying. It lasted eight weeks, with nine participating students. Other students from different programs (i.e. coastal engineering and geo-engineering) worked in close relation with the team.

The intention of the Geomatics Synthesis Project is to combine most of the subjects taught in the master programme. Next to this, the following objectives are aimed at, related to the enhancement of teamwork skills:

- Communicating via discussion, presentation and reporting;
- Experiencing the entire process from project definition, data acquisition, data processing and analysis, to presentation and delivery, and application in a neighbouring domain (e.g. civil engineering);
- Having relations with third party stakeholders (industry/government);
- And being of interest to the sections defining, supervising and controlling the project.

The project was conducted with the support from external parties. The kite photogrammetry was done with the help from Frank Krijnen of Utrecht University, who designed and constructed the platform. The radioactivity probing was done by Medusa Explorations BV, with the support of their two intern students, Martijn van der Boor and Gijs Stoel. The single beam echo sounding was done in close cooperation with Bas van Son and his team from the chair of Hydraulic Engineering at TU Delft's Faculty of Civil Engineering and Geosciences. The project team would like to extend our gratitude to the parties mentioned above.

Next to this, the team would like to thank our principle tutors, Roderik Lindenbergh and Dominique Ngan-Tillard, as well as all coaches for their support and guidance during this project. Further, the team would like to thank the Westland municipality and Hoogheemraadschap van Delfland who have given the permissions for measurements at Monster-Ter Heijde. Last but not least, we would like to thank Royal Boskalis Westminster NV, which provided this opportunity.

Delft, 17 October 2008,

The Geomatics Synthesis Project team

Contents

Summary

There are currently three active projects under development for the Delfland coast, all aiming at reinforcing the coast. The main issue is where to put the sand such that it arrives at the coast in the best place, without causing any damage to e.g. the new nature development. To answer this question, knowledge about sand transport is necessary, and for this purpose Boskalis is designing a measurement campaign within the framework of the so-called Building with Nature project.

This synthesis project contributes to this plan by investigating the capabilities of different measurement techniques for usage in coastal monitoring. Using these techniques, the team has gathered information about the coastal topography, bathymetry and grain size distribution of the coast near Monster-Ter Heijde, from the sub-aqueous zone to the first dunes behind the beach. This area is considered a hot spot on the Dutch shore because of its relative vulnerability to a break of the coastal defence.

Five acquisition methods have been used in this project:

• Photogrammetry

• Terrestrial laser scanning

• Single beam echo sounding

• Radioactivity probing

• GPS

Photogrammetry has been used to measure the topography, using two types of platforms, kite aerial photogrammetry and close range photogrammetry. The captured images from the kite aerial photogrammetry have been processed using specific photogrammetric software, leading to two results, an orthophoto and a digital terrain model, both with a resolution of 30 by 30 cm. These first results of the kite aerial photogrammetry are promising, but the achieved accuracy is not high enough yet for precise monitoring. Therefore both the acquisition and the processing method should be improved. For the acquisition method, the stability of the platform should be improved and bigger ground control points should be used. For the processing, more professional software, such as Leica Photogrammetry Suite, should be used.

Another use of the acquired photograph which has been demonstrated in this project is for land cover classification, by means of a simple classification based on the RGB value of each pixel. Although it has not been validated, this first result is promising and indicates future potential.

Another method to measure the topography is terrestrial laser scanning, using two different types of laser scanner, namely the FARO LS880 laser scanner and the Leica ScanStation, which are a

phase and pulse based scanner, respectively. The FARO laser scanner has been found to have some restrictions for the purpose of this project, since the dataset contained too much noise to easily extract topography. A night time test scan resulted in data with less noise, which indicates that sunlight could be a factor contributing to the noise. With the restricted time available, further processing of the Faro scanner data was not pursued. Instead, the results of the Leica ScanStation 2 showed to be useful and a digital terrain model of a part of the survey area has been produced. Having problems with the data acquisition, at this point it is not possible to have a fair validation of the results of terrestrial laser scanning, therefore further study is recommended.

Next to the topography, it is also found useful to gather the grain size distribution information over the entire area, which has been done with the Medusa radioactivity probing method. The measurements have been done on both the onshore and offshore part of the area. Due to lack of correlation between the grain size and the radiation properties of the samples, it was decided to work with the K (potassium) concentration that has a $1:1$ negative correlation with the grain size. As the result, K-concentration maps for the offshore and onshore survey area have been produced.

The result of the offshore area shows that the sediment in general becomes finer with increasing distance from the coastline. In all cases, more local variations in the K-concentration were found as well, which should be further investigated. On the onshore part, the tidal area shows a relatively low K-concentration, the beach has a rather constant K-concentration, while behind the dunes the K-concentration is relatively high.

The single beam echo sounding method has been used to measure the near shore bathymethry of the area, with a jet ski used as surveying platform. As a result, a bathymetric map has been produced. In this map, interesting features are visible, such as the groynes and their scour holes.

The sounding measurements have been found to have a standard deviation of 14.5 cm. The opening angle of the SBES transducer and the platform attitude contribute significantly to the standard deviation, mainly due to the fact that the jet ski is not equipped with an attitude or orientation sensor. To relate the standard deviation of the SBES measurements to several parameters (e.g. sailing speed, sailing direction, etc.), a different dataset is needed, i.e. one in which the same area is sailed many times and where only one parameter is changed at a time. These results show that the jet ski single beam echo sounding method is nearly operational. That being said, some improvements in terms of platform and surveying is still needed to achieve a higher quality dataset.

All of the aforementioned methods have used GPS for georeferencing purposes, either by measuring control points or by measuring positions of the moving platforms. Another use of GPS in this project is to measure cross-shore sections of the land area which remain wet during low tide and thus are inaccessible to the photogrammetry and terrestrial laser scanning methods.

Next to the individual results, data merging has been done for the onshore and offshore datasets. For the onshore datasets, the results of terrestrial laser scanning and kite aerial photogrammetry have been merged into a single digital terrain model of the beach. The result shows that the photogrammetry datasets has distortions near the edges of the photoblock, but it also shows that the differences between the photogrammetry, terrestrial laser scanning and the GPS measurements are small enough. However for a statement on the actual accuracy, a validation with more GPS data is needed. From this result it can be recommended that when a large area of beach is to be measured, the area near the edges of the photogrammetry block can also be measured with terrestrial laser scanning to eliminate distortions.

Further, a validation of both onshore datasets has been done by comparison with an existing airborne laser scanning dataset of the area. The comparison shows that the differences of both datasets with the airborne laser scanning dataset show the same deformation.

It is important to note that there is no overlap between the onshore and offshore datasets. During the project it was found that the jet ski was unable take valid measurements past the low water line, which means there is no sounding data available for the intertidal area. Therefore, several other acquisition techniques has been recommended to measure the intertidal area, such as videogrammetry.

On the offshore side, the K-concentration map has been overlaid with the bathymetric map, which gives a good visualisation of the spread of the K-concentration and shows the correlation between the water depth and the grain size. The general trend is that the grain size decreases with the water depth, however there is a sudden inverse relation visible between 6 m and 3 m water depth. One possible cause for this disturbance might be the sand bar present at this depth interval, which contains foreign sand as a result of earlier beach nourishment, that may have disturbed the natural gradient. The relation between grain size and topography has also been looked into, which showed a negative correlation. These hypotheses could be analyzed when a larger dataset is available in order to increase the certainty and make the correlation stronger.

At the end of this synthesis project a strong basis has been initialized for monitoring plan of the coastal reinforcement projects. The suggested monitoring plan is presented for different zones and features of the coastal area where different changes of morphology are expected. The monitoring strategy takes into consideration the capabilities and specifications of the different acquisition techniques as investigated and recommended in this project. According to the parameters of each zone, the most suitable acquisition method is described, together with its spatial and temporal resolution, together with approaches for data analysis.

While there is not a single optimum acquisition method to monitor the various events affecting the coastal morphology, it is possible to adapt different types of measurements plan to every event. Therefore the frequency and locations of measurements are relative to the different events taken into account, namely storm, (pre) beach nourishment, and annual changes. Finally, the suggested monitoring plan is summarized in the following table.

	Storms	Beach nourishment	Gradual changes
Dunes	Kite aerial and UAV photogrammetry	Kite aerial photogrammetry	ALS, photogrammetry, remote sensing
Vegetation	Kite aerial photogrammetry	Kite aerial photogrammetry	ALS, photogrammetry, remote sensing
Inter-tidal	Videogrammetry	Videogrammetry	Videogrammetry
Offshore	SBES	SBES	SBES
Sediment	Radio active, soil samples	Radio active, soil samples	Radio active, soil samples
Beach	Mobile mapping system, close range and kite aerial photogrammetry	Mobile mapping system	Mobile mapping system, close range and kite aerial photogrammetry
Event frequency	On average one per month	Dependent on protection scheme	Continuous
Measurement campaign	1 day and 3 weeks after storm	Zero measurement, every week (first month), every 2 months (first year)	Continuous and seasonal

Glossary

3D laser scanner A 3D scanning device that sends a laser pulse in a given direction and used the reflection of the pulse to determine the distance of the scanner to the reflecting object. By rotating both horizontally and vertically, a laser scanner can capture a complete 3D map of the surroundings of the scanner.

3D modelling 3D modelling refers to the creation of three-dimensional objects that are defined mathematically and geometrically (i.e. a circle extruded to a certain value to create a cylinder defined by its location, radius and length).

Accretion Accretion is the opposite of erosion: it is the gain of sedimentary material in a certain location.

Accuracy The accuracy is the closeness of a measurement to the actual value. The opposite of accuracy is uncertainty, which is an inverse perspective of the same value. See Uncertainty.

Aeolian sediment transport Aeolian sediment transport is transport induced by wind.

Aerial photogrammetry Photographing of terrain on the ground and objects in the air by cameras mounted in an aircraft; utilized in satellites, multispectral scanning and intricate data handling systems. Also referred to as aerial photo or air photo.

Aerial laser scanning Scanning of terrain and objects on the gound in the air by scanners mounted in the aircraft, also referred to as airborne laser scanner.

Atmosptheric propagation Within the atmosphere, radio waves can be reflected, refracted, and diffracted like light and heat waves.

Bathymetry Bathymetry is the topography of the offshore region.

Backrush Backrush is the returning water after wave breaking.

Backshore The part of the coast that is above the high water line and is therefore only affected by waves during severe storms.

Beach nourishment Beach nourishment is the restoring of eroded beach to create a new sandy shoreline.

Berm The berm is a sand bar that is located on the beach.

Bernouilli effect Bernouilli effect is the phenomenon that due to wind blowing over a surface, there appears a pressure gradient which can cause lift.

Bottom friction Bottom friction is often referred to as the friction between the water and the sediment bed. Bottom friction causes stirring of the upper sediment layer.

Calibrated focal length An adjusted value of the equivalent focal length so computed as to distribute the effect of lens distortion in a desired manner over the entire field used in a camera.

Camera calibration Camera calibration is the process of finding the true parameters of the camera that took your photographs. Some of these parameters are focal length, format size, principal point, and lens distortion.

Camera distance For the purpose of this project, we refer to the distance between the film plane and the average depth of the object or area photographed as camera distance. In close-range photogrammetry, it is equivalent to flying height.

Camera orientation It is the position and angles of a camera relative to its reference coordinate frame, or the process whereby the program determines the position and angles of one or more camera stations.

Camera Station A Camera Station is a single position of a camera when it took a photograph. Imagine freezing time just as the shutter was clicked to take a photograph - that frozen position and orientation of the camera is a camera station.

Check points Points of known three-dimensional coordinates and visible on both stereo images which are used to assess the quality of the absolute orientation solution.

Clay Clay is a naturally occurring material composed of fine grained material.

Close-range photogrammetry It applies to terrestrial photogrammetric applications for which the camera-object distance is less than three hundred meters.

Coast 3d Coast 3D is a Dutch coastal monitoring project (1997-2001) in order to improve the understanding of the physics of coastal sand transport and morphodynamics. The project was undertaken by 11 partners including laboratories, universities and national regulatory authorities.

Code measurement GPS measurement based on the C/A-code. C/A-code is the standard (Clear/Acquisition) GPS PRN code; also known as the Civilian Code or S-Code. Only modulated on the L1 carrier. Used by the GPS receiver to acquire and decode the L1 satellite signal; and from which the L1 pseudo-range measurement is made.

Carrier phase measurement GPS measurement based on the carrier phase. The carrier phase is the accumulated phase of either the L1 or L2 carrier of a GPS signal; measured by a GPS receiver since locking onto the signal.

Control points A Control Point is a known location in space with either X,Y or X,Y,Z values known. Control Points can be used in photogrammetry to define a known coordinate system, or to form constraints on the solutions.

Coordinates Values which indicate the location of a point with respect to a chosen system or frame of reference.

Countrate The countrate is the amount of gamma-rays measured in a certain time interval; usually per second.

Differential GPS corrections Differential corrections are corrections given by a base station in order to improve the position measurements.

Digital Elevation Model (DEM) It's a simple, regularly spaced grid of elevation points, representing the gound surface.

Design Scale A scale for which data source has been designed or selected to ensure product accuracy. In derived products the design scale is the smallest scale of individual features.

Digital Terrain Model (DTM) A Digital Terrain Model is a land surface represented in digital form by an elevation grid or lists of three-dimensional coordinates.

Ephemeris A description of the path of a celestial body indexed by time. The navigation message from each GPS satellite includes a predicted ephemeris for the orbit of that satellite valid for the current hour. The ephemeris is repeated every 30 seconds and is in the form of a set of 16 Keplerian-like parameters with corrections that account for the perturbations to the orbit caused by the earth's gravitational field and other forces.

Erosion Erosion is the carrying away or displacement of sediments, usually done by water, wind or ice.

Fetch Fetch is the extent of water over which the wind blows and forms water waves.

Fluvial sediment transport Fluvial sediment transport is transport by water which can be a river or the sea.

Flying height The distance between the aircraft and the average terrain elevation of the area photographed is called flying height.

Focal length Focal length is the principal distance when the lens of the camera is focused at infinity. Also see principal distance.

Foreshore The area between the average high tide mark and the average low tide mark.

Format size The size of a camera's imaging area in millimetres. In a digital camera, it is the size of the area of the imaging chip (known as the CCD). A 35mm film camera has a format size of approximately 36x24mm.

Frequency spectrum The frequency spectrum of a signal is a plot of the content of the frequencies with which the signal could be reconstructed. The transfer from a time signal to the frequency spectrum is also known as the Fourier transform.

Gamma radiation Gamma radiation is also known as photons which is an elementary particle responsible for electro-magnetic phenomena.

Geographic Coordinate System A system used to measure horizontal and vertical distances on a planimetric map.

Georeferencing A process of assigning map coordinates to image data to conform to map projection grid.

Grainsize The grainsize of sediment usually indicates the the size of the grains out of which the sediment is built up.

HILL An airflow model in order to do Aeolian sediment transport modelling together with the sediment model called 'SAFE'.

Holocene Holocene is the epoch which began approximately 10,000 years ago.

Horizontal tide Horizontal tide is often used as a different definition of tidal currents.

Integration time This is time interval in which a frequency spectrum is constructed and from which the K-concentration is derived.

Integranular friction Intergranular friction is the friction between sediment grains which causes cohesion and strength.

Interior orientation The determining of the interior perspective of the photograph as it was at the instant of exposure. Elements of interior orientation are the calibrated focal length, location of the calibrated principal point, and the calibrated lens distortion.

L1 frequency One of the two radio frequencies transmitted by the GPS satellites. This frequency carries the Coarse Acquisition Code (C/A code); encrypted P-Code (Y-Code); and the Navigation (Data) Message; and is transmitted on a frequency of 1575.42 MHz. Commercial GPS navigation receivers can track only the L1 carrier to make pseudo-range (and sometime carrier phase and Doppler frequency) measurements.

L2 frequency One of the two radio frequencies transmitted by the GPS satellites. This frequency carries only the encrypted P-Code (Y-Code); and is transmitted on a frequency of 1227.6 MHz. Military Y-Code capable receivers can; in addition to making L1 measurements; make pseudo-range measurements on the L2 carrier. The combination of the two measurements (on L1 and L2) permits the Ionospheric Delay to be corrected for. Dual-frequency GPS receivers intended for Surveying applications can make L2 measurements using proprietary signal processing techniques. Such measurements are essential if the Ionospheric Delay on carrier phase is to be corrected for (especially on baselines of length greater than about 20-30km) and/or where fast Ambiguity Resolution is needed.

Large-scale A description used to represent a map or data file having a large ratio between the area on the map and the area that is represented. If the map the size of this page shows only a small area such as your house, it would be described as large-scale mapping.

Lens Distortions Lens distortions are a form of optical aberration. The most important ones are radial (symmetric) and decentring lens distortions, in which image magnification decreases with distance from the optical axis. The apparent effect is that of an image which has been mapped around a sphere. If lens distortion is not taken into account by a photogrammetric program the resulting accuracy is greatly reduced.

Littoral zone Littoral zone is the complete coastal zone between the offshore and the end of the last dune row.

Map scale The ratio of a distance on a map to the true distance on the ground. For example, if the map scale is 1:1000, 1 centimetre on the map represents 10 meters on the ground. See also Design Scale.

Medusa An acquisition method to map grainsize of the sediment that is based on the natural radio-activity of the material.

Morphodynamics Morphodynamics is the term used for the change in the shape of an object or terrain but it is also used to refer to the processes rather than the shape changes.

Morphology Morphology is the shape or form of an object or terrain.

Offshore The comparatively flat region of submerged land extending seaward from beyond the region where breakers form the edge of the continental shelf.

Ordinary Kriging Kriging is a set of geostatistical techniques to interpolate the value of a random field at an unobserved location from observations of its value at nearby locations. Ordinary Kriging is the most commonly used type of Kriging which assumes a constant but unknown mean.

Orthoimage A digital orthophoto in which the effects of terrain and geometry of the photograph are removed to produce a plan view (orthographic projection) of the image.

Orthorectification A form of rectification that corrects for terrain displacement. See also Rectification.

Overlap Area covered by two photographs taken in a sequence.

Permeability The permeability is a measure of the ability of a material to transmit fluids.

Photogrammetry The art and science and technology of obtaining reliable information about physical objects and the environment through the process of recording, measuring, and interpreting images and patterns of electromagnetic radiant energy and other phenomena.

Pixel It is a minimal picture element with assigned intensities representing grey shades (monochromatic) or colours.

Point cloud A point cloud is the computer visualization of the XYZ coordinates that describe a physical object or environment. Each point represents an actual point on the object or in the environment, and collectively describes its shape and measurements.

Pore water pressure Pore water pressure if the pressure of the water between sediment grains which affects the inter-granular friction between the grains.

Potassium Potassium is an atom which is also denoted as K, which tends to show radio-activity.

Precision It is the repeatability of performing a measurement.

Principal distance The distance between the imaging surface plane (piece of film in a 35mm camera or CCD chip in a digital camera) and a point where all light rays intersect inside the lens. A principal distance of 50mm means that the distance from the point where all the light rays focus to the imaging plane is 50mm long.

Principal point The location in a camera where the optical axis of the lens intersects the imaging plane. It is the reference point in the image to which all marks and lens distortion parameters are related.

Projection Either the process or the end result of displaying the rendered 3D model superimposed on the projects photographs. That is the 3D model rendered from exactly the same view point as the photograph so that they match up.

Radionuclide A radionuclide is an atom or ion that radiates gamma-, alfa-, or beta-particles.

Raster data Data that are organised in a grid of columns and rows.

Real time kinematic RTK is a technique used in survey based on the use of carrier phase measurements of the GPS singals where a single reference station provides the real-time corrections to a centimeter level of accuracy.

Rectification The process of projecting a tilted or oblique photograph onto a horizontal reference plane.

Registration The process of aligning neighboring scans together.

Rectification A process of making image data conform to a map projection.

Rip-channels Rip-channels are cross-shore directed channels through which water currents can be high.

Resolution A level of detail in data. For example, ground pixel distance in aerial photography.

SAFE A model to estimate sediment transport by wind which is used together with HILL to do sediment transport predictions.

Sand Sand mostly consists of loose particles of silica with only small amounts of fine-grained material.

Sheet flow conditions Sheet flow is flow that affects the bottom the least because it is associated with no turbulence.

Shoaling Shoaling is the change of the wave height when the wave enters shallow water.

Shoreface Shoreface is the part of the shore that is for a large extent affected by wave-action and also by wind action.

Single beam echo sounder Single beam echosounder uses one emitting and receiving transducer, which releases a series of energy pulsed in the form of sound waves into a small area underneath the boat, the time between the emitting and returning echo is used to calculate the water depth beneath the boat.

Skewness Skewness is a measure for the symmetry of the distribution of the observations.

Sorting The sorting of sediment is the spread in the grainsizes of the grains in the sediment. A low spread of this grainsizes corresponds to a good sorting.

Spatial resection Spatial resection is the non-linear problem of computing the co-ordinates of a point from spatial directions measured from that point to at least three targets with known co-ordinates.

Spectral fingerprint The spectral fingerprint is the typical spectrum from a certain radionuclide.

Stereoscopy The science and art that deals with the use of binocular vision or observation of a pair of overlapping photographs.

Storm surge Storm surge is the effect of rise of the water table associated with a low pressure weather system and strong wind. It is the combined effect of wind set-up and the influence of the air pressure.

Swash Swash is a bar over which waves wash freely.

Targets A target is a point in a scene or on an object that can be easily identified and easily marked when viewed in an image. Typically, a target is a high contrast dot or filled circle. Such a target can be marked with high precision with the sub-pixel marker (manual or automatic).

Tidal amplitude The total difference between high tide and low tide.

Tidal current Tidal currents are currents associated with the tidal cyclus.

Topographic map Map that presents the horizontal and vertical positions of the features represented.

Transient Transient processes only last for a short period of time.

Triangulation Using trigonometric functions to calculate measurements, used in certain types of 3D laser scanners to determine point locations based on transmission and reflection positions of the laser beam. In 3D modelling, triangulation also refers to the generation of triangles out of point cloud data in creating 3D surfaces.

Uncertainty The uncertainty is the quantity of how much a measurement is unknown compared to the actual feature. Uncertainty is the inverse perspective of accuracy, which is defined as the closeness of a measurement to the actual feature. The uncertainty essentially describes how much of a measurement is uncertain. See Accuracy.

Undertow Undertow is a seaward directed current that arises from a strong onshore directed wind.

Variogram The variogram is a function describing the degree of spatial dependence of a spatial random field, defined as the expected squared increment of the of the values between two locations.

Vector data Data that represent physical elements such as points, lines and polygons.

Videogrammetry The process of taking precise measurements by using video images taken from two or more video cameras taken at different angles.

Wind setup Wind set-up is the effect that a strong wind causes frictional stress with the water resulting in a rise of the water table.

List of abbreviations

ALS Airborne Laser Scanning

ATV All Terrain Vehicle

BGO Bismuth, Germanium and Oxygen

CAD Computer-Aided Design

CCD Charged Coupled Device

CTD Conductivity Temperature Depth

D-GPS Differential Global Positioning System

DEM Digital Elevation Model

DSL Digital Subscriber Line

DTM Digital Terrain Model

EGNOS European Geostationary Navigation Overlay Service

ETRS89 European Terrestrial Reference System 1989

EU European Union

FSA Full Spectrum Analysis

GCP Ground Control Point

GIS Geographic Information System

GNSS Global Navigation Satellite System

GCP Ground Control Points

GPS Global Positioning System

GSM Global System for Mobile communications

GSP Geomatics Synthesis Project

HDS High Definition Surveying

HSDPA High-Speed Downlink Packet Access

JARKUS JAaRlijkse KUStmetingen

KAP Kite Aerial Photogrammetry

KPN Koninklijke PTT Nederland

IMU Inertial Measurement Unit

INS Inertial Navigation System

ISDN Integrated Services Digital Network

LAN Local Area Network

LARC Lighter Amphibious Resupply Cargo

LEDs Light Emitting Diodes

MMS Mobile Mapping System

NAP Normaal Amsterdams Peil

NMEA National Marine Electronics Association PC Personal Computer

PPS Parts-Per-Million

PPT Parts-Per-Trillion

PVC Plasticized Vitreous Compound

RD Rijksdriehoeksmeting

RINEX Receiver Independent Exchange Format

RMSE Root Mean Square Error

RTCM Radio Technical Commission for Maritime Services

RTK Real Time Kinematic

SBES Single Beam Echo Sounding

TIN Triangulated Irregular Network

TLS Terrestrial Laser Scanning

UAV Unmanned Aerial Vehicle

USB Universal Serial Bus

List of figures

List of tables

1 Introduction

There are currently three coastal engineering projects planned for the Delfland coast. The first one is a large-scale beach nourishment program, which will start in December 2008, and will be finished in 2011 [25]. In this project, an extra row of dunes will be added from Hoek van Holland to Kijkduin, on the seaside of the current dunes. This requires 18 million m^3 of sand, which will be dredged from the North Sea and transported by pipes to the beach. In the end, the coastline will be moved 170-200 m to the west.

The second project concerns nature compensation for the Port of Rotterdam's new industrial area 'Maasvlakte 2'. One of the key requirements for constructing this industrial area is that no nature is lost, which means some nature needs to be created elsewhere. Therefore, a spot has been selected between Monster-Ter Heijde and Hoek van Holland, where 15 acres of nature reserve will be added to the dunes.

The third project is the 'sand engine' (*'zandmotor*' in Dutch), which is still in the pilot phase. The general idea behind it is to add an enormous amount of sand in front of the Delfland coast (i.e. under water) which then will be transported to the beach by natural processes and in that way strengthen the coast. The main issue is where to put the sand such that it arrives at the coast in the best place, without causing any damage (e.g. to the new nature reserve). To answer this question, knowledge about sand transport is necessary, and for this purpose Boskalis with its Building with Nature research project is setting up a regular measurement campaign, preferably on a monthly basis, along the coastline from Hoek van Holland to Kijkduin.

This synthesis project contributes to the Building with Nature project by investigating capabilities of different measurement techniques, i.e. terrestrial laser scanning, photogrammetry, single beam echo sounding, radioactivity probing and GPS positioning, for usage in coastal monitoring. Further, using these techniques, the team has gathered information about the coastal topography, bathymetry and grain size distribution of the coast near Monster-Ter Heijde, from the sub-aqueous zone to the first dunes behind the beach. A challenge for the team is to elaborate a methodology to fuse the datasets from these different techniques with different temporal and spatial resolution and quality.

The synthesis project focuses on the Delfland coast near Monster – Ter Heijde, which is considered a hot spot on the Dutch shore because of its relative vulnerability to a break of the coastal defence. There are two main objective of this project. The first objective is to measure the initial situation of the coast near Monster-Ter Heijde, before the start of the enforcement works. The second objective is to design a spatio-temporal monitoring strategy for the enforcement works.

The synthesis project has been carried out in three stages. In the first stage, the team has looked into the capabilities of the chosen measurement techniques, with respect to their usage for coastal area surveying. The second stage is the actual measurement campaign, which was done in two parts. The first part was done between 15 and 19 September 2008, at which time the measurements with all techniques were done. The second part was done on 29 September 2008, when additional measurements

with photogrammetry and terrestrial laser scanning were done. The last stage is the processing of the data gathered from the measurements, and merging the different datasets.

This report is the final report of the project, in which the processes and outcomes of the project are described in detail. The morphological background of the Dutch coast in general and of the Monster-Ter Heijde coast in particular is given in chapter 2. In chapter 3, for each acquisition method the working princlple, the measurements and the results extracted from the acquired data are described. Chapter 4 discusses the data merging of different datasets. A review of the used measurement techinques and recommendations for a future monitoring project are given in chapter 5. Finally, conclusions are drawn in the last chapter.

2 Coastal morphology

The Dutch coast is of great interest for commercial purposes and recreation but it is also the barrier between the North Sea and the Dutch hinterland. The goal of this chapter is to get a good understanding of the morphodynamic processes that are of importance for our coast. The coast can be analyzed by first looking at the energy input or boundary conditions and then looking at the resulting morphological features (see figure 2.1). This approach is schematically depicted in figure 2.1, which shows the relation between the energy input parameters and the morphodynamics.

First this chapter presents the energy input or boundary conditions (section 2.1), then a description of the coastal zone (sections 2.2 and 2.3) and finally a discussion on how to measure these morphological features. Great use is made from the research program called Coast3D and the corresponding articles that dealt with morphodynamic processes and sediment transport near Egmond (a small town at the Dutch coast) . Some aspects about the Monster coast are better understood using analogies with Egmond although these analogies are not justified in all cases due to differing characteristics of the regions like wave action, tidal current strength, etc.

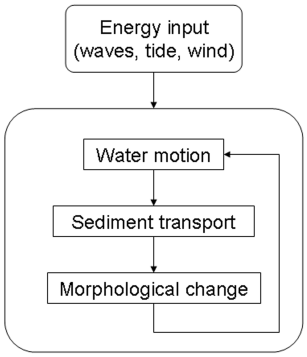

Figure 2.1: The morphology consists of the energy input components and the morphodynamic loop [53].

2.1 Energy input

The Dutch coast is dominated by broad sandy beaches and extensive dune ridges. All this sandy sediment is susceptible to transport in several ways. The transportation rate and direction, determines the shape of the coast and its character in the sense of net erosion or net accretion. We distinguish the energy input as being transport by water (fluvial) or by air (aeolian).

2.1.1 Wind

Wind can have several effects on the processes governing coastal morphology. These include wind stress on the water surface, inducing short-term above normal sea elevations or storm surge and furthermore wind stress and sand sand particles resulting in aeolian transport of sediment on the beach, or in the dunes.

Before the wind can transport particles, it must lift them from the ground surface. Particles are raised by 'lift', which is produced by the Bernoulli effect and the local acceleration of wind, and bombardment by particles already in the air [88]. The Bernoulli effect arises from the fact that wind speed increases swiftly away from the ground surface so that a surface particle sits in a pressure gradient; the top of the particle experiences a lower pressure than the bottom of the particle. However the most effective mechanism for getting particles airborne is bombardment by particles already in flight.

Roughly three types of wind transport can be distinguished [88]:

- Saltation. Sand grains bound, land and rebound, imparting renewed imperus to other sand grains. Such motion is confined to short distances and heights of about 2 m.
- Reptation. On hitting the surface, saltation grains release a small splash-like shower of particles that make small hops from the point of impact.
- Suspension. Particles of silt and clay lifted into the atmosphere become suspended and may be carrier great distances.

It must be stated that saltation is the most important process [59]; once saltation is in, it facilitates all the other processes.

Storm events are of great importance for sand transport. These events result in large transport rates of larger particles due to high energetic winds. Storms are defined as periods of wind speeds over 20m/s [39]. For morphodynamic purposes it interesting to look at storm duration. But since the main goal of this project is to set up a monitoring strategy, the frequency is also of great importantce. This is important because measuring after a storm event is advisable due to the rapidly changing morphology during such an event.

The average storm duration every year is published by Augustijn [39] over a total time span of 42 years. This long time period provides enough information to asses the statistics of storm duration and frequency:

- The average storm duration between 1964-1996 is 500 hrs/year: 90 hours during summer (April-August), 410 hours during winter (September-March).
- The variation in the amount of storms is large: 13 storms in 1989, 48 storms in 1970.
- The average frequency of storms is 35 per year. On average 1 storm every month in the period April-August and 5 storms every month in the period September-March.

One effect that can be observed during storm events is known as undertow. Undertow or downwelling is a seawards directed current, directly above the seabed. When the waves break due to shoaling, the water retreats which is known as the backrush. But in the case of strong landward directed winds, a strong reversed current can occur over the tilted surface of the shoreface, which is depicted in figure 2.2. This current is much stronger and has more effect over a larger area than just the backrush has. It furthermore transports sediment as bedload or suspended load seawards which may therefore contribute to shoreface erosion [83].

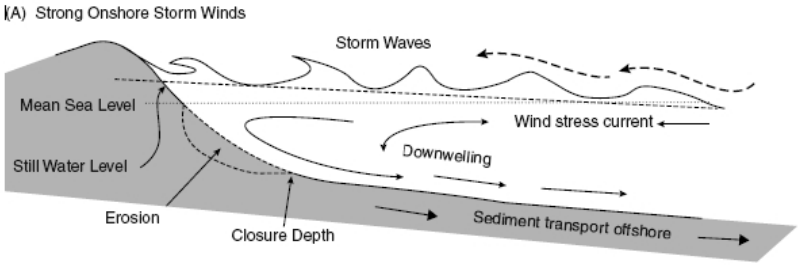

Figure 2.2: Undertow current, depicted in this figure by 'downwelling'.

Storm surge is the effect of water level rise associated with a low pressure weather system [83]. It is partly caused by the frictional wind stress on the water surface inducing a current in the surface water. When waves are abundant, the wind also 'pushes' against the waves resulting them to steepen and get a smaller wavelength. This phenomenon is called wind-setup and is one component of the total storm surge effect. Apart from the frictional effect of wind on water, the low pressure at the center of a weather system also has an effect. The low air pressure results in a sea water level rise, which can be significant depending on the bathymetry.

The storm surge effect enhances the beach erosion process along open sandy duned coastlines by raising the water table in the beach and lowering intergranular friction between the sand grains, so that the pore water pressure from the raised water table induces the sand from the lower beach face to flow out into the surf zone. As a result of the onshore winds and storm surge, the tidal cycles within estuaries are altered to a much higher than normal tides and reduced low tide [83]. The total storm surge with respect to the still water level during the flooding in 1953 was at its maximum 3 m, which is considerable compared to the average tidal amplitude of 1.6 m [49].

2.1.2 Waves

Waves are periodic disturbances formed by wind blowing over a water surface [59]. They are caused by turbulence in airflow generating pressure variations on the water. Once formed, waves help to disturb the airflow and are partly self sustaining. Energy is transferred from the wind to the water within the wave-generation area. The amount of energy transfer depends upon the wind speed, the wind duration, and the fetch (i.e. the extent of water over which the wind blows). Waves formed in water deep enough for free orbital motion to occur are called waves of oscillation. The waves are called waves of oscillation, because the water particles have roughly circular motion; forward on the crest, upward in the front, backwards in the trough and downward on the back. When the waves encounter shallower water, their appearance and the water motion changes.

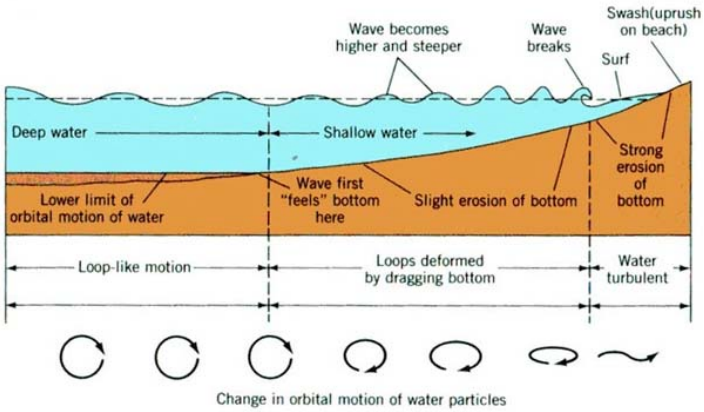

Figure 2.3: Change in wave properties (amplitude, waveheight, orbital motion) when approaching the shore.

As depicted in figure 2.3, when waves feel the bottom, the circular motion becomes elliptical, and finally the motion is linear motion directed towards the beach. When a wave 'feels' the bottom, it slows down due to loss of energy by bed friction [59]. This effect is called shoaling. The wave-induced shear is usually too transient and non-directional to drive sediment very far. However, once sediment is lifted into the water, other background currents such as those resulting from the angle the waves make with the shoreline, from tides, or direct wind stresses can take over and move the suspended sediment [30].

When waves approach the shore they are also refracted. Wave refraction occurs because the inshore part of a wave crest moves more slowly than the offshore part, owing to the shallow water depth, and the offshore part swings forward. The refraction phenomenon results in the alignment of the waves with the bathymetric contours [83].

Two important characteristics of a wave are its wavelength and wave height. For rough planning purposes, waves are often characterized as regular or 'monochromatic', meaning that successive waves in the incoming field are assumed to have the same, constant height and period, and the wave form is sinusoidal in shape. But when doing quantitative sediment transport analysis, this simplification is not legitimate. The reason such analyses are important and are performed is that wave energy and the resulting sediment transport potential are proportional to the square of the wave height [30].

Alongshore variations in the wave time series cause gradients in energy which can have significant impact on any existing or proposed coastal structures. In addition, because the water depth at which a wave is affected by bottom friction depends on the wave height and steepness, the different waves in the time series in a given section of shoreline will break over some cross-shore width. This width is representative for the degree of variability in the wave series. This visible 'surf zone' is important because it may affect total sediment transport volumes and the position and prominence of features such as submerged bars or rip-channels.

The shoaling of the wave and thereby functioning as a stirring agent, was already described. The other important aspect of a wave is breaking. When the water depth is too shallow to sustain the height of the growing wave, the wave becomes unstable and breaking ensues.This point of incipient breaking is commonly estimated to be when the wave height reaches roughly 80% of the water depth. After the wave breaking the water retreats, which is denoted as the backrush. The net effect of the backrush and uprush is directed seawards, which causes beach erosion.

2.1.3 Currents

Along most sections of the coast, any sediment suspended by wave action is typically transported parallel to the shoreline by background currents [59]. These currents most often result from the fact that the breaking wave crests form some angle with the shoreline. Waves surging obliquely toward the beach and reflecting at the complementary angle produce net alongshore water movements which are roughly proportional to the size of the approach angle and the square of the wave height. This alongshore and cross-shore currents are depicted in figure 2.4.

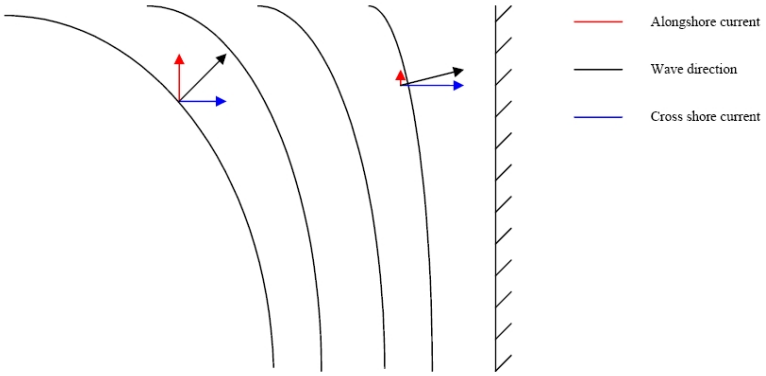

Figure 2.4: Oblique incoming wave will result in alongshore and cross-shore current.

The along-shore and cross-shore currents may be either reinforced or opposed by other water movements resulting from tides, local wind shear on the water column, or any similar force which results in a dynamic setup of the water surface. Although alongshore transport currents are relatively weak under average conditions, they are persistent and can be much stronger during storms when the wave heights are larger and the seas more directional.

The changing tide is the result of the changing positions of the Moon and Sun relative to the earth coupled with the effects of Earth's rotation and the bathymetry. Besides the sea level change itself, tidal currents occur. These tidal currents are often referred to as the 'horizontal' tide, whereas the seal level change is known as the 'vertical' tide.

Because most sediment transport is related to the wave climate at a particular location and time, the instantaneous transport magnitude and direction may change as the wave field changes. The most common pattern of change is a seasonal one in which higher energy periodic winter storms approach a shoreline from a consistent direction (like northeasters) which is different from the prevailing wave direction under average, milder summer conditions. In such cases there will be associated reversals in transport direction for varying lengths of time

2.1.4 Study area

The literature study presented in previous sections indicates that tidal currents and wind waves are both important sediment stirring agents [70]. It is therefore important to look at the magnitude of these effects in the region of interest.

The tidal amplitude varies between 1.5 m (neap tide) and 2 m (spring tide). The maximum surface tidal currents in Egmond vary between 0.7 and 1.1 m/s, while the current velocities at 1 m above the bed are typically 0.2-0.5 m/s during fair-weather conditions. The northward directed flood current is dominant in the North Sea [70]. The residual (tide-averaged) water motion is dominated by wind- and density-driven effects [71].

Most of the winds along the Holland coast come from the North Sea. The prevailing wind direction is southwest (23%), followed by west (16%), east (13%) and northwest (12%) [86]. The storm winds causing the largest wind set-up along the coast are coming from northwest. [84]. The wind generates along-shore currents in the direction of the along-shore wind component, while it creates a vertical circulation in cross-shore direction driven by the cross-shore wind component (see figure 2.2) [70].

The wave climate in the region of interest is dominated by sea waves with a mean annual significant wave height of about 1.1 m. Characteristic storm conditions in the Dutch North Sea, derived from the work of [71], are wave heights of 3-4 m and currents of 1 m/s. These values are derived from data obtained in the Egmond coast, which is not protected against longshore transport by groynes.

The influx of river water in the North Sea at Hoek of Holland is stabilized by water locks. These locks foresee a constant flux of around 1500 m^3/s. This sweet water influx results in a density-driven cross-shore current directed towards the coast, in the order of cm/s [89]. This density gradient gives rise to an estuarine type of vertical circulation, with near-bed residual currents directed towards the coast, compensated by a return flow higher in the vertical. This current must not be disgarded since its region of influence reaches up to 20 km to the north, as defined by [37].

2.2 The large scale coastal zone

The coast can roughly be divided into three parts; each having its own morphological and morpho-dynamical properties. A cross section of the beach and near-shore region is depicted in figure 2.5. The following parts of the coast can be distinguished: offshore, foreshore and backshore. These three parts will be discussed one by one.

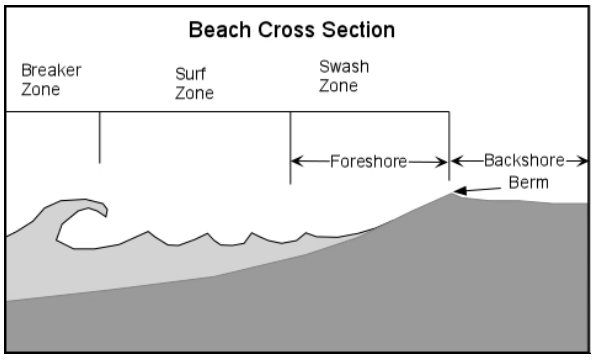

Figure 2.5: The three regions and subregion of the coastal zone [22].

2.2.1 Offshore

Within the surf zone, wave breaking is the dominant hydrodynamic process which drives near shore currents and sediment transport [64]. At any particular location in the nearshore, the vast majority of entrainment and suspension occurs as the wave crest passes, creating a 'cloud' of sediment. Outside the surf zone this cloud may be quite small, both in size and in concentration, especially if the entrainment is associated with sand ripples that are present on the bed. Near the break point, large, long-period waves can create what is known as 'sheet-flow conditions', in which the bed is scraped flat and, although there is strong entrainment, there is limited suspension due to a lack of turbulence. In both of these situations, the cloud of sand settles back to the bed before the next wave crest arrives. However, in the surf zone the sediment cloud may take several wave periods to settle back to the bed, and may in fact be resuspended by a subsequent wave. It is for this reason that sediment concentrations inside the surf zone are generally several times greater than those outside [83].

2.2.2 Foreshore

After breaking in the surf zone, the waves (now reduced in height) continue to move in and run up onto the sloping front of the beach, forming an uprush of water called swash. The water then runs back down again as backrush [83]. The hydrodynamics and sediment transport in the swash zone are important for various of reasons.

First, an important part of the littoral sediment transport occurs in the swash zone; sediment concentrations are often high in the swash zone, and may typically be several orders of magnitude higher than in the inner-surf zone [42, 76]. Secondly, swash run-up influences engineering design and also leads to the erosion of dunes. Thirdly, swash zone mechanics determine to a high degree the mechanism of beach recovery after storms. Swash hydrodynamics additionally determine the interaction between marine processes (inner surf zone) and terrestrial processes (coastal water table, coastal dunes) and therefore influence much of the nearshore littoral zone. For example, the swash zone plays an important role in the ecology of the intertidal zone [69] and groundwater levels in subaerial littoral beaches and low-lying islands [52, 74].

2.2.3 Backshore

The main type of sediment transport in the backshore region is the aeolian transport, since seawater does not enter this part of the coast. Therefore several aeolian deposition types such as sand dunes and ripples can be observed. A small positive gradient of the ground surface can be observed directed seawards. This gradient is rather consistent, besides from the intertidal ridges and berms that result in local maxima and minima, when analyzing a cross-shore section. These morphological features are described in detail in the next section.

2.3 Small scale morphology

The seabed of the Dutch part of the North Sea mainly consists of fine to medium sands which are deposited during the Holocene [50]. This fine grained material is transported and deposited by the

earlier described sediment carriers. The morphology (or 'shape') of the coastal zone is the result of these carriers and their zone of influence. Therefore a representative part of the Dutch coast is highlighted and all important zones in it, are described by their morphological features. The following features in their corresponding zones are analyzed; subaqueas bedforms, groyne-related features and the beach-and dune-related features.

2.3.1 Subaqueous bedforms

There are certain bedforms that can be distinguished in the North Sea bed. Wave-like forms occur in regular patterns and are usually called sand dunes or sand waves. If the velocity of the flow is sufficient to transport sediment either as bed load (particles moving along the bottom) or suspended load (particles moving in a stream without touching the bottom), an initially flat bed is deformed into a bed containing bed forms. There is a constant rate of erosion and accretion, that results in the formation of sand dunes. These sand dunes are not stationary, they usually migrate via bed load transport processes, with erosion occurring on the stoss surface and deposition being observed downstream form the crest, along the lee face [81].

The subaqueous bedforms can be characterized by wave length, amplitude, orientation, asymmetry and migration velocity [81]. A relative flat surface will develop if the flow velocity is larger than a critical value into small-scale features called ripples. With higher velocities the ripples will transform into larger bedforms, named sand dunes. Dunes can either have a sharp or a flat crest. Sharp crested dunes present a degree of asymmetry similar to that of ripples, where dunes with a flat crest are more symmetrical in shape [81].

With a further increasing flow velocity, no sand dunes or ripples form and the dunes are gradually transformed into a plane bed. Finally, under very high flow velocity conditions, bed features reappear and formations known as antidunes can occur. These four stages are depicted in figure 2.6. The type of bed forms and its main characteristics depend to a large extent on the flow intensity. Furthermore, grain size plays a significant role in the development of bed forms, and some bed form features will only be observed within a specific range of grain size [81].

There are roughly three types of sand bodies present in the Dutch coastal zone. The largest structures is called shoreface connected ridges which are positioned the farmost offshore. These structures are usually present at a waterdepth of around 18 m depth. The ridges are 2 m high and can reach a length of up to 5 km. These ridges slowly migrate in the northward direction with a velocity of 1 m/year[71]. These shoreface connected ridges are depicted in figure 2.7.

Along the entire Dutch coast are sand bars present, varying from 1 to 4 sand bars. The cross-shore size of these sand bars is around 200 m and they are positioned on a small oblique angle with respect to the shore. Large changes to these sand bars usually take place during storm conditions [94]. Wijnberg also stated that as long as the outer bar stays in place, the inner bar will not move in the seaward direction. The degeneration of the outer bar is determined by two factors that counteract. The sand bars are for a large part degenerated by assymetric waves during mild storm conditions. On the other hand symmetric breaking waves during heavy storm events contribute to preservation of the outer bar. The balance between these two determines the accretion or degeneration of the outer bar. The fact that the outer bar conditions determines the conditions of the total sand bar system is the reason for doing suppletions further offshore than the existing sand bars.

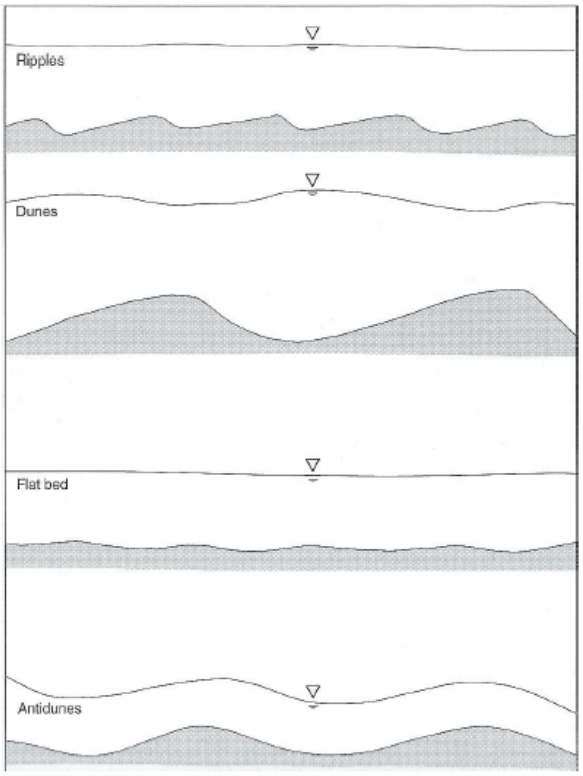

Figure 2.6: Bedforms associated with certain flow velocity [81].

The intertidal bar, which is often visible during low tide is for a large extent determined by the wave climate. In figure 2.8 a typical intertidal bar is depicted together with bar related features. One of these features is the so called feeder channel which forms as a result of longshore currents a the landward side of the bar. If a narrow breakthrough in the bar is present, a 'rip channel' may form. In these rip channels current velocities are higher [21]. The rip currents are the most pronounced during storm conditions and during onshore winds.

Besides from these longshore directed sand bodies (shoreface connected ridges and intertidal bars), there are also sand structures positioned perpendicular to the coast. These structures are present in the form of sand waves and migrate in the alongshore direction. Sand waves are often several kilometers long and their shape is quite stable for a period of months to decades. These sand waves have a large impact on the coast in such a way that they result in local shore accretion. This local accretion results in more intensive erosion further away from the sand wave [45]. These sand waves migrate which makes their position of great importance for the local shore development. The migration rate of the sand waves is between 100 m and 300 m every year.

2.3.2 Groynes

Groynes have impact on the coastal morphology as well. This impact is relevant for our test area since one groyne is present in our area. Groynes tend to prevent longshore drift by physically blocking a longshore current. The groyne has two sides with their own sedimentation characteristics, known as the updrift side and the down drift side. Accretion occur at the updrift side and strong erosion occurs

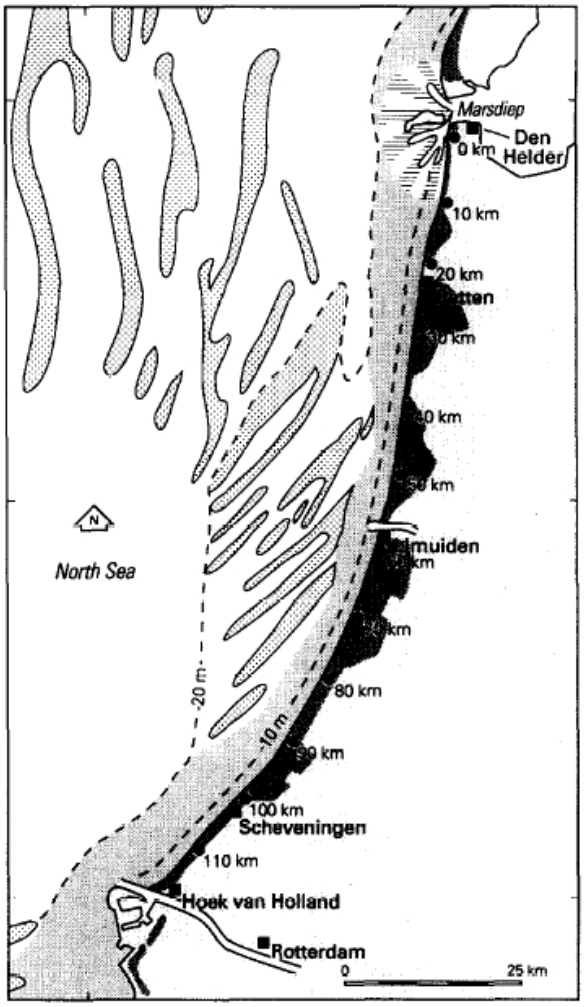

Figure 2.7: Shoreface connected ridges along the Dutch coast [93].

at the downdrift side. This is depicted in figure 2.9. Grain size of the sediment has a strong impact on the way of transport, which can be bedload transport or suspended load. Since the effect of the groynes on sedimentation is different for the two sides of the groyne, sorting is taking place.

Another consequence of groynes is the occurrence of 'scour holes'. These holes are abundant just at the far-end, downdrift side of the groyne. They are the result of high velocity eddy currents at the groyne tip that inherit local erosion [88].

2.3.3 Beach and dunes

The morphological features that are formed by wind consist mainly of dunes and smaller scale features like ripples [59]. It is still not completely clear why and how dunes form but stays the fact that the wind speed must be low enough to allow particles to fall out of the conveying wind. This reduction in wind speed can be behind an object, like small vegetation or a relatively large grain or pebble. When the premature dune is there, it traps saltating grains by making rolling over the surface harder due to the steep windward side of the dune.

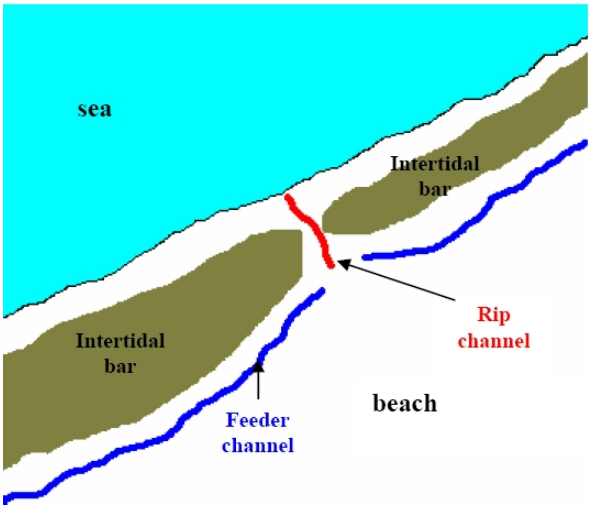

Figure 2.8: Monster coast morphology with; beach, rip channel, feeder channel, intertidal bars.

When dunes are vegetated in sufficient quantity, grasses will continuously trap sand as they grow and the dunes increase in size. Profile data taken at several beaches show dune crest elevations growing at an average rate of about half a meter per year for several years to reach elevations of 3 to 8 m [85]. The development of the dune shape after its birth is determined by two factors: wind variability and the sand supply [92].

Sand transport is also influenced by the local topography. At the dune tops is the wind mainly directed perpendicular to the dune crests. This is even the case when the large scale wind direction is oblique with respect to the dune crests [36]. The relation between sand transport and wind speed is determined by Adriani and Terwindt [36], which is shown in table 2.1. From this table it can be derived that below 7 m/s wind speed the sand transport can be neglected.

Wind speed (m/s)	Sand transport (10^6 m^3/s/m)
4.5	-
7.0	1
10.0	3
12.5	14
15.5	31
19.5	86
22.5	165
26.5	310
31.0	408

Table 2.1: Relation between sand transport and wind speed.

For this reason it is important to analyze the frequency and duration of storm events in order to predict morphodynamical behaviour. And it is also important for monitoring planning; measuring after storm events might be advisable.

In [91], a aeolian sand transport model was adopted ('SAFE') together with an airflow model ('HILL') to simulate the sediment deposition and erosion in a (Dutch) coastal area after beach nourishments.

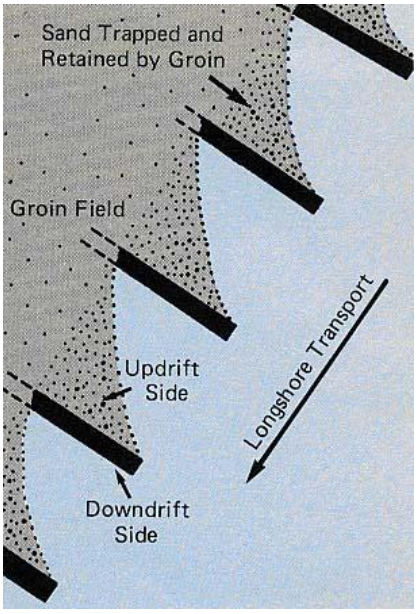

Figure 2.9: Groyne together with its implications to sediment accretion.

The two models gave a good indication of the expected sediment transport and might be useful to use in planning beach nourishments and coastal monitoring by Royal Boskalis Westminster N.V.

2.3.4 Monster coast morphology

In the backshore area, two rows of sand dunes adundant have formed. These sand dunes are both of approximately the same height and are both vegetated with dune grass and some small bushes. Behind the dunes is a flatland that continues up till the bicycle path. This flatland is characterized by intensive vegetation and only small variation in the topography. Tese dunes have been stabilised in the past 150 years. At present, aeolian activity in the coastal dunes is restricted to small features like blowouts [38].

The beach has an almost constant gradient of 1:57 up to the point where a local minimum is visible in the section shown in figure 2.11. The local maximum that is visible in figure 2.11 at 610 m horizontal distance represents an intertidal bar. The intertidal sand bar is situated just shoreward of the mean low water level. When water level is rising, it responds highly dynamically due to their response to changing wave conditions and tide [68]. The behaviour of the intertidal bar is of importance for beach erosion, since the bar dissipates and breaks the wave energy that impacts the shore.

The intertidal bar morphology is characterized as being a slip-face intertidal bar, as defined by [68]. The slip-face morphology shows large migration rates and is largely dependent on the tidal range, wave action and the relative position of the bar with respect to the mean-water level. The net sediment transport associated with intertidal bar migration in the Egmond region was around 0.3 to 1 m^3/m/day. The monitoring results will lead to exact values of bar migration rate in Monster. There is also a large sand bar visible offshore in the profile at 1000 m horizontal distance. This sand bar extends over 200 m cross-shore which represents a large volume. The sand body is the result from an earlier performed beach nourishment in order to reduce beach erosion. It will be interesting to monitor the behaviour of this sand bar.

The offshore part of the Monster coast is characterised by an almost constantly increasing depth up to 9 m at the outer boundary of our survey area. When going further out of the survey area and looking at the farshore bathymetry, the water depth slowly increases and large-scale sand waves can be observed. This large scale bathymetry of the Dutch coast is depicted in figure 2.10.

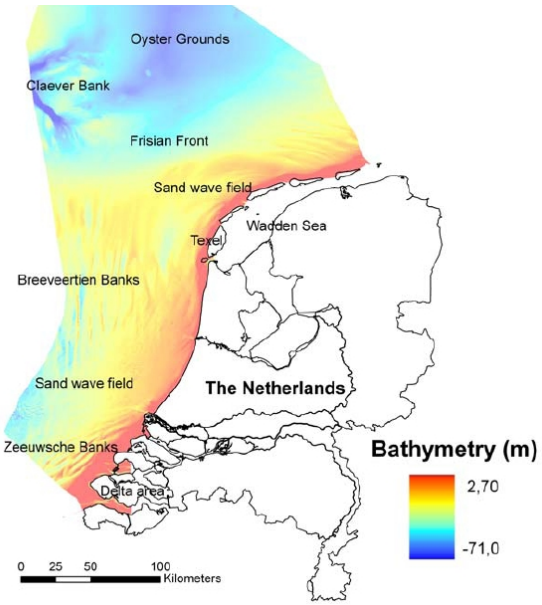

Figure 2.10: Large scale barthymetry of the Dutch coast [84].

In order to monitor the coast, it is important to know the magnitude of the net sand transport rates. In [80] is described how a linear trend analysis of the JARKUS measurements [15] between 1963 and 1992 resulted in an overall profile. The JARKUS measurements consist of a complete profile of the dunes up till 1000 m offshore. Van Rijn did this trend analysis after eliminating the effect of earlier suppletions which gives the ability to predict the coastal behaviour.

Every profile of the coast was separated into two parts:

- Regiom 1: from the dune top untill the foreshore (NAP -7 m until -3 m).
- Region 2: from the foreshore to the deep coastal zone (NAP -13 m until NAP -7 m).

The analysis of every region seperately makes it possible to analyze the volumes for every region. The following average volume changes were observed for the Monster-Ter Heijde region:

- Region 1: -35.000 m^3/year;
- Region 2: -275.000 m^3/year.

These volumes are important in order to compare future monitoring results with volumes from the past. This allows to make long term and short term predictions possible.

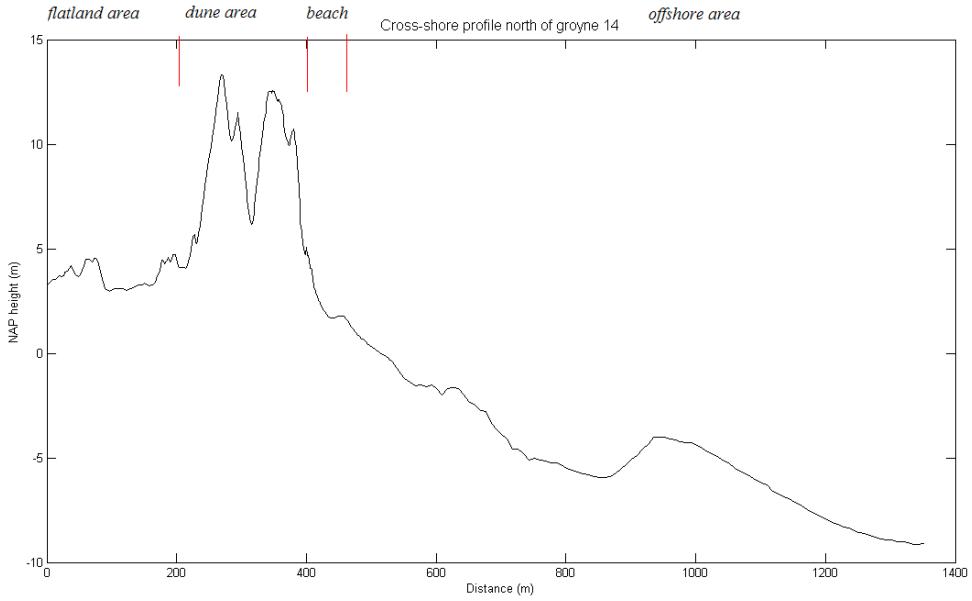

Figure 2.11: Section of coastal area in Monster-Ter Heijde, derived from SBES data and RTK-GPS data, measured between 15 and 19 September 2008.

2.4 Measuring morphological features

There are two aspects that one must keep in mind, while planning coastal monitoring. One aspect is the spatial scale and the other important aspect is the temporal scale. Furtermore there is one hidden aspect that is of importance, which is the financial aspect. Before a monitoring strategy can be constructed, it must be clear what the results should contain, how often the data should be updated and what the available budget is.

Sand waves with superimposed megaripples (see figure 2.12) are common observations in acoustic surveys of continental shelves, including the North Sea [87]. But these ripples are usually too small to be observed on multi-beam and side-scan sonar records [77].

The time scale of the subaqueos morphodynamics is the other factor of importance. Bathymetry field data collected in the continental shelf show that the morphology of sand wave crests changes in response to tidal and wave conditions. Megaripples on the other hand are more dynamic features [54]; migration of megaripples of dm/day is common in tidal and subtidal environments [92]. With this information one may reconsider what the monitoring objectives should be.

Another main concern of monitoring coast morphology is the limitations of the measurement techniques. There are many types of sensors which have all their advantages and disadvantages. It is the task of the engineer to asses the sensors and come up with the optimal selection of sensors. The limitations of laser scanning is taken below as an example.

Data from laser scanning can be used to construct a high resolution digital terrain model of any terrain. The laser scanner does this by sending out light and measuring the backscatter. From the time interval between sending and receiving the light, it derives the distance between the scanner and

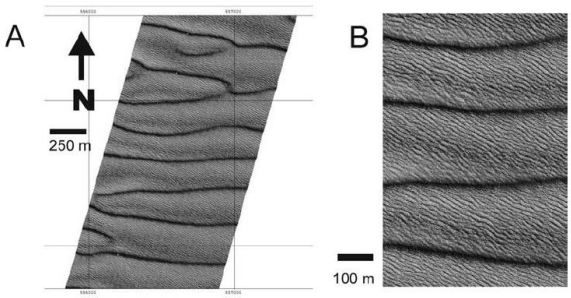

Figure 2.12: An area with sand waves (A) and superimposed megaripples (B) [77].

the reflection point. This method is very effective but only applicable when the terrain has a high backscatter strength. This is of course not the case for water and nor for wet sand. As a result, laser scanner is not very suitable for the intertidal area. The characteristics of sensors in combination with coast characteristics must be analyzed in order to construct the most suitable monitoring plan.

Summarizing; the four important factors that determine the best monitoring program are determined by:

1. Spatial scale of interest;
2. Temporal scale of interest;
3. Budget;
4. Sensor requierements and limitations.

The next chapter describes the assessment of the data quality and applicability of five different sensors used for coastal surveying purposes.

3 Data acquisition

Part of this project is to conduct measurements for a part of the coastal area near Monster-Ter Heijde, using five different techniques: photogrammetry, terrestrial laser scanning, Medusa radioactivity probing, single beam echo sounding and GPS. These techniques are determined prior to the project by a panel of experts, and are considered to be suitable for gathering information of the coastal area. The measurement campaign covers both an onshore and offshore part of the area, as illustrated in figure 3.1.

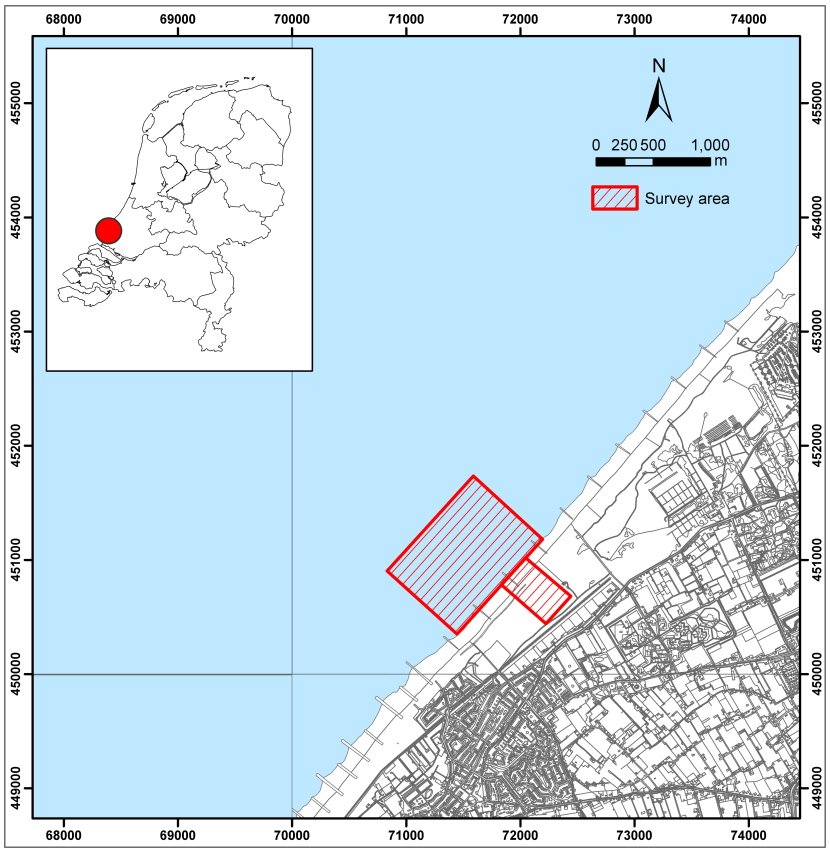

Figure 3.1: The survey area (modified from TOP10 vector map) .

The measurement campaign was done in two parts. The first part was done between 15 and 19 September 2008. During this time, measurements were conducted with all techniques. To support the campaign, a bungalow was rented at a camping site approximately 800 m from the survey area. The second part of the campaign was done on 29 September 2008, where additional measurements with photogrammetry and terrestrial laser scanning were done.

In this chapter, the measurements and results of the five acquisition techniques are discussed.

3.1 Photogrammetry

Photogrammetry is the art, science and technology of obtaining reliable information about physical objects and the environment through the process of recording, measuring and interpreting photographic images and patterns of electromagnetic radiant imagery and other phenomena [5]. There are several photogrammetric techniques to obtain this information. Most of them are designed to capture aerial images, commonly from aircrafts, satellites and sometimes from balloons or kites, however there are other techniques which are designed to acquire terrestrial images through a camera stationed on or close to the Earth's surface [66].

In this project kite aerial photogrammetry (KAP) has been used, which allows to capture aerial images from a height of a few meters to hundreds of meters through a camera mounted on a kite [4], together with close-range photogrammetry that allows to acquire oblique images from a close distance.

3.1.1 Working principle

The largest application of photogrammetry is to extract topographic information, such as a digital terrain model (DTM) from aerial images. It has also been applied to process satellite images and close-range images in order to acquire topographic and non-topographic information of photographed objects.

The general working principle can be summarized in three parts: interior orientation, exterior orientation and orthorectification of imagery. These form the orientation procedures that allow the reconstruction of a 3D model of terrain from stereo pairs of images.

Interior orientation defines the internal geometry of the camera as it existed at the time of image capture. This procedure is primarily used to transform the image pixel coordinate system to the image space coordinate system (figure 3.2).

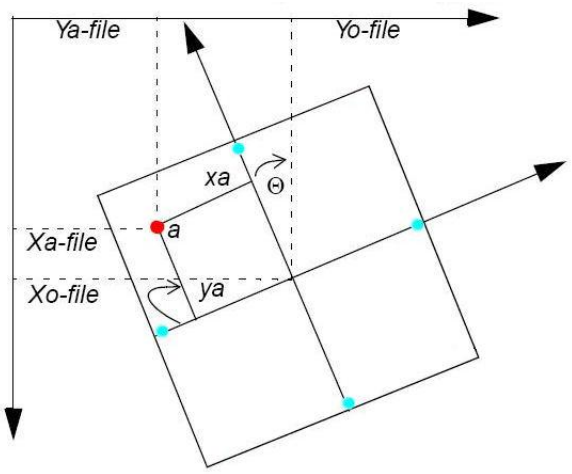

Figure 3.2: From pixel coordinate system to image space coordinate system [31].

Tthe objective of the exterior orientation is to identify the relationship between the images taken from a camera and the real contest on the ground. In practice we have to convert the images into the local coordinate system of the ground control points (GCPs).

The location of an object in the image can be measured and the outcome of this measurement is called image coordinates. The relations between the image coordinates, the object coordinates and the location and orientation of the camera for one image are given in the collinearity condition equations:

$$x = -f \frac{r_{11}(X-X_0)+r_{21}(Y-Y_0)+r_{31}(Z-Z_0)}{r_{13}(X-X_0)+r_{23}(Y-Y_0)+r_{33}(Z-Z_0)} \tag{3.1}$$

$$y = -f \frac{r_{12}(X-X_0)+r_{22}(Y-Y_0)+r_{32}(Z-Z_0)}{r_{13}(X-X_0)+r_{23}(Y-Y_0)+r_{33}(Z-Z_0)} \tag{3.2}$$

where x and y are the image coordinates of an object, f is the focal length of the camera, X, Y, and Z are the object coordinates of the same object, X_0, Y_0 and Z_0 are the object coordinates of the projection centre of the camera and $r_{ij}(i,j=1,...,3)$ are the elements of a 3D rotation matrix, that represents the relationship between the image space coordinate system and ground space coordinate system through the three rotation angles ω, φ and κ of the camera (figure 3.3).

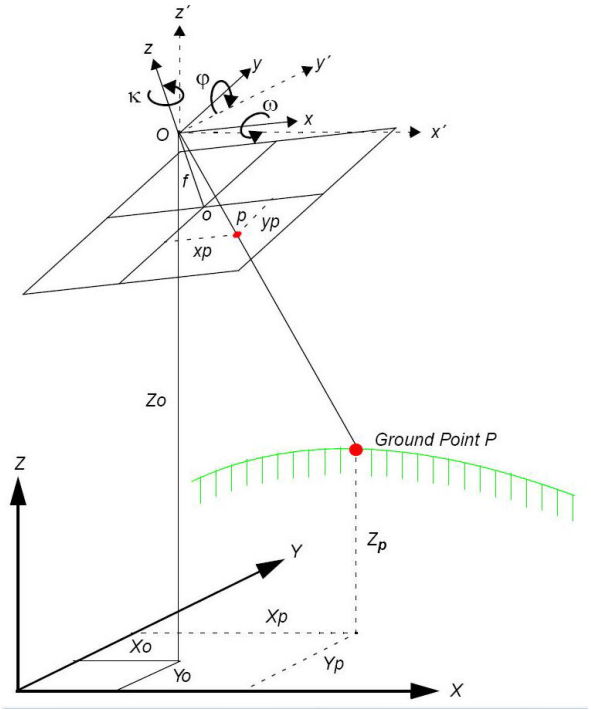

Figure 3.3: Elements of exterior orientation [31].

In the collinearity condition equations x and y coordinates are the observations, the X, Y, and Z coordinates are the unknowns and the $r_{x,y}$ entries and X_0, Y_0 and Z_0 coordinates are the known parameters. Having only one image of the object will result in only two observations and three unknowns, thus insufficient to solve the equation. Therefore at least two images are needed, which will give four

observations and three unknowns and then the object coordinates can be determined using the space forward intersection (figure 3.4).

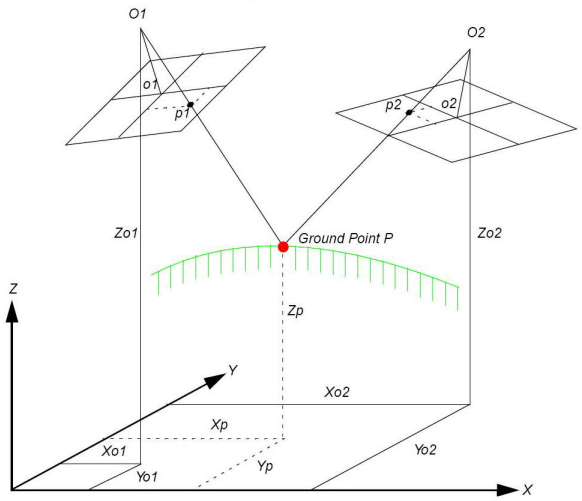

Figure 3.4: Space forward intersection [31].

Space forward intersection techniques assume that the exterior orientation parameters associated with the images are known. Using the collinearity condition equations, the exterior orientation parameters along with the image coordinate measurements of point p_1 on image 1 and point p_2 on image 2 are the input to compute the X_P, Y_P and Z_P coordinates of the ground point.

On the other hand, the exterior orientation parameters of images in an image block can be determined using bundle block adjustment using GCPs. A block of images contained in a project is simultaneously processed in one solution and the statistical technique known as least squares adjustment is used to estimate the bundled solution for the entire block while also minimizing and distributing error [63].

Bundle block adjustment uses the collinearity condition equations as the basis for formulating the relationship between image space, the camera and the ground space. Once the relationship has been defined the orthorectification of imagery can be created.

3.1.2 Acquisition platform

The main acquisition platform used in this project is a camera mounted on a kite. The kite aerial photogrammetry (KAP) technique is probably one of the oldest and most used systems of low budget aerial photography [4]. A camera is lifted using a kite and is triggered either remotely or automatically to take aerial images. The camera rigs can range from the extremely simple, consisting of a trigger mechanism with a simple camera, to complex apparatuses using radio control and digital cameras. In this project, we have used the following kite aerial photogrammetry rigs:

- Kite;
- Flying line;

- Cross beam suspension;
- Camera cradle;
- Radio control;
- Camera.

The most important aspect of any kite used to lift a camera is the stability. Generally, single lined kites are used as they allow very long line lengths and need less intervention from the flyer. Almost any stable kite design can be used to lift lightweight camera rigs, up to approximately 500 grams [43].

Figure 3.5: Kite used for the measurements.

The camera can be mounted directly to the kite, but it is usually secured to an adjustable rig suspended from the flying line at a distance from the kite. This distance reduces excessive movement being transmitted from the kite to the camera and allows the kite to be flown into higher altitude.

The cross beam suspension is a simple levelling method that involves suspending the camera from a rigid length of material below the kite line. A line runs through eyehooks or small pulleys so that the weight of the rig causes it to settle naturally into a level position [47].

The camere used is a Canon EOS 350D (see figure 3.6), which has a focal length of 18 mm and a sensor size of 22.2 by 14.8 mm. The pixel resolution is 3456 by 2304 pixels, which means that a pixel is about of 7 microns in size [6]. The camera has been set to a high shutter speed to reduce motion blur. The shutter release mechanism is radio controlled, using an infrared signal to instruct the camera to release the shutter.

In the close-range photogrammetry campaign the same camera has been used, but with a lens with a larger focal length of 20 mm.

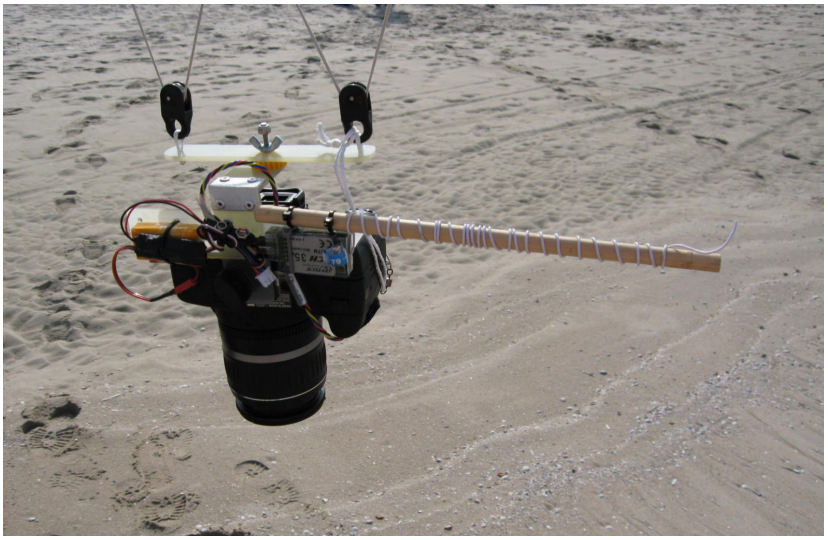

Figure 3.6: Camera mounted on the cradle.

3.1.3 Measurement campaign

The photogrammetry measurements are structured in three different campaigns, two campaigns using kite aerial photogrammetry and the other one using close-range photogrammetry (figure 3.7).

Kite aerial photogrammetry measurements were subdivided in two different campaigns: a high-resolution acquisition campaign of a small area of about 200 by 100 m and a low-resolution acquisition campaign of the entire survey area that is about 500 by 300 m .

This subdivision is driven by the ground pixel size of the measurements. A pixel resolution (i.e. the ground coverage on 1 pixel in the image) of about 20 mm is the best choice to have a good final result, but not practical for the entire survey area. This would result in many images, requiring too many GCPs and consequently too many measurements. Therefore another measurement campaign has been realized, the low-resolution measurement campaign, with a pixel resolution of about 50 mm, which covers all the survey area. Next to this, a third measuring campaign has been done, taking the dune face from the beach using close-range photogrammetry (see figure 3.7). Examples of the images captured from the different campaigns are presented in figure 3.8.

In every campaign the same georeferencing method has been used. Several ground control points were put in place such that different grids of GCPs were created (see figure 3.9).

In the high-resolution acquisition campaign 24 targets (GCPs) of about 30 by 30 cm were distributed on the survey area in order to be easily identifiable from the sky. For the same function, in the low-resolution acquisition campaign 12 targets of 60 by 60 cm were placed on the ground. In the close-range measuring campaign 60 GCPs were put in place at about 5 m from each other such that a grid of 12 by 5 GCPs was created. All these GCPs were measured with RTK-GPS. This was the longest part of the measurement campaigns, which took approximately 1 hour for each campaign.

The image acquisition of the high resolution acquisition campaign has been performed at a flying height between 70 and 80 m. As a result, the area covered on the ground in each image is of about 70

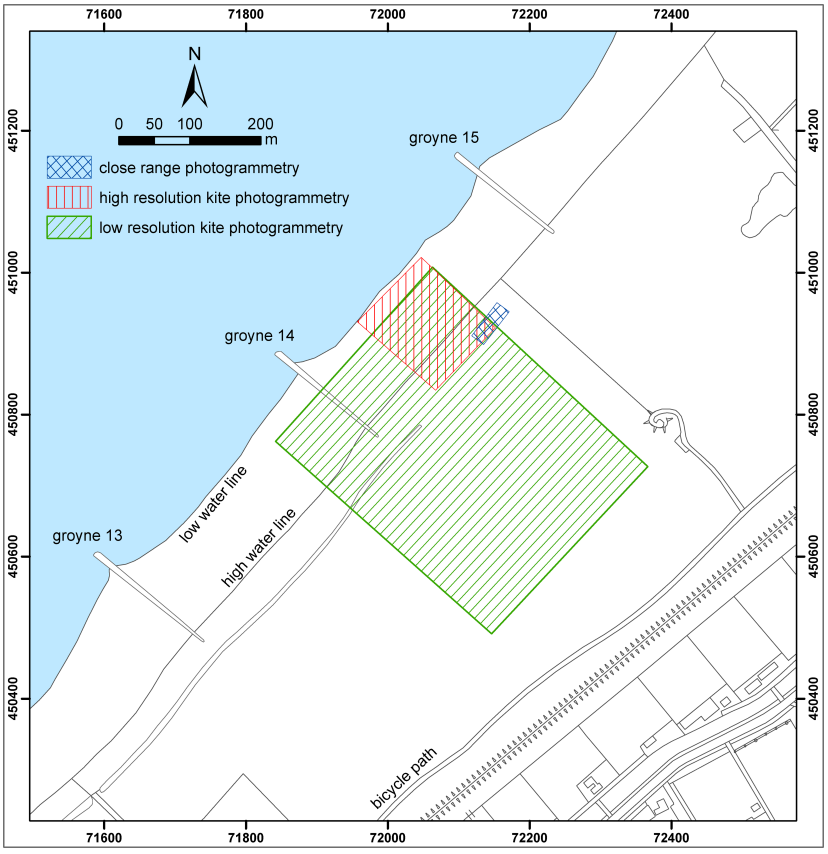

Figure 3.7: Areas of photogrammetry acquisition campaigns.

by 45 m with a ground pixel size of about 18 by 18 mm. This survey took about 30 minutes, resulting in 176 images.

The image acquisition of the low-resolution campaign was planned to be performed at a different flying height of 140 m, to cover a ground area in each image of about 200 by 120 m with a ground pixel size of about 50 by 50 mm. However, due to the weather conditions the campaign has been performed at a flying height between 90 to 100 m. This campaign lasted about 30 minutes and resulted in 262 images.

On the other hand, in the close-range photogrammetry measurement campaign, the image acquisition has been completed at a distance of aproximately 15 m between the camera and the surface of first dunes. Here 27 images were taken and the acquisition lasted no more than 5 minutes.

3.1.4 Data processing

The aim of post-processing the photogrammetric data is to extract geographical information out of the photographs. The achieved end result is an orthophoto (i.e. a photo which is geographically oriented and wherein height distortions are removed) of the whole measured terrain and a digital terrain model (DTM). To achieve this, two things must be done: determining the exterior orientation parameters (i.e. location of the camera in the terrain and its rotation angles to find out where each picture is taken

(a) High resolution campaign

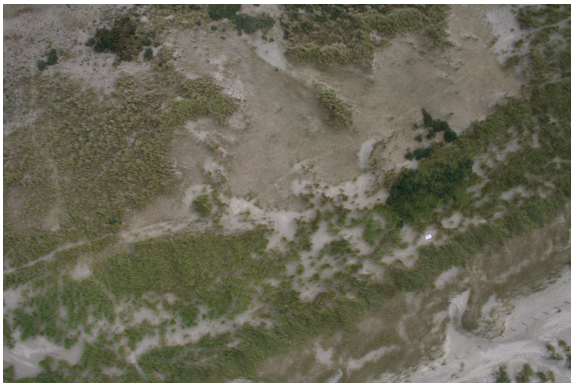

(b) Low resolution campaign

(c) close range photogrammetry campaign

Figure 3.8: Examples of images from different campaigns.

from) and determining the terrain coordinates of unknown points by locating them in at least three photographs [62].

The post-processing was done in PhotoModeler [24], due to the lack of more advanced photogrammetry software (e.g. Leica Photogrammetry Suite [16]). Futhermore MATLAB [19] is used to create a data grid and to interpolate the resulting point cloud in this grid.

To determine the exterior orientation for the high resolution campaign, 11 photos were chosen in such a way that every GCP was included and there was enough overlapbetween photos. This ensured that terrain coordinates could be calculated from the photographs. The GCPs were measured in each picture. After pinpointing the GCPs in every picture, PhotoModeler processed the project and gave the exterior orientation parameters as a result. PhotoModeler can calculate and export an orthophoto automatically when the exterior orientation parameters of the photographs are determined.

The exterior orientation parameters can be used to determine the ground coordinates of objects measured in the photos by means of the so-called forward intersection method. In PhotoModeler every object would have to be measured manually in every picture. This is not a problem when the objects are clearly visible in the pictures and not too many objects need to be measured. The ideal way of creating a DTM though is to calculate the ground coordinates of a grid of points. In PhotoModeler, this would mean that every gridpoint needs to be measured manually in the photographs. Again, to

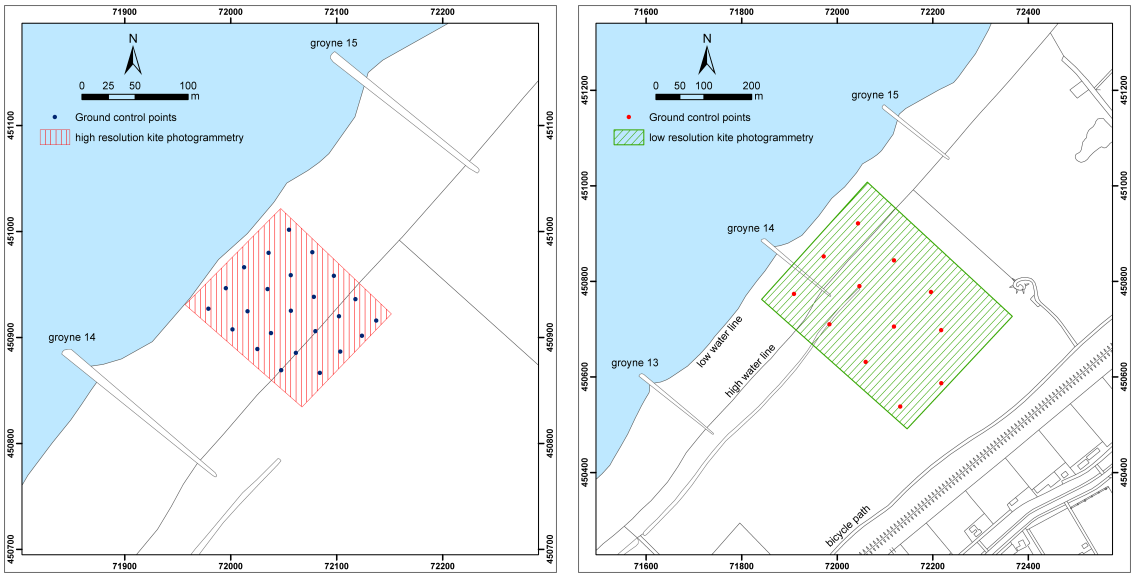

(a) High resolution campaign.

(b) Low resolution campaign.

Figure 3.9: Ground control points grid of the high and low resolution campaign.

measure objects manually in the photos it is necessary that the objects are clearly visible in the photos. When creating a point grid, this may very well not be the case (especially on the beach). Therefore a software which can automatically generate a point cloud (i.e. a large group of points taken from the pictures for which the coordinates of every point is determined) from pictures is necessary. For this, the trial version of PhotoModeler Scanner [24] is used. This software is able to create a point cloud out of a block of oriented photos.

PhotoModeler Scanner needs the photos to be oriented very accurately to be able to create a point cloud. Due to inaccuracies in the coordinates of the ground control points this needed accuracy could not be obtained using the spatial resection method. Therefore another processing method has been used. The GCPs are still pinpointed in each picture, but are considered to be a tiepoint (i.e. the ground coordinates of the points were not known). With this method the pictures were calculated to each other (the location of a picture is known relative to the other pictures). Now it is possible to determine the location of an object by measuring it in at least three pictures, but the coordinates of the object are still given in a local model coordinate system. The GPS coordinates of the GCPs are used to determine the transformation between this model coordinate system and the terrain coordinate system (i.e. the Dutch RD/NAP system). This transformation is calculated in MATLAB.

The point cloud, which was created by PhotoModeler scanner, is exported to a text file containing only x, y and z values. This file is then imported in MATLAB. In MATLAB the heights are interpolated on a grid using a linear grid interpolation which uses a Delaunay triangulated irregular network (TIN). Next, the original point cloud data is triangulated into a TIN and from this triangulation the heights of the gridpoints are calculated.

3.1.5 Results

The achieved result is an orthophoto of the area measured with the high resolution campaign, bounded by the outer GCPs and a data grid with interpolated heights, as shown in figure 3.10.

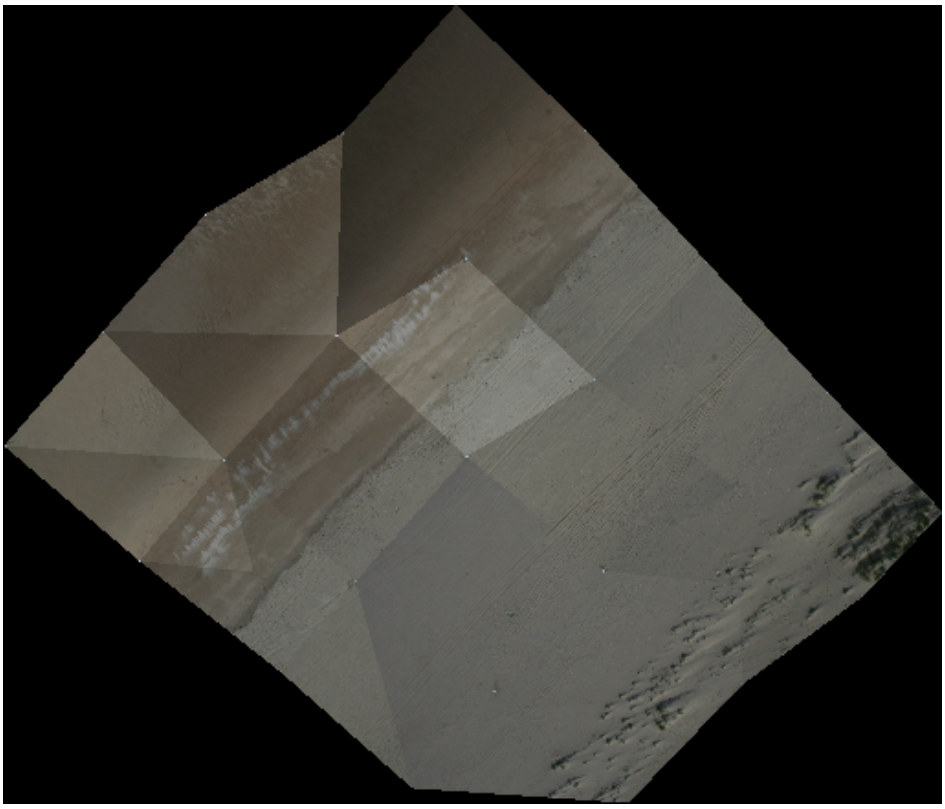

Figure 3.10: Ortophoto of photographed area from the high resolution campaign.

Only the area within the GCPs is textured, the outside area is black. PhotoModeler creates the orthophoto textures from surfaces created by the user in the PhotoModeler project. In this case, the created surfaces where quadrangles with the GCPs as corners, therefore there is no texturing outside the area defined by the GCPs.

If the figure 3.11 is zoomed in, some gaps which exist in the interpolation grid are visible.. This has to do with the fact that at that location, insufficient data is available from the point cloud. The area outside the bounding region of the point cloud (i.e. the region where the outer points of the point cloud are lying on, which is the white area in the image) does not have height values, since this would require extrapolation instead of interpolation.

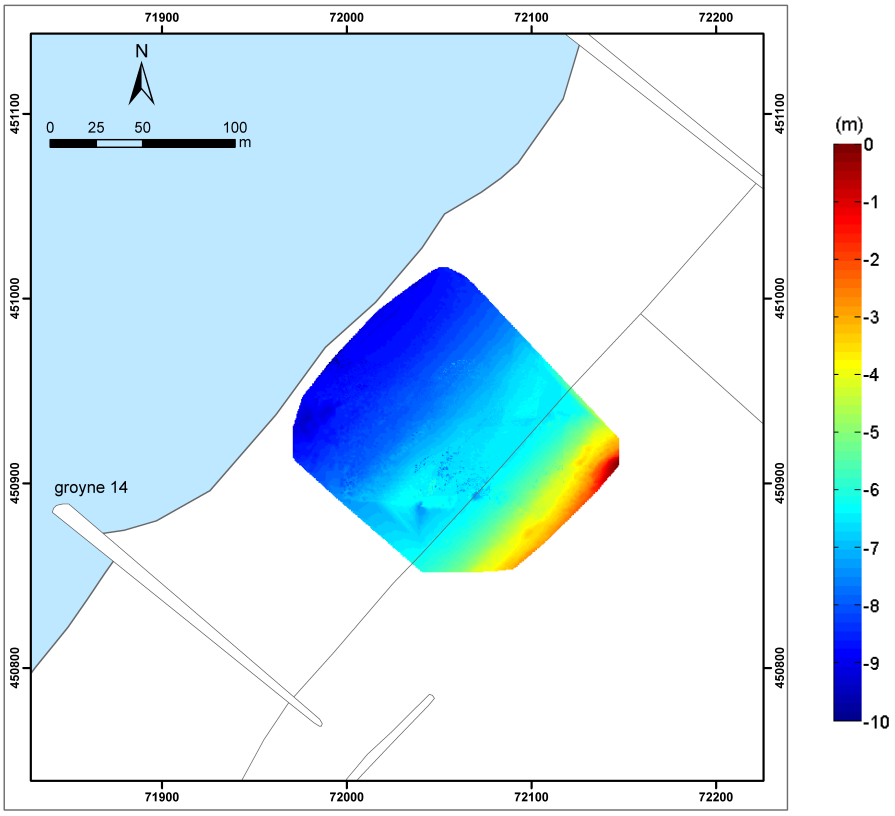

Figure 3.11: Data grid with interpolated heights (in m above NAP).

3.1.6 Quality assessment

Resolution

This subparagraph will describe the point density of the results. The point cloud which is created by PhotoModeler is not on a grid, thus the distances between the points of the point cloud are not regular. The distance between the points of the point cloud is usually about 1 to 2 dm but larger gaps also exist. The more to the edge of the block of photos, the larger the distances between the points occurs.

The zoomed part shows the distances of 1 to 2 dm between points. It has been decided that the interpolation will take place on a grid of 30 cm, so that the laser scanning group can use the same grid. This will mean that the data of these two techniques can easily be compared.

The orthophoto has a size of 512 by 436 pixels and covers an area of 158 by 135 m; this also gives a resolution of 30 by 30 cm.

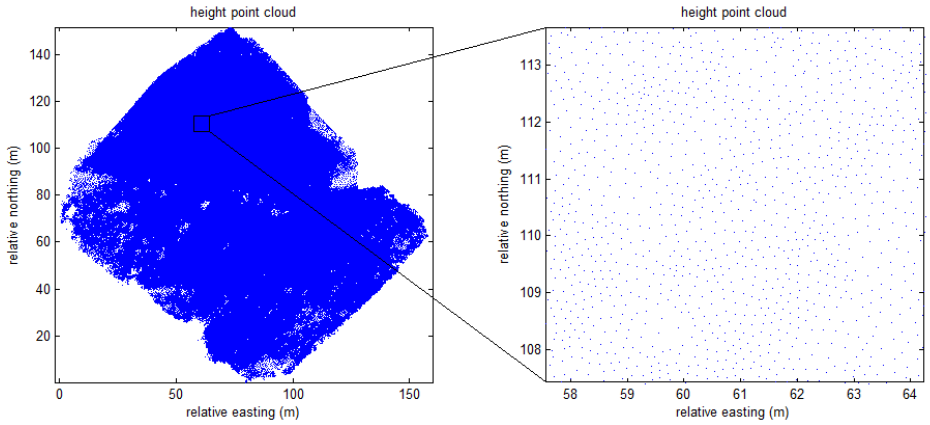

Figure 3.12: The point cloud with gaps and lower resolution near the edges of the cloud.

Accuracy

The overall accuracy of the measuring results obviously depends on the accuracies of several steps. For the two products, the accuracies of these steps will be described one by one. For the orthophoto, the overall accuracy is influenced by:

- *Accuracy of ground control coordinates.* The ground control coordinates were measured by RTK-GPS. The accuracy of the spatial resection will depend on the accuracy of the GPS measurements. The accuracy of the GPS measurements is described in detail in section 3.5. In PhotoModeler both a horizontal and vertical accuracy of 5 cm is used, because this gives the optimal terrain accuracy (the terrain coordinate residuals in PhotoModeler were the lowest with this setting).

- *Accuracy of GCP measurements in the photos.* The ground control points are pinpointed in the photos manually. When PhotoModeler processes the project after the ground control points are pinpointed in the photos, a table containing quality information can be opened. This table gives, among other parameters, the pixel residuals of the point measurements in the photos. The largest pixel residual in the project was about 2 pixels, but this seems to be an outlier, since most residuals stay within 1 pixel. Nevertheless, an inaccuracy of 2 pixels in the photo, taken from a distance of about 85 m, would give us a horizontal inaccuracy of 5 to 6 cm.

For the height model, the overall accuracy is influenced by:

- *Accuracy of tiepoint measurements in the photos.* The pixel residuals give a measure of the accuracy of the tiepoint pinpointing in the photos. Reviewing of the point quality table in PhotoModeler showed that these residuals all stay within 1 pixel, which would give us a horizontal accuracy less than 3 cm (with a camera height of about 85 m). To check if these exterior orientation parameters have reasonable values, a 3D model of the GCPs and the camera position is reviewed.

- *Accuracy of the model/object coordinate system transformation.* The transformation between the model coordinate system created in photomodeler scanner and the RD/NAP system describes the relation between these systems. The accuracy of the transformation parameters

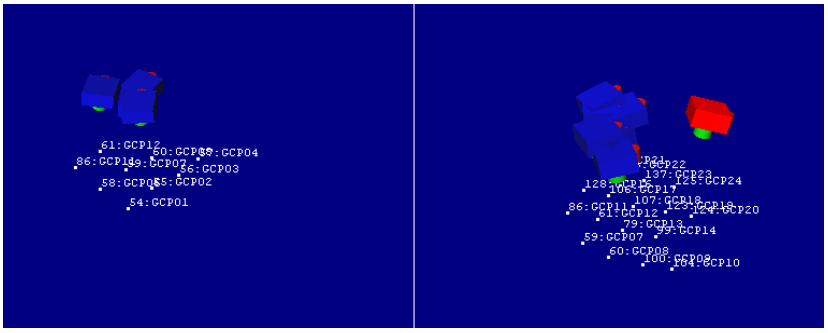

Figure 3.13: The ground control points of the two models used to create the point cloud with the camera stations.

(scale, rotation angles and a translation vector) are dependent on the accuracy of the measured coordinates in both systems. In the terrain coordinate system these are the GPS measurements of the GCPs, which accuracy is already discussed. In the model coordinate system the accuracy is determined by the pixel residuals and the accuracy of the height determination, described above. With an accuracy of 5 cm for the GPS measurements and 3 cm (in the terrain) for the tiepoints, a total accuracy of 8 cm is expected. To assess the accuracy, a couple of GCPs is used to determine the transformation orientation parameters with the remaining GCPs as checkpoints. The calculated ground coordinates of these checkpoints are then compared with the GPS coordinates. The differences, called the residuals, tell how accurate the exterior orientation is. To assess this accuracy, the means and the root mean square (RMS) are determined. Because the processed pictures didn't have enough tiepoints to make one block of pictures, the pictures needed to be processed in two blocks. The statistics can be seen in table 3.1. These residuals are larger than expected, especially in block 2. Expected were residuals of 2 to 3 cm, which would coincide with the pixel resolution that comes forth from the chosen flying height. Nevertheless they all fall within the chosen grid resolution of 30 cm.

	Mean X	Mean Y	Mean Z	RMS X	RMS Y	RMS Z
Photo block 1	0.0004	0.0178	-0.0368	0.0205	0.0192	0.0429
Photo block 2	-0.1470	-0.1022	0.0903	0.0588	0.1369	0.1528

Table 3.1: Statistics of model/object coordinate system transformation (in meter).

- *Accuracy of height calculations when the point cloud was created.* The initial point cloud created by PhotoModeler Scanner contained notable noise in the height values of the points. This noise could be filtered out by lowering the allowed height differences in the photomodeler scanner. These were set to 30 cm, because of the residuals seen in the previous paragraph. Now the height data doesn't look very noisy, but outliers up to 30 cm vertically can still exist (outliers of more than 1 m are filtered out). Because the height values of the points in the point cloud are not known otherwise, it's difficult to assess the actual accuracy of the height data (without the outliers). It is possible to look at the height difference between two points close to each other. On a distance of 10 cm, especially at a flat beach, not much height difference is expected. This was checked by zooming in to a flat beach area on an interval of about 50 cm in X and Y direction, selecting the points lying in this interval and checking the heights. The

height differences within the whole area stayed within one cm and the differences between two neighbouring points were a couple of mm.

All these inaccuracies somehow influence the accuracy of the end products, but with a chosen resolution of 30 by 30 cm, the total accuracy is good enough for this resolution.

Error budget

In the previous section the errors of the several steps are summed up. Now the factors causing these accuracies will be described.

Accuracy of ground control coordinates. The inaccuracies of ground control coordinates are caused by factors which influences the GPS accuracy, for a detailed description, see section 3.5.

Accuracy of GCP measurements in the photos. The accuracy of the ground control point measurements in the photos is influenced by factors which make it difficult to pinpoint the ground control points in the picture exactly. These factors are pictures being blurry, and the ground control points being not big enough in the picture. Very small shifts of ground control points in the terrain might also be possible, because we used wooden boards which were lying on the terrain. If someone accidently bumped into a board, then it is moved slightly, causing an extra inaccuracy. It is uncertain whether this has actually happened, because when the movement is larger then 1 cm, a print in the sand would have been visible. Then it was clear that one of the GCPs had moved and the measurements would have to be done again.

Accuracy of tiepoint measurement in the photos. To create a point cloud in photomodeler scanner, the GCPs were used as tiepoints. No further tiepoints were used, so the factors influencing the tiepoint measurements are the same factors that influenced the pinpointing of the GCPs in the photos, which are described above.

Accuracy of height calculations when the point cloud was created. The accuracy of the calculated heights is influenced by the accuracy of the orientation of the pictures, which is in turn influenced by the accuracies of the measurements of the ground control points in both the terrain and the picture. The height values are calculated with the help of the so-called parallax differences, then the height of an object will result in a small distance between the foot and the top of the object in the picture. This distance (the parallax) is different in two pictures showing the same object. From this difference (the parallax difference) the height of the object is calculated. The bigger this difference, the more accurate the height calculation. To make sure this difference is big enough the distance between two picture centers should be big enough. If this distance is too small, the heights will be inaccurate.

Accuracy of the model/object coordinate system transformation. As was seen in the previous paragraph, the residuals between the resulting coordinates after the relative orientation of the photo's and transformation of the model coordinate system to the RD/NAP system were larger than expected. This is probably due to the fact that these results show the final accuracy of the project, which is influenced by all inaccuracies which has been described so far.

Finally, all the mentioned factors are summarized in table 3.2.

Factor influencing uncertainty	Order of magnitude	Possible correction methods	Resulting uncertainty
Inaccuracy of GPS measurements	< 5 cm	Using static GPS instead of RTK-GPS	Up to 1 cm
Blurry photo	2 pixels (photo) or 6 cm. (terrain)	Using a more stable platform for the camera	Within 0.5 pixel (photo) or 1.5 cm (terrain)
Ground control points too small in pictures	3 pixels (photo) or 9 cm (terrain)	Taking photos from lower height or use bigger GCPs	Within 0.5 pixel (photo) or 1.5 cm (terrain)
Small shifts of ground control points	1 cm	Anchoring GCPs or using paint instead of wooden plates	Within a mm
Photo centers being to close to each other	Couple of mm to 1 cm, with possible outliers up to 1 m	Using pictures further apart; taking pictures on a longer time interval (a picture every 10 seconds instead of 5	Not much more accurate than it is now but probably with less outliers

Table 3.2: Error budget for photogrammetry.

3.2 Terrestrial laser scanning

Laser scanner technology that has developed during last two decades and has already been proven to be very useful in many applications, e.g. cultural heritage, highway engineering surveys, forest intervention, modeling smaller objects as statues, ships, pipelines and objects in industry environment, architectural and archaeological surveys. The shape of an object is usually remarkably complex, and in this sense the laser scanning method provides accurate and complete 3D models of the acquired objects that enhance the visual interpretation and realistic representation. In comparison with the traditional methods as tachymetry and photogrammetry, the acquisition itself is cheap, fast and, after defining some initial values as for example portion of the object to be acquired and the density of the points, completely automatic. On the other hand the analysis, the processing and the modeling phases of the laser scanner data need more time and attention.

In this project the terrestrial laser scanning technique has been used to measure the topography of the coastal area and to obtain the elevation of the terrain as accurate as possible according to expected terrain morphology changes. The aim is to measure the initial situation of the coastal area and monitor the changes of the surface and objects on it (e.g. dunes, groyne, and vegetation) over time. A plan for repeated measurements is given in chapter 5. The research is also focused on the direct impact of large storms, thus it is important to measure the area accurately and immediately after the event. In comparison with the aerial laser scanning method and photogrammetry, which are commonly used for terrain modeling, the terrestrial laser scanning method is preferred while it offers higher resolution and accuracy, bigger flexibility of the acquisition process and time, and lower costs for multitemporal

monitoring. The comparison of the data sets is given in chapter 4.

3.2.1 Working principle

Terrestrial laser scanners can be divided into two different categories, namely time of flight and phase shift distance-meters. The first one measures the time interval between emitting the laser pulse and receiving its back-scattered echo. The second one compares the phase of the emitted pulse with the phase of the returned echo and compute the phase shift. Finally the measurement principle is the same in both cases; they both measure the time, which is then used to compute the range. For each acquired point a distance is measured in a known direction, so we obtain polar coordinates, which are further on recomputed to Cartesian coordinates. The result is a 3D cloud of points, where for each point of the model the X, Y, Z coordinates and the intensity value (e.g. the energy reflected by the measured point) are known.

The 3D point cloud has a predefined resolution according to the scanner specifications and an accuracy that depends on the measurement geometry (i.e. range and angle measurements) and instrumental effects of the scanner. When one scan is not enough to cover the complete area of interest, more scans must be taken, which are later on combined in post-processing. For this reason the scans must have certain overlap and some well detectable (in sense of the laser point cloud) referencing objects must be placed in this area. To obtain the final 3D model of the area it is necessary to align scans together, which is done in the so-called registration step. Further on, in order to compare laser scanner data with other techniques and also to allow multitemporal analysis, the terrestrial laser scanning (TLS) model should be transformed into the global coordinate system in the so-called georeferencing step. For this reason GPS measurements were done.

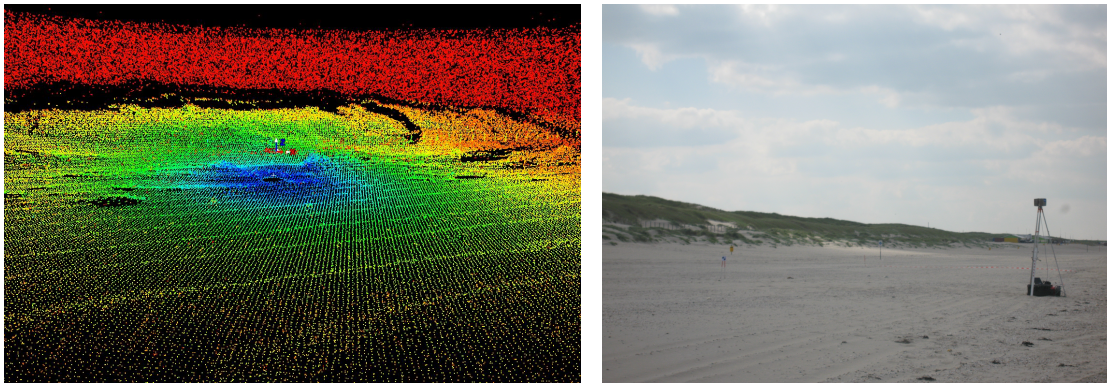

(a) Resulting cloud of points with color coded representation of intensity values.

(b) Image of the scanned area

Figure 3.14: Resulting cloud of points (left) and the measured area (right)

An example of the color coded intensity values is shown on figure 3.14. The intensity values show how much energy is reflected back from the surface according to the emitted energy and is a relative value. Therefore the intensity values become smaller further away from the scanner position (from blue to orange and red) as can be seen on the figure 3.14 and change regularly in concentric circles around the scanner. Intensity is really small for the points in the air, which mostly represent noise. It is

mainly dependent on the reflectivity coefficient of the surface material, and can be used to determine different surface materials after the normalization for the distance from the scanner. Further analysis should show, whether the intensity can be used for segmentation of different surface materials (e.g. to separate sandy area from grass area).

3.2.2 Acquisition platform

To acquire TLS data, mostly the Faro LS880 laser scanner [10] (figure 3.15, left) was used. But according to some filtering problems, that will be discussed in the following section, also a Leica ScanStation 2 [17] (figure 3.15, right) was used, which was borrowed from the Leica Geosystems.

(a) FARO LS880. (b) Leica ScanStation 2.

Figure 3.15: The Faro LS880 scanner and Leica ScanStation 2 scanner.

The Faro scanner LS880 is a phase-based scanner, which emits an infrared beam. The laser scanner splits the laser beam into three component parts operating on three different modulation lengths 76 m, 9.6 m and 1.2 m, as shown in the wave modulation diagram in figure 3.16. With the use of three varied ranges a higher degree of accuracy can be achieved over a greater distance as the specific range is measured with a resolution of 17 bit or 0.58 mm [10]. The initial range is determined by means of the lowest frequency, which also defines the largest unambiguously measured distance, e.g. 76 m, and the finest one improves the range measurements to within few millimeters. The measuring principle is based on the phase shift, which is used to compute the distance from the laser to the object or surface.

Lecia ScanStation 2 is a pulsed or 'time-of-flight' scanner, which sends out the pulses with visible green wavelength. It is a new generation of pulsed scanners with a high scan rate that is 10 times faster than the normal pulsed scanner. Table 3.3 shows the specifications of the two laser scanners used in the project [10, 17].

The scanners differ in the distance measurement principle, which results in their important characteristics. As can be seen in table 3.3, the phase difference method is faster and more points per second can be acquired than with the time-of-flight method. This influences the best resolution one can get in

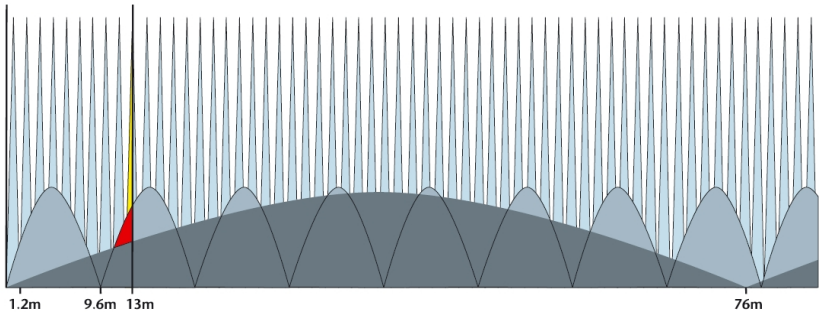

Figure 3.16: Modulation diagram of the Faro LS880 [10].

Scanner	FARO LS880	Leica ScanStation 2
Scan method	phase difference	time of flight
Field of view, H × V (°)	360 × 320	360 × 270
Range (m)	0.6 - 76	300 @ 90%; 134 @ 18% albedo
Angular resolution, H and V (°)	0.00076 and 0.00900	0.0002
Systematic distance error	± 3 mm / 25 m	± 6 mm / 50 m
Wavelength (nm)	785 (infrared)	532 (visible green)
Beam divergence (mrad)	0.25	0.06
Spot size	19 mm / 76 m	≤ 6 mm / 50m
Scan frequency (points/sec)	≤ 120,000	≤ 50,000
Camera	add-on option	integrated
Inclination sensor*	yes	compensator

**Leica ScanStation 2 is able to compensate for changes of main axis inclination during measurement, so it is assumed that the XY-plane of the scanner coordinate system is horizontal, while Faro LS 880 uses corrections only for post-processing (in the registration of scans).*

Table 3.3: Specifications for the FARO LS880 and Leica ScanStation 2 laser scanner.

certain time. Another important feature of a TLS is the measurement range, since range determines to a large extent the types of application. Since laser scanners operate in non-contact mode, the range depends also on object reflectivity. Therefore the maximum range is accompanied with an indication of the reflectivity percentage (also called albedo). Scanners using the time-of-flight method can measure longer distances and are more suited for long-range applications (more than 250 m). The phase difference scanners measurements have higher accuracy, but signal-to-noise ratio increases with the range and depends on lighting conditions. Therefore phase-shift systems are particularly suited for high-precision short-range (up to 25 m) and medium-range applications (up to 250 m), for which high point densities are required [65].

The two scanners use also different wavelength of the light send out into the environment. According to the physical properties of the electromagnetics waves, it is expected that visible green light penetrates shallow water and measures also the topography of surface few decimeters under the water. The infra red light in case of the FARO laser scanner specularly reflects on the water surface, so there are no points.

The Faro scanner offers the possibility to mount a digital camera on top of it, but the camera was not available in our case. The additional image data would be very useful to provide an overview of the scanned objects.

3.2.3 Measurement campaign

To cover the whole coastal area that is of interest (i.e. where changes are expected), more scans were needed. But due to the time limitation for the measurements and the maximum range that can be covered with the laser scanners used, a restricted number of areas to be measured have been chosen as can be seen in figure 3.17. The measurement campaign was done in four days.

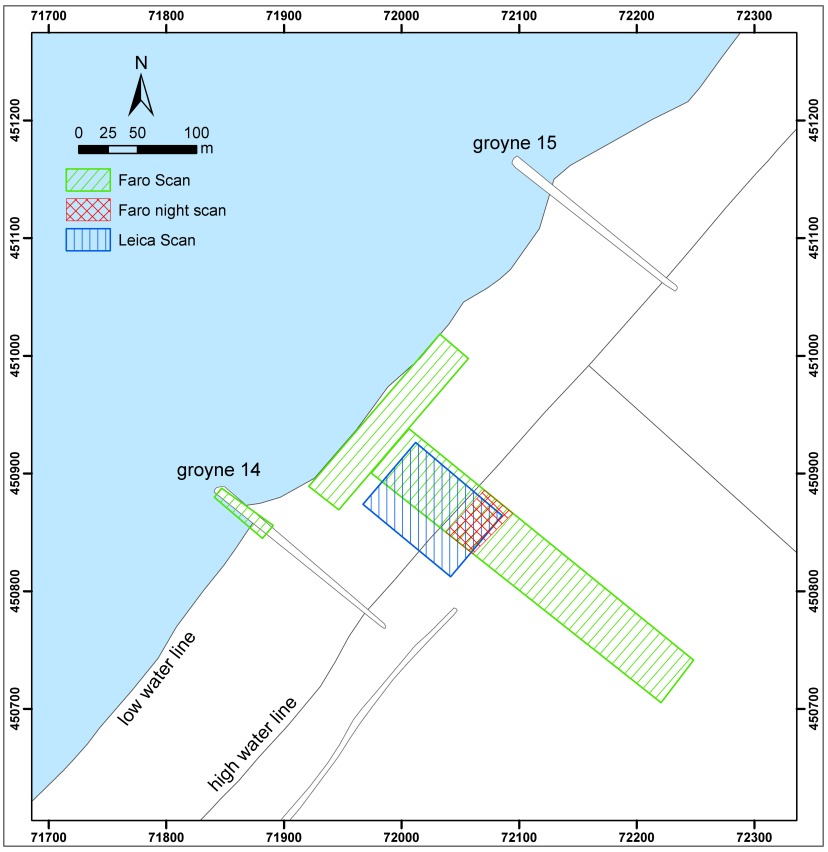

Figure 3.17: The areas of TLS measurements.

The aim was to make one line of measurements perpendicular to the sea line to obtain all different surfaces that occur in this costal area that are firstly a sandy wet part (tidal area), secondly the sandy dry beach, both are relatively flat, and thirdly the sloped dune area, overgrown with grass and bushes.

Using the Faro scanner, three scans along the sea line in the tidal area have been done with the aim to enable an overlap with the single beam echo sounding technique. Further, one scan has been on groyne 14, to obtain detailed measurements of this feature, which is important for beach safety. After

first processing of the data, a big amount of the noisy points became apparent. Therefore an additional scan during the night has been made, in an attempt to research the relationship between sunlight and the noise of Faro scanner. The day and night scan are expected to differ, since the daylight influence on the returned signal as an additional input.

To further assess the noise presence in the scans made at the beach, additionally two scans with the pulsed-based laser scanner Leica ScanStation 2 were tried.

To obtain an unobstructed viewing angle from the 3D scanner locations and also to assure larger incidence angle further away from the scaner, the scanner should be positioned as high as possible. For this reason a special high tripod has been used to elevate the scanner up to 2.5 m height.

Adjacent scans were acquired one after another with a certain overlap, which serves as a referencing area to connect the scans together in a unique local reference system. In order to define the minimum overlapping area between two adjacent scans, some tests have been performed. Using an overlap of 30% the final precision is compatible with the range accuracy of the used laser scanner [46].

For the purpose of registering the scans together in one point cloud and also for georeferencing this point cloud into the global coordinate system, some objects, that are visible in the point cloud, must be acquired during scanning. Since in the measuring area there are no stable benchmarks available (e.g. houses and poles), artificial targets were placed. The size, shape and target's material should fit the scanner characteristics (resolution, range, high reflectivity targets), such that the target is well defined and visible in the point cloud. According to the type of the target, its position depends on the laser-object distance, the used angular resolution and the mean inclination of the measuring directions. In this project three different types of targets have been used, as can be seen on the figure 3.18.

(a) Planar paper target. (b) Spherical white target. (c) High reflective target.

Figure 3.18: Targets used in the project.

Twenty planar targets size 20 by 20 cm were designed from a wooden plate on whicha paper was pasted, printed with a pattern as can be see in figure 3.18, left. At least five of them were placed along the line of two scans, so to be visible from both positions of a scanner and enable the registration of scans. Five white spheres with a diameter of 15.24 cm (6 inch) were fixed on the tripod (figure 3.18, middle) and placed in the overlapping area of two scans to be used for registration and georeferencing. The global coordinates of the sphere's centre were measured with RTK-GPS. Another type of target, one high reflectivity HDS circular planar target with a diameter of 15.24 cm (6 inch: figure 3.18, right), was used when scanning with Leica ScanStation 2.

At least three, but to assure redundancy five identical points, in two adjacent scans are needed to register them together. Also for georeferencing at least three but preferably more points are needed per point cloud to be transformed from a local laser scanner coordinate system to a global one. The schematic position of the scanner and targets (spherical and planar) is shown on the figure 3.19.

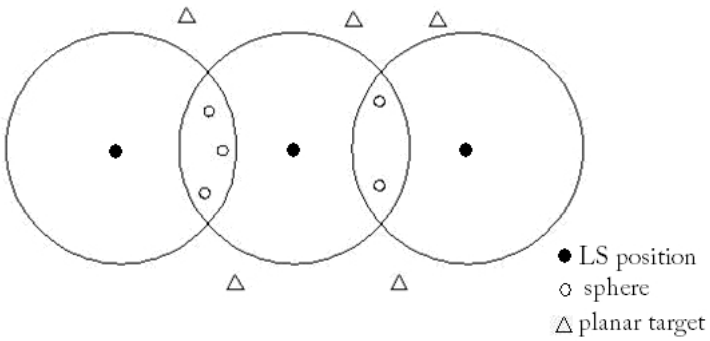

Figure 3.19: The relative positions of spheres, targets and scanners.

3.2.4 Data processing

As mentioned earlier, a problem with the Faro scanner data is the noise present in the 3D data, which must be removed before further use of the data. The noise, that is usually a result of gross errors and outliers, was estimated with different tests. Smoothing filters are used to reduce noise and remove points not belonging to the scanned surface. The amount of noise depends on the type of surface, laser beam divergence and on the environmental conditions in which the acquisition is carried on. When the Faro LS880 scans towards the sky, normally nearly no laser light is reflected back into the scanner. However in this case the scanner still gives a measurement, which is pure noise and completely useless. Finding the right filter for the data is therefore very important for the next processing steps. A filter should eliminate as much noise as possible, but at the same time keep the details of the surface [35].

The filtering step was done in Faro Scene, which offers four different filters. The most useful and effective were the stray and the dark points filters. The first one divides the point cloud into regular meshes. The size of the mesh is chosen by the operator and is in a theory a function of the acquisition scan step and of the point density one wishes to obtain at the end of the filtering phase. For each mesh that contains at least four measured points, the median of the distances is estimated and the deviations of the single values are computed from their median. The operator defines the percentage of points that are rejected, starting with points that have the biggest deviation. The rest of the points are used for the estimation of the real distance using the mean. The second filter works on the intensity values and eliminates all points with smaller intensity value than the threshold specified by the operator.

Also after setting different parameters values for the mentioned filters, no satisfactory results were obtained. As can be seen on the figure 3.20 the filtered data is too noisy to see the spheres in the cloud of points.

One of the possible reasons of such a noisy data set might be daylight. It apparently influences the reflectance of the beam from some small particles and water vapor in the air. To research this

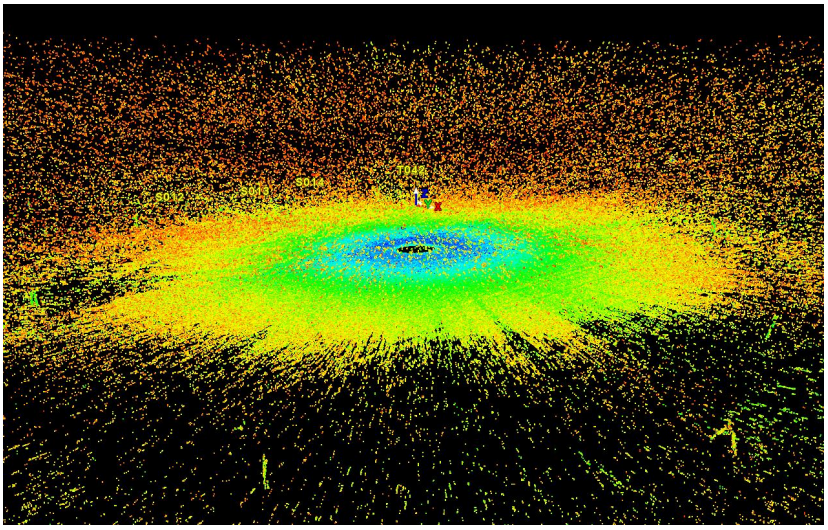

Figure 3.20: Filtered data.

phenomenon, two scans have been at the same position (on the beach, on the bottom of the dune foot) on different times, one at around 18.00 which at the time was during daylight and another at around 21.00. Results can be seen in the figure 3.21.

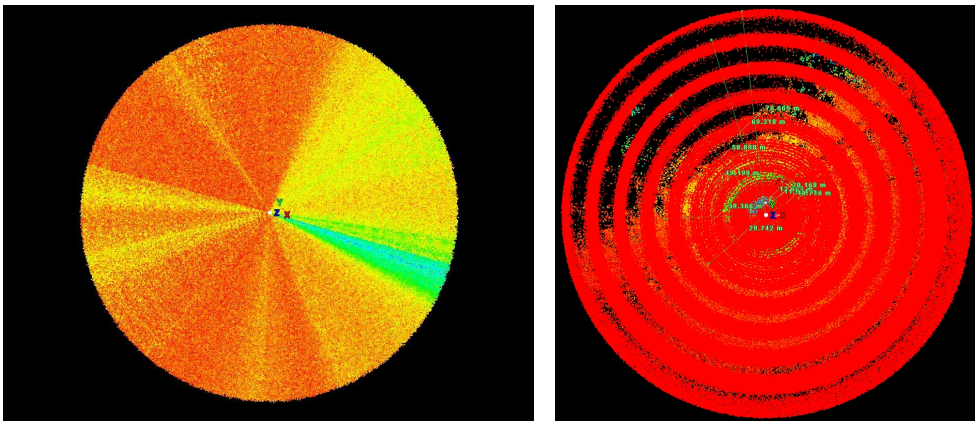

(a) Day time scan. (b) Night time scan.

Figure 3.21: Day and night time scans of the same area (aerial view).

The day scan is completely noisy and since there are so many points on the sky it is difficult to separate the surface points from the noisy points. The night scan shows some unexplained pattern of concentric circles, that occur closer to the scanner with a frequency of approximately 1.2 m and further away with the frequency of around 9.6 m. Those distances show that the pattern depends on the frequency modulation of the laser signal, but a more exact explanation is not known yet.

Both scans were filtered with the same filter and the results can be compared in figure 3.22. The filtered day scan is still very noisy, but the filtered night scan is now clean and usable for the next processing steps.

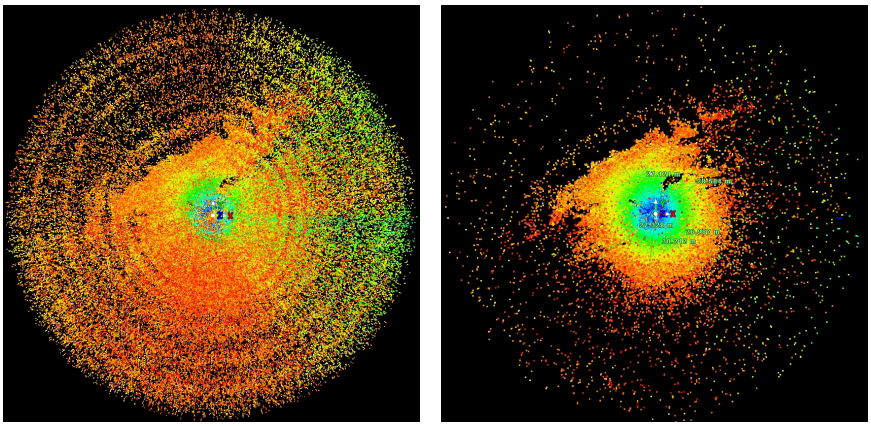

(a) Filtered day time scan. (b) Filtered night time scan.

Figure 3.22: Filtered day and night time scans (aerial view).

The second attempt to solve the noise present in the Faro LS880 data set was to use another sensor. Fortunately the Lecia ScanStation 2 was available at the time and it was borrowed for a day to make two trial scans on the beach. From figures 3.23 and 3.24, it can easily be seen there is a great difference between the data acquired by the two sensors. Although many noise points are presented in the Faro data also after filtering, the Leica data gives a very clear view of the terrain, and almost no noise points can be found after filtering.

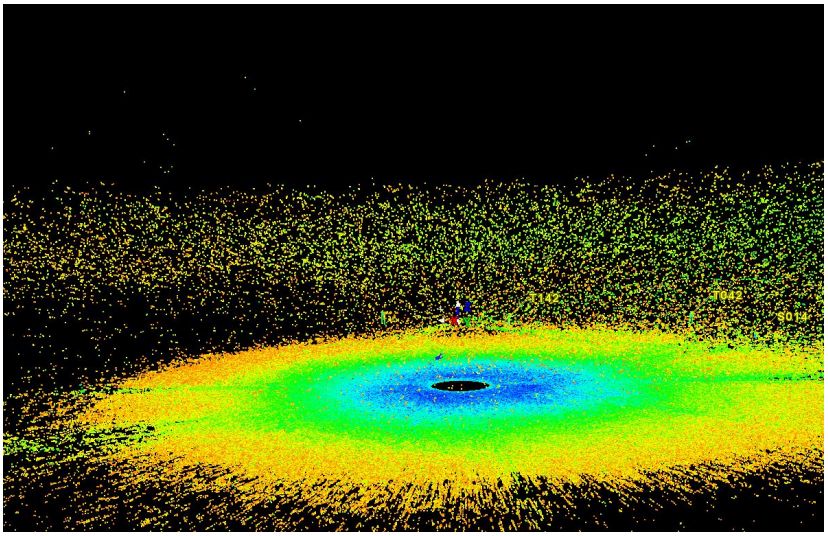

Figure 3.23: Data acquired by FARO LS880.

The registering and georeferencing step was done in Leica Cyclone. For the registering process first three translation and three rotation parameters are computed according to the tiepoints, visible and selected in both point clouds. Then the transformation parameters are used to recompute all points of the second scan into the coordinate system of the first scan, which has been chosen as the reference system. Figure 3.25 shows the point clouds before and after registration. The pricinple and procedure

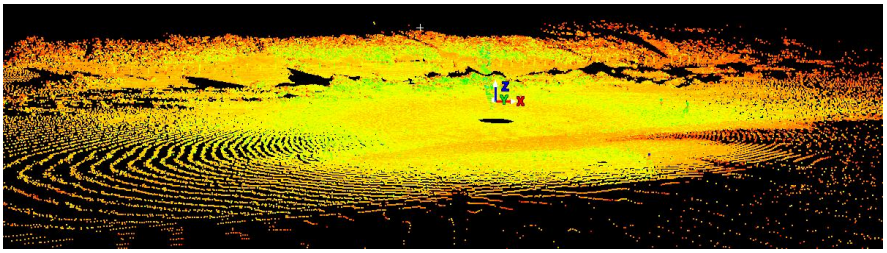

Figure 3.24: Data acquired by Leica ScanStation 2.

for the georeferencing is nearly the same as registration. But in this case the ground coordinates of the spheres' center, which were measured with the RTK-GPS method, are used to convert the local scanner coordinate system of the integrated point cloud in to a geographical coordinate system (in our case Dutch RD/NAP system). Finally, an intergrated point cloud with global coordinates is obtained (see figure 3.26).

The registration and georeferencing was done for both Faro and Leica data. But since it was still impossible to remove all noise points in the Faro data, only the Leica point cloud was considered for further analysis (e.g. constructing a DTM and merging with the other data sets). Unfortunately the accuracy of the registered and georeferenced Leica data is very bad (the error is about 16 cm), due to the low scanning resolution. It was not possible to fix the exact center position of the targets by using only 1 or 2 points. In a normal case the error is smaller than 6 mm, according to Leica Geosystems HDS Technical Support.

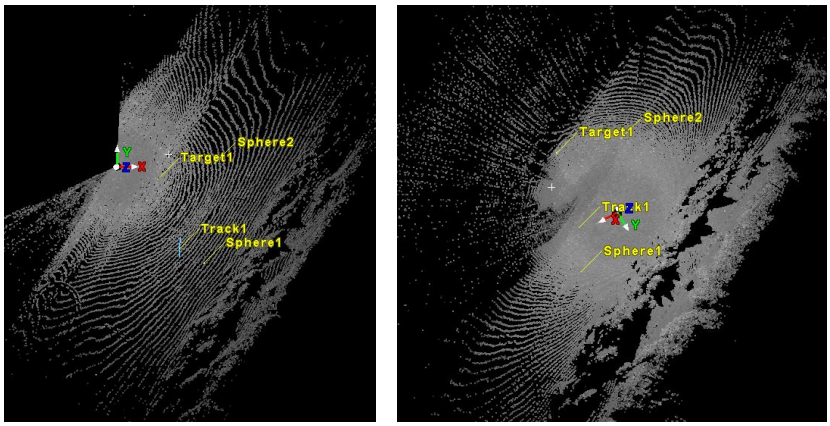

Figure 3.25: Two scans before registration with four pairs of reference points.

For the purpose of analysis and comparison, a digital terrain model was made. To get a reliable DTM, the objects on the ground must be manually removed before modeling the surface.

3.2.5 Results

After referencing, georeferencing and filtering the non-terrain points, a digital terrain model can be obtained in Cyclone. Here only the Lecia data was used with two scans in one georeferenced point

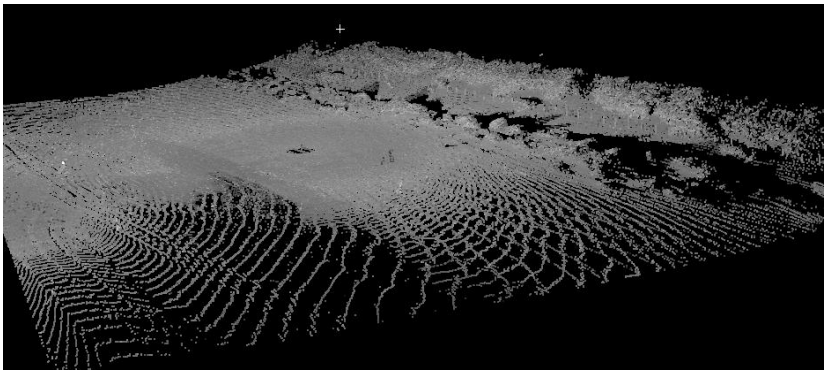

Figure 3.26: Results after registration.

cloud, since it is almost impossible to get a DTM out of the Faro data. Cyclone uses TIN for the interpolation and the result is shown in figure 3.27.

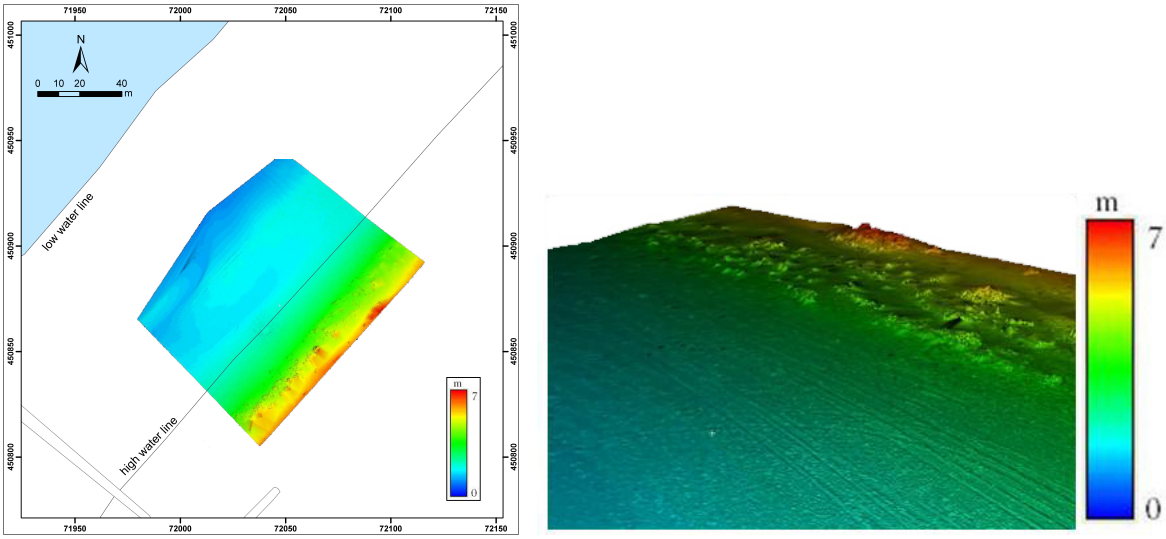

(a) DTM overview.

(b) Zoomed in DTM.

Figure 3.27: DTM derived from the Leica scanner data: the left picture shows the overview of the DTM and the right one is a zoomed-in picture showing more details.

The grid interpolation in MATLAB is also used for creating the DTM, since it is necessary to use the same grid interpolation as other techniques for the data fusing, which can be seen in the figure 3.28.

Another option for using the laser scanner data is to make a profile of the DTM. By comparing the profiles of the beach in different time, it is possible to monitor how the beach changes by looking at the difference between the two profiles.

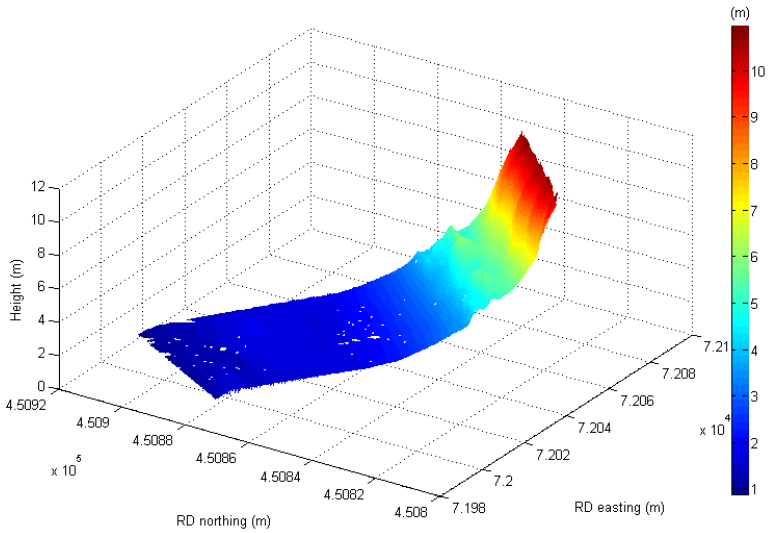

Figure 3.28: DTM in MATLAB, the grid size is 30 by 30 cm.

3.2.6 Quality assesment

Resolution

A big advantage of laser scanners is that they records millions of points just in a few minutes. The point density or the scanning resolution is a very important parameter, as it influences the accuracy of the final products and defines the size of features that can be seen or modeled from the raw data. For most of the TLS systems the resolution can be set by the operator before the acquisition starts.

If it is assumed that the area is flat, as it mostly is on the beach, and that the scanner is positioned 2.5 m above the ground, it is possible to compute the point density on the ground (horizontal plane), given the vertical and horizontal angular resolution. The point density decreases very fast with increasing range. Figure 3.29 shows the change of along-sight resolution (in the direction that the laser scanner looks) with increasing range (left graph) and with increasing incidence angle (right graph). It can be seen that the resolution changes very fast and gets worse, once the incidence angle exceeds 82°, what correspond to the range is bigger than 20 m. To obtain satisfactory resolution also further away from the scanner, the TLS platform should be placed higher.

The point density was defined in Faro's scan settings by an angular step. One of the four possible resolutions can be chosen (see table 3.4). According to the limited time available, usually 1/4 resolution was chosen. The Leica ScanStation 2 enables to fix a linear grid, setting its spacing on the basis of acquisition distance. The operator can independently set vertical and horizontal scan density. The minimum scan angle step in horizontal and vertical direction is 0.0002°. This gives a resolution of 0.02×0.81 m at a distance of 76 m for a scanner height of 2.5 m.

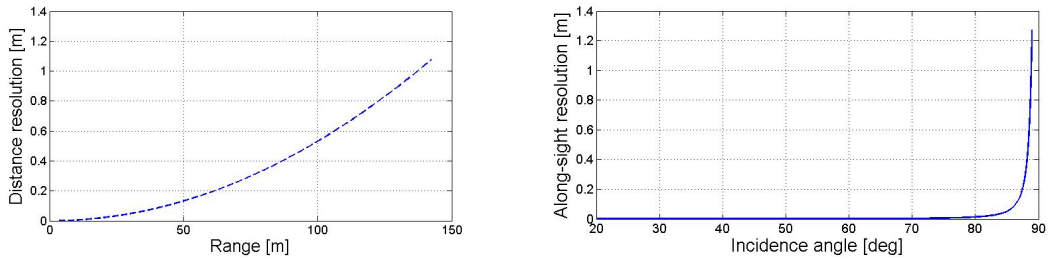

Figure 3.29: The along-sight resolution depending on the range (left) and on the incidence angle (right).

Resolution	Scanning Time	Vertical resolution	Horizontal resolution	Number of points per scan	Resolution on flat terrain at 76 m*
1	> 60 min	0.009°	0.00076°	> 25 000 000	1.19 cm × 3.06 cm
1/2	40 min	0.018°	0.00152°	21 398 561	2.39 cm × 6.13 cm
1/4	8 min	0.036°	0.00304°	12 612 493	4.78 cm × 12.26 cm
1/10	2 min	0.090°	0.00760°	2 132 273	11.94 cm × 30.65 cm

**The height of the scanner from the ground is set to 2.5 m.*

Table 3.4: Different resolution values that can be chosen in the Faro scanner settings.

Accuracy

When considering the accuracy of the TLS data, one would like to assess the horizontal and vertical accuracy of the acquired points. It depends on the accuracy of the laser scanner components which give two measurements: range (laser range) and angle (scanning component). The range and scan angle accuracy is given in the specifications for each scanner. For the scanners used in this project the specifications are listed in table 3.3.

The higher the point density is, the higher is the spatial resolution, and the more precise the position of the points can be determined. To obtain some reliable estimation of the position accuracy, the TLS data should be compared with some reference data (for example with GPS measurements). But in the scope of the project just the theoretical values written already in the previous section (table 3.4) can be reported. The spatial resolution is in our case of the flat terrain changing with the range.

The vertical accuracy of the measured points firstly depends on the range measurement accuracy. The nominal value of the systematic distance error, given in TLS specifications (see table 3.3), is valid in the line of sight direction, but its influence on the vertical error changes with the incidence angle. In case of a flat terrain the incidence angle becomes smaller further away from the scanner. On the base of simple geometry rules and if the 3 mm range error is assumed, the theoretical vertical error was computed . It increases very fast when the incidence angle approaches to 90°, i.e. when the scan beam is parallel with the surface (see figure 3.30, left).

In order to reach an expected precision, the range must be limited to corresponding value, where the point density is still reasonable (table 3.4) and the vertical precision of the points still acceptable (figure 3.30, right).

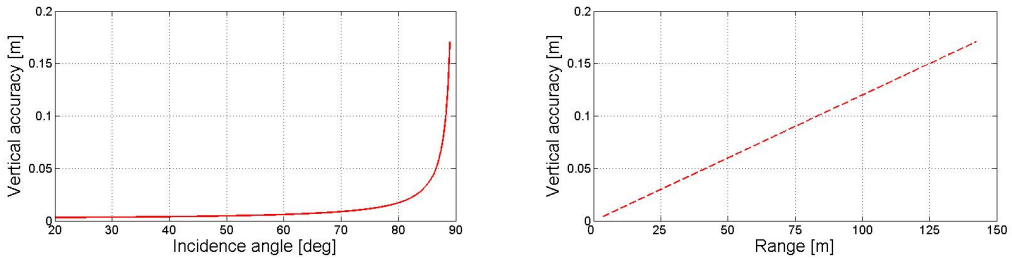

Figure 3.30: The vertical accuracy depending on the scan angle (left) and on the range (right).

Beside the measurement errors, the accuracy of the point cloud also depends on the systematic errors, which are the trunnion axis error, eccentricity of the scan centre, collimation axis error at 3 mgon, horizontal axis error at 30 mgon (accuracy and leveling the TLS), angle of incidence and surface properties [82]. Again the systematic error could be assessed in comparison to the reference data.

Finally the accuracy of the results obtained from the TLS point cloud depends on the processing steps that have to be done. In this project the main result is a DTM of the beach area that was computed from the TLS points with linear interpolation. Beside the vertical and horizontal error of the points the biggest contributions to the DTM accuracy are errors in registration and georeferencing procedure. In case of the Leica data the mean error (i.e. the average in X, Y, Z direction of the local and RD coordinate system) is in the range of 15 cm and for the Faro data 2 cm (values are obtained from the automatically generated report of the registration and georeferencing in Cyclone). Such difference exist mainly due to the error in registration and georeferencing, which will be explained in the next paragraph.

Error budget

According to the errors discussed in the previous section, a short summary and list of them is given in table 3.5. According to the acquisition problems (noisy data, not well planed trial measurements) the TLS data set does not represent the best what can be achieved with this method. Therefore table 3.5 contains also suggestions for possible improvements of the measurements and processing and gives an idea what the resulting, best accuracy could be.

As shown in the table 3.5, the sources of the biggest error are registration and georeferencing procedures. It is mainly due to too low resolution on the targets' surface, so they can not be determined exactly. Another reason is the low number of the targets (just three could be used) that were visible in two adjacent scans. Also for georeferencing just three spheres with RD/NAP coordinates were used, so there was no redundancy to compute the transformation parameters.

Finally, it is suggested to put the targets closer than 20 m from the laser scanner.

3.3 Medusa radioactivity probing

One important aspect that could give more insight in the sediment transport is the sediment type *[55].*There are certain types of sediment like mud, clay and sand. These sediments have different

Factor influencing uncertainty	Order of magnitude	Possible correction methods	Resulting uncertainty
Range accuracy	4 mm at 50 m	Limit the range of scanning or use another sensor	< 4 mm
Scan angle accuracy	0.009°	Using higher resolution for scanning or use another sensor	0.0002°
Systematic error	-	Improve the precise leveling	< 4 mm [82]
Registration accuracy (horizontal / vertical)	Horizontal 20 cm Vertical 7 cm	Setting higher scanning resolution, using bigger targets, positioning targets closer to the scanner, using more targets in the process	6 mm
Georeferencing accuracy (horizontal / vertical)	Horizontal 20 cm Vertical 2 cm	See registering accuracy.	2 cm (or the accuracy of the GPS method)

Table 3.5: Error budget for terrestrial laser scanning.

physical characteristics and a different dominant grainsize [79]. The differences in grainsize are the result of the sedimentary environment in which the sediment was eroded *[57].* In the Medusa measurement method the sediment type by based on grain size distribution is derived from natural radioactivity using the measured natural radioactivity.

The Medusa data adds valuable grain size information to the bathymetry, since spatial sorting takes place in the coastal zone. Besides from the fact that different sediment types are eroded in a different environment, the sediment type also influences the landscape itself. This feedback or loop was mentioned in chapter 2. One example is that when a lot of clay is abundant in the ground, water is not able to penetrate, which results in surface water, while sand (especially with large grains and low cementation [75]) is permeable for water and little or no surface water will stay on a sandy soil [23]. It also allows mapping susceptibility to erosiom, since some sediment types are more susceptible to erosion than others, which is important for future beach nourishment planning [75].

3.3.1 Working principle

In order to monitor the sediment type, the fact is used that K^+-ions tend to stick to mud and clay particles, which results in radioactivity. Sand particles on the other hand, do not attract these K^+-ions, which results in a relatively low radioactivity *[95].* This difference in radioactivity is used to quantify the mud content in the sediment.

The radioactivity probe measures the natural radioactivity that impacts the sensor. For all practical field applications, only γ-radiation (also known as photons) is of importance, because α- and β-

radiation have not much penetrating potential and will in general not escape the ground and will not reach the detector *[58].*

The sensor consists of a crystal ('NaI crystal' or 'BGO crystal') that tends to show scintillation when it is impacted by γ-radiation [61]. Scintillation is the phenomenon that when certain matter is hit by radiation, it sends out a light flash. This light is picked up by a light-sensitive sensor that transforms the lightflash into an electric signal.

These electric signals are stored for a certain time, known as the integration time. After this usually short time period (usually 1 s) the computer constructs a frequency spectrum of the recorded electrical signals. The frequency spectrum is a plot of the frequency as function of the countrate (or number of γ-rays per second). From the frequency spectrum and known 'fingerprints' of Th, U and K, it extracts the concentration of these atoms. From this concentration the grainsize of the sediment can be derived due to a 1:1 correlation between these two properties.

3.3.2 Acquisition platform

The measurement campaign consists of offshore and onshore measurements. The onshore measurements are done using a radiation sensitive sensor mounted on a backpack frame. The system is worn as a backpack (see figure 3.31) and a person carries it while walking tracks. The sensor is connected to a handheld PC which stores and processes the incoming data. The data can afterwards easlily be uploaded to another data carrier via an USB connection.

The offshore system is towed behind a small vessel (see figure 3.32) that sails cross shore directed lines. The offshore sensor is mounted in a PVC housing in order to protect the sensor against bumps while it is towed directly over the sea bottom. The sensor is connected to the boat by a strong cable through which the data is transferred to a computer onboard.

The housing of the sensor is around 6 m long and considerably heavy. It is therefore recommendable to have at least three pairs of hands available when loading and unloading the sensor in the water.

Figure 3.31: Medusa sensor used onshore.

Figure 3.32: Medusa sensor used offshore.

There are two additional sensors mounted on the Medusa sensor used offshore, namely a temperature sensor and a pressure sensor. These two sensors are used for two different purposes. The temperature sensor measures the temperature inside the housing. This temperature is important since the reference spectra are susceptible to temperature changes. The spectra tend to shift, which can be compensated for using the temperature data. The pressure sensor on the other hand is used to calculate the sensor depth.

For the positioning of the measurement equipment a DGPS system is used. DGPS works the same as a simple handheld GPS; it uses signals received from GPS satellites to calculate its position. A DGPS system uses also actual corrections that are transmitted by a ground station in the vicinity or from geostationary satellites. There is a station in Hoek van Holland that transmits a signal with actual corrections about the satellite position and satellite clock error for instance. This station is used for the onshore survey. The differential corrections that are transmitted improve the positioning accuracy to 1 m. When these differential corrections are not used the accuracy would be much lower (in the order of ten meters).

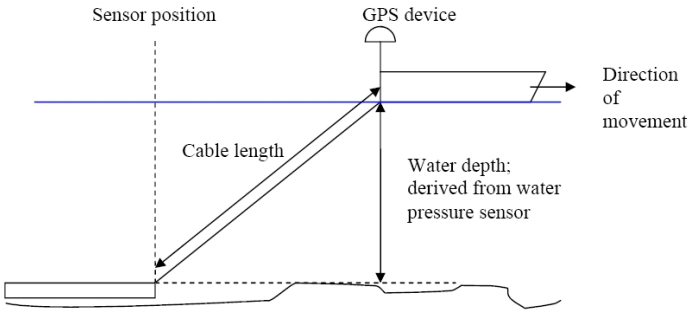

Figure 3.33: Georeferencing of the sensor offshore.

The positioning of the sensor offshore is difficult due to the fact that GPS signals do not penetrate water. Therefore the boat is equipped with a GPS device instead of the Medusa sensor. The sensor position is calculated afterwards by using the pressure sensor that is mounted on the Medusa sensor.

From the pressure data the depth of the sensor in the water can be extracted. Using this depth, the x, y position of the sensor can be calculated using simple goniometry. The sensor position is derived with the assumption that the sensor is situated behind the boat in the direction of movement. This is depicted in figure 3.33. Furthermore it is assumed that the cable runs in a straight line from the boat to the Medusa sensor. Medusa assumes a position error of around 10% of the cable length; for our surveying this results in a 2.5 m horizontal accuracy.

3.3.3 Measurement campaign

The measurement campaign consists of two different components; one offshore and one onshore. The offshore campaign was performed on the first day of the measurement week.

The sensor used for the offshore measurements is towed behind a small boat. The sensor is attached with a 25 m long cable as a result in the fact that the sensor can not come as close to the shore as one might wish. The offshore limiting factor is the cable length with respect to the water depth; at some point the sensor loses contact with the ground which results in sudden signal loss (due to the fact that water has a high absorption for γ-radiation). It is possible to get further offshore by attaching more cable on the sensor but for this region 25 m of cable was sufficient.

The onshore part was measured by walking tracks with the Medusa backpack. The beach, dunes and flatland behind the dunes were all done with a different track-spacing. This resulted in a different spatial resolution which forces to deal with each of these region seperately in the processing steps. Apart from the spatial resolution, the integration time on the first day was set at 0.2 s instead of 1 s, which was a mistake by the operators. The surveyed tracks are depicted in figure 3.34 and a table with the measurement parameters is depicted in table 3.6.

	offshore	onshore (beach)	onshore (dunes)	onshore (behind the dunes)
survey speed (km/h)	7	5	5	5
grid spacing (m)	30-40	30	3-5	15
integration time (s)	2	day 1: 0.2; other days: 1	1	1

Table 3.6: Medusa measurement parameters.

It is stated before that the main goal of the Medusa measurements is to do grain size mapping. The first step in reaching that goal was to get the nuclide concentrations of K, Th, U by surveying the area of interest with the radiation sensor. Getting from the radiation to concentrations is automated in the onboard computer connected to the sensor and is therefore only mentioned for transparency of the method.

The total time spent on sailing the tracks is of course strongly related to the survey speed. The tracks of this campaign were sailed at an almost constant speed of 6 to 7 km/h, which resulted in a total survey time of around 4.5 hours. There is another two hours spent on preparing the equipment and (un)loading the equipment in the small boat. The net area that is surveyed per hour is around 0.2 km^2 with a cross-shore distance from the shore of 600 m. The onshore measurements which were acquired with a much smaller spacing between the tracks took three full days of 8 hours surveying. This resulted in a total measuring time of 24 hours for a total area of 2.4 km^2, corresponding to 0.1 km^2/h.

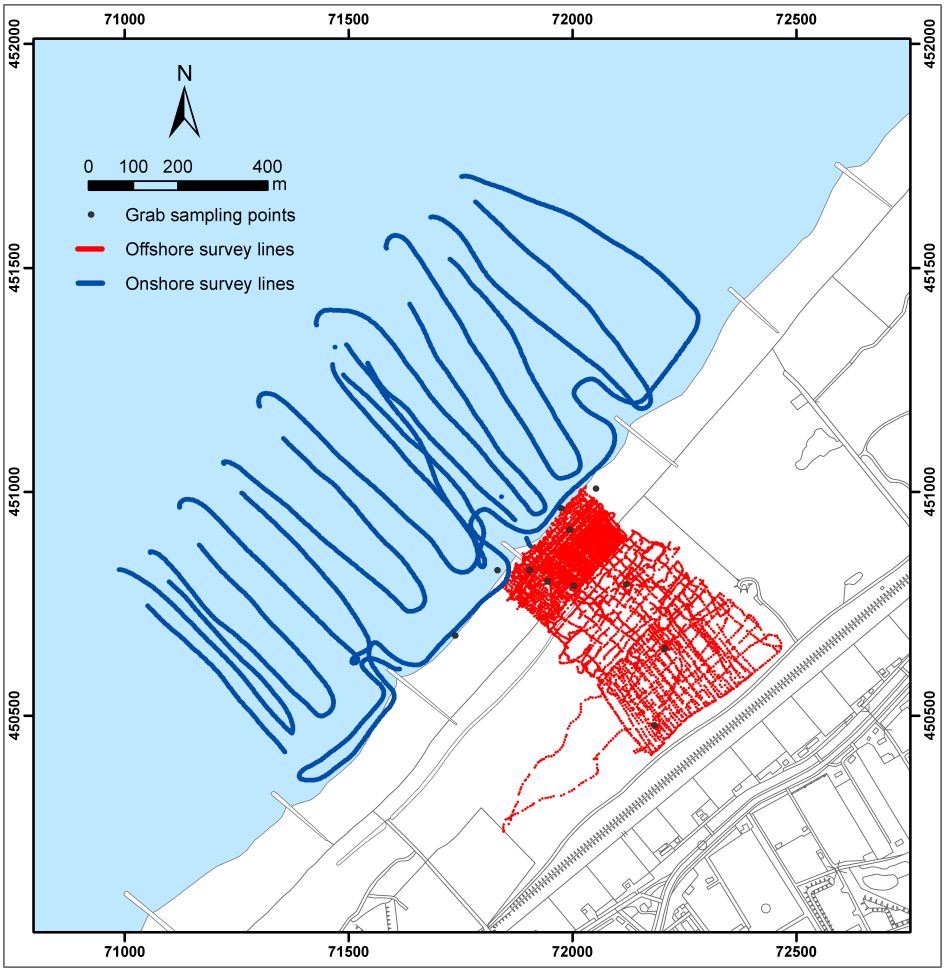

Figure 3.34: Medusa survey tracks.

3.3.4 Data processing

As a result of the variable nature of the underwater and beach environment, it is impossible to cover the area properly with sediment samples alone. Therefore, a geostatistical approach is used to describe the spatial variation of the grain size. As shown in figure 3.34 a number of measurements took place onshore and offshore in order to build a complete map, a function or surface is needed to fit a collection of the scattered data points. Geostatstical interpolation refers to finding values for points between the given points. A well known and often used interpolation method is ordinary Kriging [90].

First it is necessary to remove outliers of the nuclide concentration. After this outlier-removal, the spread and the normality of the data is analyzed (a further discussion on this normality can be found in paragraph 3.3.6). The raw dataset consists of two subsets; one dataset with the offshore data and one dataset with the onshore data. The first step in the further data processing is to seperate datasets that might show differing characteristics. Based on the morphological regions earlier defined, the dataset is divided into four parts; these subsets are:

- Offshore area;

- Beach area;
- Dune area;
- Flatland area.

Then the interpolation step is done to get an overall coverage of the region. Kriging can be used as an interpolation method to estimate values in a regular grid using irregularly spaced data [90]. Ordinary Kriging serves to estimate a value at a point of a region for which a variogram is known. The Kriging method has two advantages; it takes the error of the observations into account (filtering the nugget) and it uses the spatial correlation derived from the data itself. For these reasons the ordinary Kriging method is chosen for the data interpolation.

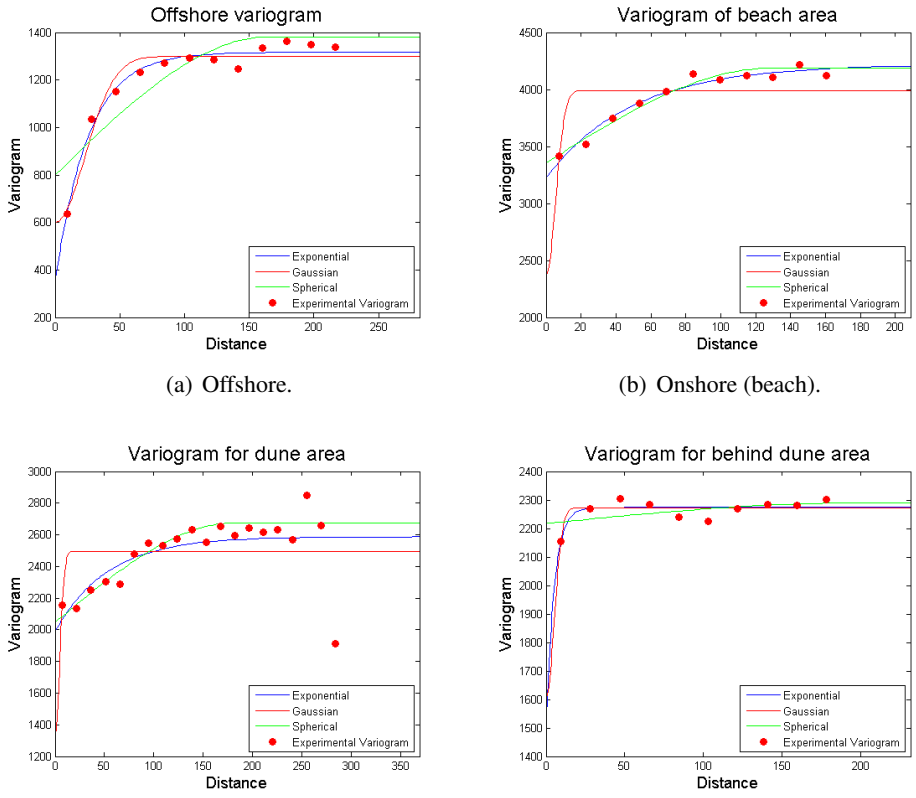

(a) Offshore.

(b) Onshore (beach).

(c) Onshore (dunes).

(d) Onshore (flatland).

Figure 3.35: Experimenal variograms with model fits.

Figure 3.35 shows the different isotropic variograms for the four locations. Together with these variograms and the original data ordinary Kriging interpolation was preformed in the offshore, beach and dune area.

This interpolation was done for two grids that cover the entire measurement area (offshore: 1 by 1 m; onshore: 0.3 by 0.3 m). These two grids cover the data from all acquisition methods: photogrammetry, laser scanning, GPS and single beam echo sounding. These grids are used for the further processing of all sensors in order to make comparison and data fusion more easy.

The flat area behind the dunes was very noisy and there was nearly no spatial correlation present. Furthermore the variogram range of only 26 m is not large enough to find a reasonanle amount of observations to interpolate with. Consequently a nearest neighborhood interpolation was used and afterwards smoothed by a moving average filter. This filter has a kernel of 33 by 33 grid cells, which corresponds with an area of 10 by 10 m on the ground. The final results of the K-concentration interpolation are depicited in figure 3.36.

(exponential) model parameters/area	offshore	beach	dunes	flatland
sill [Bq/kg]	1317	4139	2555	-
range [m]	76	118.23	150	-
nugget [Bq/kg]	345	3203	2015	-

Table 3.7: Variogram parameters.

It is important to mention that the resulting images presented are the K-concentration and not the grain size. The reason for this is that the lab results for the grain size determination did not show a direct correlation with the spectra. Therefore it was chosen to work with the concentration; the higher the K-concentration, the smaller the grain size (negative correlation). They relate 1:1 to each other which makes the K-concentration well interpretable.

3.3.5 Results

Grain size is a sediment characteristic which is one of the relevant parameters for sediment transportation along coastal areas. A grain size map can be used as a reference map for grain size monitoring on the long term. This will give the chance to understand how the grain sizes are correlated with the cross-shore gradient profile.

The maps in figure 3.36 show some interesting features related to the sediment transported as a result of the groynes. Groynes are built to preserve the coastal line and to reduce the erosion. It is important to realize that a relatively stronger current is able to transport larger grains [73]. This behavior can clearly be seen in the figure; high water current (at the groyne tip) flushes away larger particles after which erosion-resistant clay remains.

Typically at many locations there is a considerable variation in the grain size, depending on the distance from the coastline; i.e. the sediment becomes finer with increasing distance from the coast line. This contrast can roughly been seen in figure 3.36 and can give valuable information about the development of the coast.

Grain size variations in coastal dune sands have been widely used to infer transport and depositional mechanisms [40]. In figure 3.37 it is visible that the tidal area shows a relatively low K-concentration. However, it is not really well understood if this is really a sandy area, or weak signals due to water absorption, as the onshore acquisition is executed without direct contact with the sediment layer.

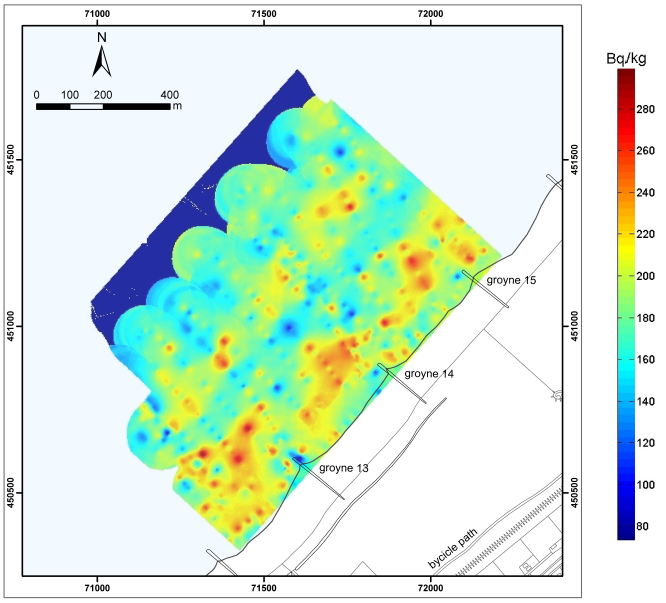

(a) K-concentration offshore.

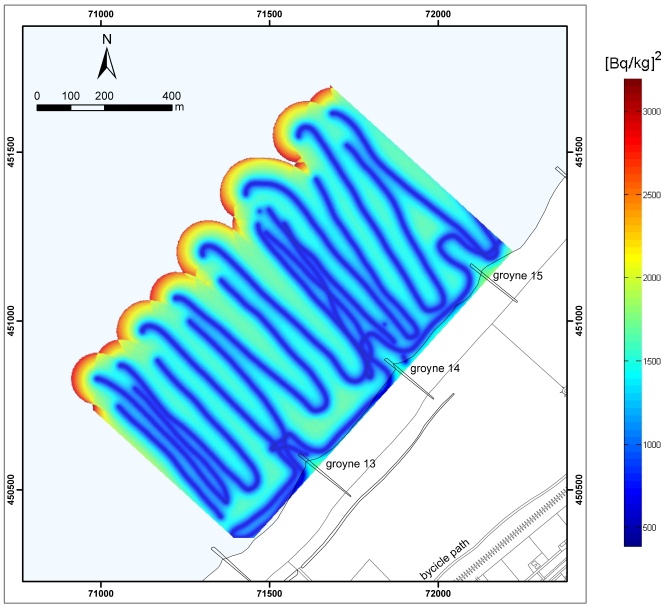

(b) Kriging error variance offshore.

Figure 3.36: Ordinary Kriging results for offshore observations.

The dune area shows a positive trend, starting from the end of the beach till behind the dunes which is vegetated. Grain size coarsening of the dune sands may be due to wind deflation of the fine grains, leaving behind the coarse fraction on the sands [60]. It is not easy to conclude if the finer material behind the dunes is just due to the fact that vegetation can trap finer particles. Another reason for this fine material could be the relatively low wind speed, which causes finer particles that fall out of saltation.

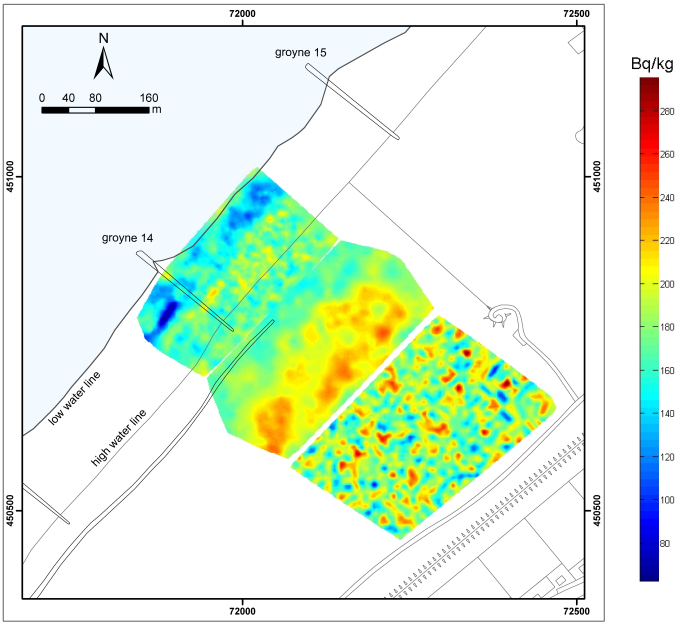

Figure 3.37: K-concentration onshore.

The flat area behind the dune was not so promising as it showed a noisy signal. Furthermore there was no spatial correlation, as can be seen in figure 3.35 which depicts the variograms of the four regions. One aspect that might be interesting for further research is the comparison of this rather noisy signal with vegetation data (for example from photogrammetry). It could well be that the normal distribution of the signal corresponds with the vegetation, which in itself is a rather normal distribution.

3.3.6 Quality assessment

Resolution

The resolution of this measurement system can be divided into the spatial resolution, temporal resolution and the sensor resolution. The spatial resolution is the spatial interval between two measurements which is determined by a couple of things. First is the survey speed, second is the sampling rate. In the case of offshore surveying the speed is often around 3 m/s and with a sampling rate of 1 s, there will be a measurement every 3 m.

The sensor resolution is the smallest detectable particle which is often expressed as the 'full width at half maximum'. This is the width of the γ-ray peak in the spectrum at half of the highest point on the peak distribution *[61]*. For BGO this 'full width at half maximum' is around 3.3% which is the sensor resolution. This 3.3% is small compared to the error of the derived nuclide concentrations (which is 10%).

Directly related to the sensor resolution is the efficiency of the sensor. There are always particles that pass through the sensor which will not be detected. The percentage that will be scintillated is called the efficiency. It can also be defined as the 'probability that an emitted γ-ray will interact with the detector and produce a count' *[61]*.

It is not possible to quantify the effect of the sensor resolution and efficiency in the field because they both contribute (they have a combined effect) to a certain error in the data and a certain uncertainty.

Accuracy

Every measurement system has a certain accuracy or bias. The accuracy is the degree of closeness of a measured or calculated quantity to its actual (true) value. This accuracy is determined by measuring a known (true) radioactivity with the sensor in a controlled environment and calculate the offset. With this offset the calibration factors are determined which are used to compensate for this bias. One factor that can create such a bias is Radon gas trapped in the sensor housing. Radon is a decay product of Uranium that radiates γ-rays and can therefore result in higher radiation values than expected. When performing this calibration step, it is also possible to calculate the uncertainty of the measurements by calculating the spread around this 'true' value. In *[58]* the uncertainty of the sensor is found to be at maximum 10%.

There is a relation between the amount of photons that are used to determine the spectrum and the uncertainty of the spectrum; more photons per spectrum result in a lower uncertainty. Since the number of photons per second is rather constant, the integration time (which is selected manually) is the most important factor concerning the uncertainty. Medusa chooses to do the surveying relatively fast with a high sampling rate which results in a relatively large uncertainty of the nuclide concentration (order of magnitude of several procents), but resulting in a shorter surveying time and higher spatial resolution.

The average standard deviation of the nuclide concentration around the mean for every measurement is given for every nuclide in table 3.8. These standard deviations represent the 68.3% confidence interval around the measured value. It is based on the spectra and the consistency of the measurements within every epoch (within the integration time).

	K	Th	U
Onshore data (Bq/kg)	48.1	5.9	4.3
Offshore data (Bq/kg)	26.1	2.9	2.0

Table 3.8: Average standard deviation.

One thing that was curious about the dataset was the fact that all data seems to be rather normal distributed, except for the beach area. This is depicted in figure 3.38, in which it is clearly visible that the beach area does not fit to a normal distribution (skewness). The cause of this might be the fact that the wet areas have a small radiation intensity due to the absorption of the water present. But it could well be that the water currents in these wet areas cause that smaller material is deposited there. The resulting K-concentrations are given in figure 3.36, in which it is visible that the wet areas show a low K-concentration (and so a relatively large grain size).

Error budget

The error budget of the Medusa radioactivity probe is shown in table 3.9.

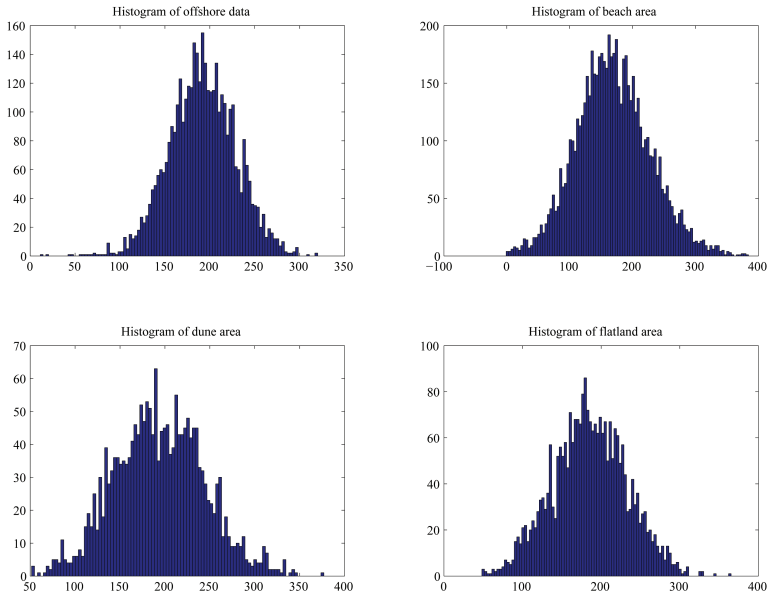

Figure 3.38: Histograms of the data from all four regions.

3.4 Single beam echo sounding

In the previous paragraphs, two techniques were discussed to measure the topography of the beach near Monster-Ter Heijde. Since morphological changes don't only occur on land but in the sea as well, it is necessary to also measure the near shore bathymetry. For this purpose, a fourth acquisition method is applied: single beam echo sounding.

3.4.1 Working principle

The single beam echo sounder (SBES) used for measuring is the SyQwest HydroBox [12]. The HydroBox includes a transducer with an opening angle of 8°, operating at a frequency of 200 kHz, which is able to measure the bathymetry in increments of 1 cm.

As with all echo sounders, the basic principle behind it is to measure the time it takes for a transmitted pulse to be reflected on the sea bottom and be received again at the point of transmission. To convert this time to depth, knowledge about the average sound speed in the water column is necessary. Although the HydroBox has an option to set the sound speed between 1400 and 1600 m/s, its value is not measured.

Instead of only a depth value, the HydroBox actually records the full waveform of the returned signal. However, this data is not useful, since the signal of the transducer is so strong that clipping occurs in the receiver. Manual adjustment of the emitted power is not possible either; hence just the depth value is used, given by the time of the first returned signal, multiplied with the sound speed as set in the HydroBox.

Factor influencing uncertainty	Order of magnitude	Possible correction methods	Resulting uncertainty
Radon and other radioactive matter inside the sensor housing	10 %	Calibration of the sensor in a controlled environment subjected to a known amount of radiation	Considerably small
Position of the sensor offshore	2.5 m	-	2.5 m
Position of the sensor onshore	1 m	Real time kinematic positioning	< 10 cm
Cosmic radiation	400,000 counts/hr	For airborne surveying: one sensor 'looking' up to allow for compensation	For land based purposes: considerably small
Temperature related spectral drift (offshore)	-	Temperature sensor inside housing allowing for spectral corrections	-
Temperature related spectral drift (onshore)	-	Using LEDs	-
Site specific radiation	-	FSA processing	Considerably small
Resulting nuclide concentration	-	-	< 10%

Table 3.9: Error budget for the Medusa radioactivity probe.

3.4.2 Acquisition platform

The platform used to measure the near shore bathymetry is a Yamaha VX Deluxe jet ski, provided by the chair of Hydraulic Engineering at TU Delft's Faculty of Civil Engineering and Geosciences (see figure 3.39).

The use of a jet ski as an acquisition platform is relatively new to bathymetric surveying, but has several advantages over traditional platforms:

- A jet ski has a large power-to-weight ratio, providing great acceleration for maneuvering to avoid danger of breaking waves in the surf zone.
- It has the ability to sail in very shallow water due to pump drive propulsion.
- It is light enough to be launched and retrieved from a trailer on the beach (four people are needed to carry the jet ski though), and is therefore useful to survey areas that are rather inaccessible and far from protected harbours.

On the jet ski, the SBES is mounted, as well as a GPS receiver and a portable computer, which logs all the measurements. Hydrographic software (HYPACK 2008 [13]) is installed on the computer to

Figure 3.39: SBES survey platform.

combine the echo sounding and GPS data, and to provide real-time output on a display screen for the driver.

3.4.3 Measurement campaign

The SBES measurements were done on 16 September 2008, during high tide in an attempt to cover as much of the intertidal area as possible. With a total survey time of 4 hours, an area of 800 by 1200 m was covered, as shown in figure 3.40.

Because most morphological changes occur in the cross-shore direction, the area was surveyed with most tracks perpendicular to the coast line, and fewer tracks along the shoreline. The distance between the cross-shore tracks is approximately 30 m. However, as can be seen in figure 3.40, further away from the coastline this distance becomes larger.

What can be seen in figure 3.40 as well, is that the actual measurement campaign has some differences with respect to the original plan. For example, the planned distance between the cross-shore tracks was 20 m and uniform for the whole survey area. In practice, it turned out that following exact tracks is rather difficult, hence the tracks became as shown in the figure.

Next to this, it was expected that the SBES survey would have some overlap with the land measurements in the intertidal area by surveying during high tide. However, in practice it turned out that the jet ski was unable take valid measurements past the low water line, which means there is no SBES data available for the intertidal area.

Another observation from figure 3.40 is that some tracks show gaps where no echo sounding data is available. This is likely caused by the jet ski sailing too fast, hence the HydroBox does not detect the reflected signal. Experience has shown that the maximum sailing speed in m/s is roughly equal to the water depth in meters. Along the shoreline there are also parts where data is missing because the water is too shallow (i.e. less than about 1 m).

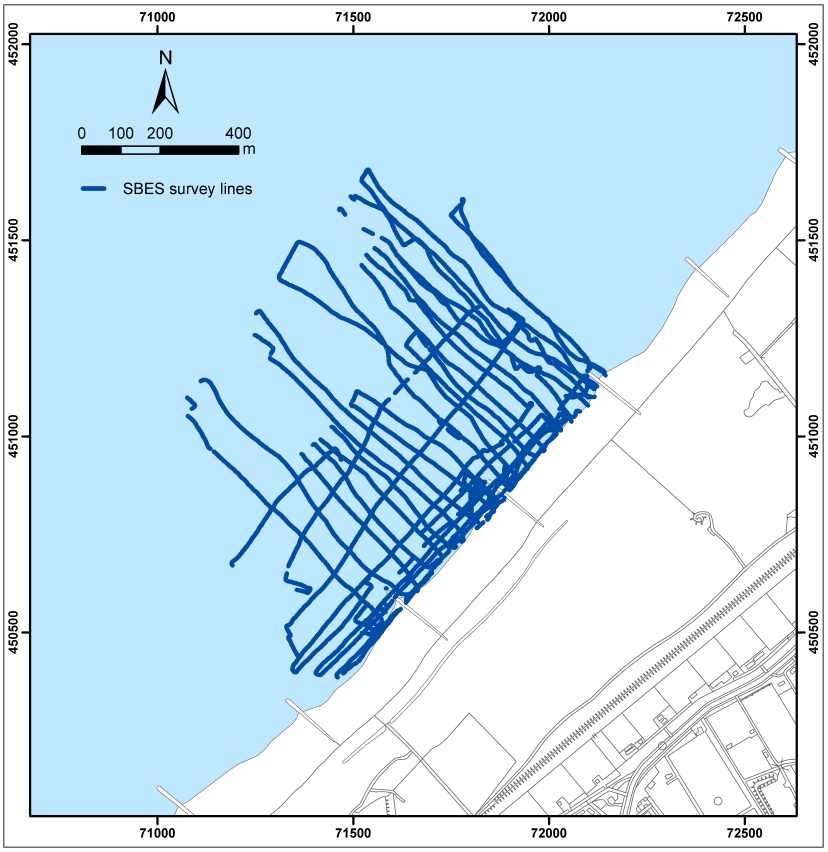

Figure 3.40: The jet ski survey tracks.

During the survey, georeferencing of all sounding data was done by real time kinematic GPS positioning, with positioning information received via a mobile Internet connection from a reference station in Hoek van Holland. For more details, see paragraph 3.5.

3.4.4 Data processing

After the survey, the data from the SBES and GPS receiver is processed with the primary objective of obtaining a bathymetry map. Before the real data processing can take place, some pre-processing of the data is necessary, e.g. to get the data in the right format to be used with other software than HYPACK.

As mentioned before, HYPACK combines the GPS and SBES data, which is considered to be the raw output. More specifically, HYPACK stores the GPS output in NMEA sentences, together with the depth values received from the HydroBox.

It is important to note here that the GPS position is logged only once a second, while the echo sounder emits a pulse ten times per second. Because these measurements are not fully synchronized, this causes a time offset, although both the HydroBox and the GPS receiver work in the same time frame.

For further data processing, the GPS and SBES data are extracted from the HYPACK file with a custom made Python [26] script. All GPS coordinates are transformed from ETRS89 to the Dutch

RD/NAP coordinate system using Coordinate Calculator v.4.1, freeware software from the Dutch Cadastre [7].

Next to this, there are some time periods when SBES data is recorded but no GPS position is available, which may be caused by having too few satellites in view or by a loss of connection to the GPS reference station. This SBES data is filtered out to make sure no GPS positions are extrapolated in the further processing.

The rest of the data processing is done using MATLAB [19]. As a first processing step, the vertical offset between the GPS antenna and the SBES transducer is corrected for. During the survey, the GPS height has been assumed to be the same as the transducer height, where it is in fact 113.6 cm higher. A correction is applied by simply subtracting the offset from the GPS height in the local coordinate system.

The second processing step is to correct for the actual sound speed. The sound speed has been fixed at 1500 m/s in the HydroBox, while during the survey it was likely different. Since no sound speed profiles have been measured during the survey, an attempt is made to derive the actual sound speed from the water temperature and salinity. This is possible using an empirical relation, for example the one of Mackenzie [67]:

$$\begin{aligned} c &= 1448.96 + 4.591T - 5.304 \cdot 10^{-2}T^2 + 2.374 \cdot 10^{-4}T^3 + 1.340(S-35) \\ &\quad + 1.630 \cdot 10^{-2}D + 1.675 \cdot 10^{-7}D^2 - 1.025 \cdot 10^{-2}T(S-35) \\ &\quad - 7.139 \cdot 10^{-13}TD^3 \end{aligned} \tag{3.3}$$

where T is the surface water temperature in °C, S the salinity in ppt and D the depth in meters.

According to Rijkswaterstaat [3], the water temperature during the survey was rather constant at 18 °C. The salinity at the time of measurement is expected to be between 34 and 35 ppt, as given by [20]. Since the sound speed is not very dependent on the salinity, either value can be used in equation 3.3. Besides, it is noted that the empirical sound speed hardly varies with depth in shallow water, and therefore results in a constant value of 1515 m/s for the time of the survey.

After the sound speed correction is applied, the GPS positions are interpolated to the times of the SBES measurements using cubic spline interpolation, to keep the periodic nature of the data (e.g. caused by waves). This removes the time offset between the GPS receiver and the SBES as mentioned earlier.

Next, the depths as measured by the SBES are subtracted from the GPS height (after the offset correction), to yield the water depth. The result of this is shown in figure 3.41.

Having applied all the necessary corrections, filtering and GPS interpolation, the data can be used to create a bathymetry map of the surveyed area. For this purpose, an interpolation of the estimated height values to a regular grid is needed. The method chosen for this interpolation is ordinary Kriging. With ordinary Kriging, the uncertainty in the individual observations is incorporated, as well as the spatial continuity of the measurements.

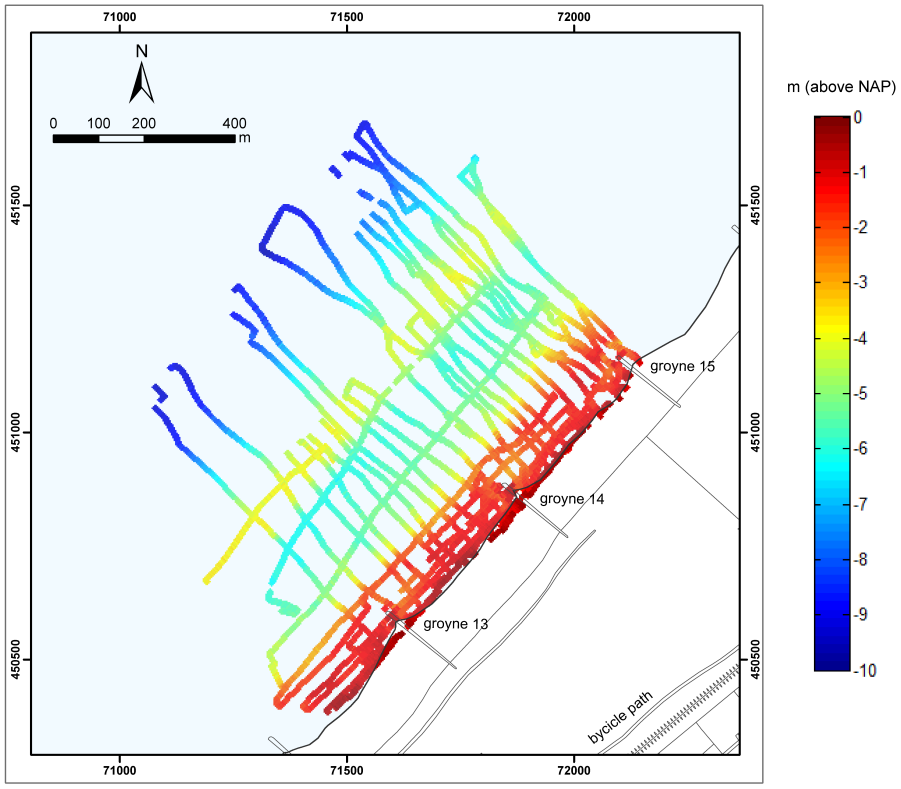

Figure 3.41: SBES measured height.

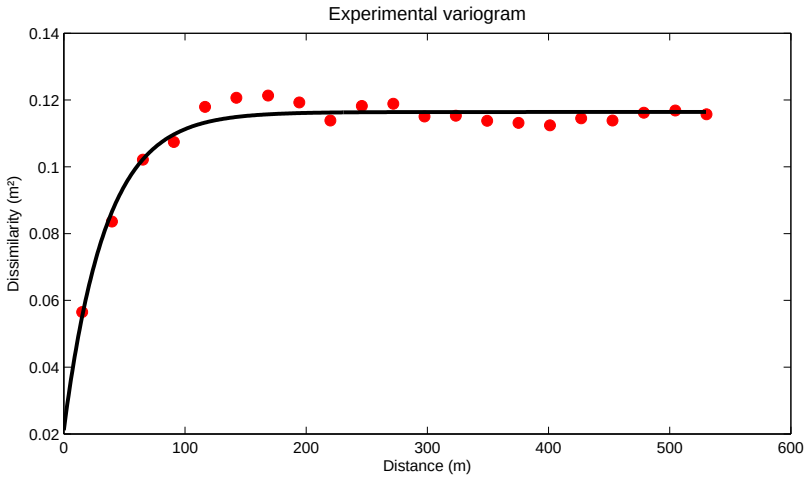

Figure 3.42: Experimental variogram with best function fit.

To do Kriging, an isotropic variogram needs to be constructed. This is done by first calculating the average cross-shore profile, by summing the height values in the along shore direction. Next, this profile is subtracted from the measured heights, resulting in a dataset of residuals that is second

order stationary. From this new dataset, dissimilarities between pairs of points are calculated. These dissimilarities are grouped by their distance, and the average of each group is computed. This average is shown by the red dots in figure 3.42.

Once the experimental variogram is constructed, a variogram model is fitted to it (see figure 3.42). The exponential model is found to give the best fit to the variogram, resulting in a nugget value of 0.02 cm^2 and a range of 102.8 m at which the dissimilarity becomes constant. The nugget gives valuable information about the standard deviation of the measurements, which will be discussed in the next section.

Now that the variogram function is known, it can be inverted into a covariance function, after which the ordinary Kriging system can be constructed. Solving this system for the nearest 500 points in a 1 by 1 m grid results in a bathymetry map and an estimate of the corresponding standard deviation (see figures 3.43 and 3.44).

3.4.5 Results

The bathymetry map obtained by ordinary Kriging is shown in figure 3.43. Note that in the figure some interesting features are visible, like the three groynes and their scour holes.

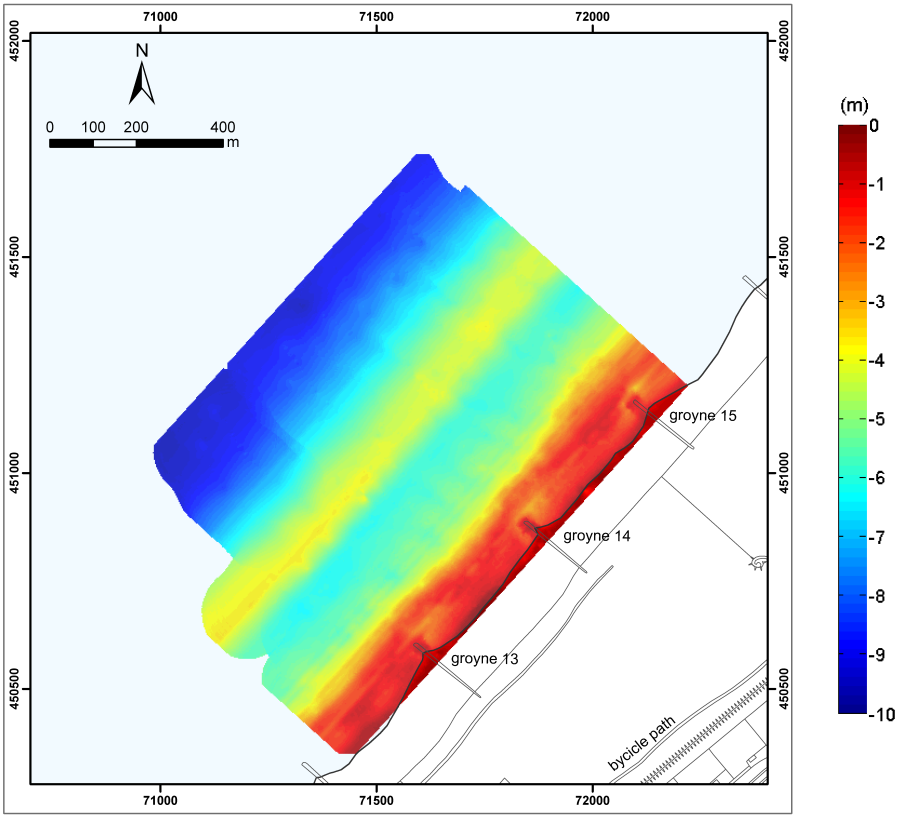

Figure 3.43: Result of ordinary Kriging.

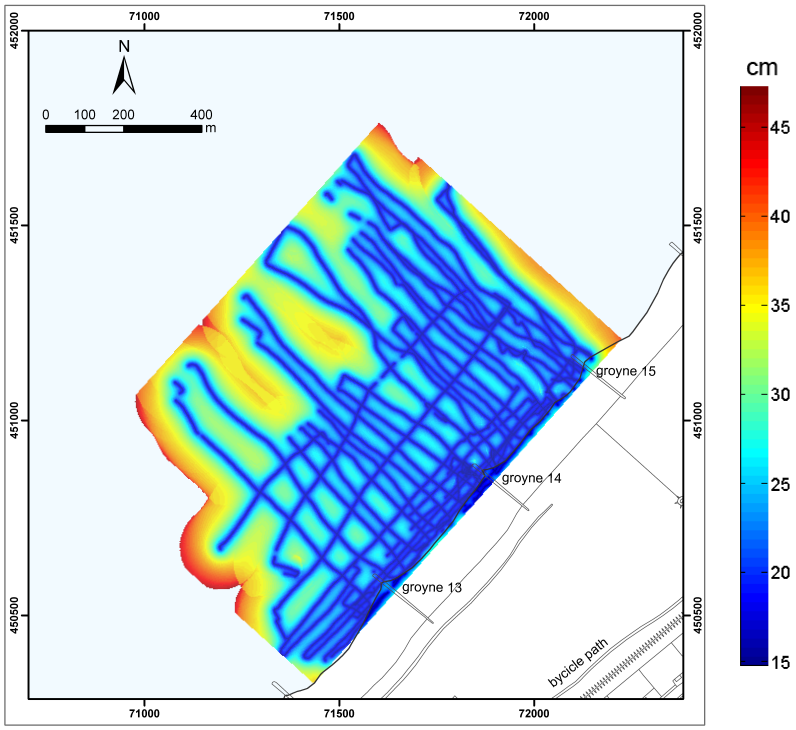

Figure 3.44: Ordinary Kriging standard deviation.

An estimate of the standard deviation corresponding to the ordinary Kriging result is shown in figure 3.44. Note that the error is smallest near the sailed tracks, and that the uncertainty grows larger when moving away from the tracks, especially at parts where the depth values are extrapolated.

3.4.6 Quality assessment

In the previous sections, the data processing steps were discussed that eventually resulted in a bathymetry map. In this section, the quality of the bathymetry map and the SBES measurements itself will be assessed.

Resolution

The average spatial resolution or distance between the SBES measurements is 30 m in the along shore direction and 25 cm in the across-shore direction. The big difference in resolution arises from the fact that most tracks have been sailed in the across-shore direction, and that the distance between two consecutive measurements is much smaller than the distance between the tracks.

However, since most height differences occur in the across-shore direction, it is still possible to reasonably interpolate the data to a 1 by 1 m grid, as shown in the previous sub paragraph.

Precision

Regarding the precision of the SBES measurements, it was already said that the variogram function provides information about the standard deviation. More precisely, the nugget value corresponds to the variance of the depth values, i.e. the standard deviation is the square root of the nugget. In this case, the standard deviation is found to be 14.5 cm.

With this number, it is possible to calculate the confidence intervals of the observations, as shown in figure 3.45. This figure is interpreted as follows: suppose that exactly the same spot on the sea floor is measured many times under the same (average) conditions as during the survey, then 90% of the recorded depth values is expected to be within 24 cm of the mean value. This mean value can differ from the true value though, because of a systematic error or bias.

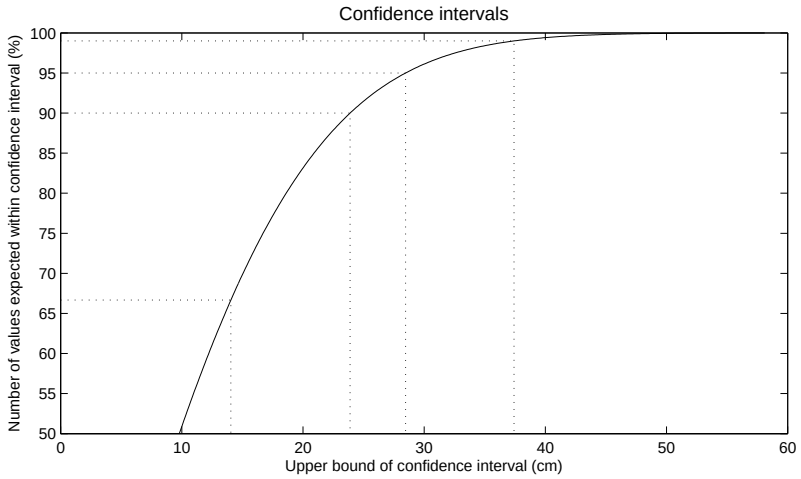

Figure 3.45: Confidence intervals of the observations.

Apart from the SBES measurements itself, the precision of the bathymetry map can be assessed. Figure 3.44 showed what standard deviation of the measurements corresponds to the result of ordinary Kriging, but this does not say much about the variance of the bathymetry map itself. For that purpose, it is necessary to look at the difference of the ordinary Kriging result with respect to the individual measurements. In this case, that is done by subtracting the measurements from the Kriging interpolation and constructing a variogram for the residuals (see figure 3.46).

As can be seen in figure 3.46, the variogram shows mostly a nugget component corresponding to a standard deviation of 7.3 cm. This can be interpreted as being the standard deviation of the bathymetry map. However, it is also visible that the depth values of points close to each other appear to be somewhat more random. This randomness has been found to decrease with the number of points used for Kriging and is therefore considered to be a Kriging artifact rather than a property of the dataset.

Besides the variogram, the residuals have been averaged in a regular grid to see if there is any spatially dependent signal left. The result is shown in figure 3.47. From this figure, it is concluded that there is no clear signal present, which justifies the use of an isotropic variogram as mentioned in the part on data processing.

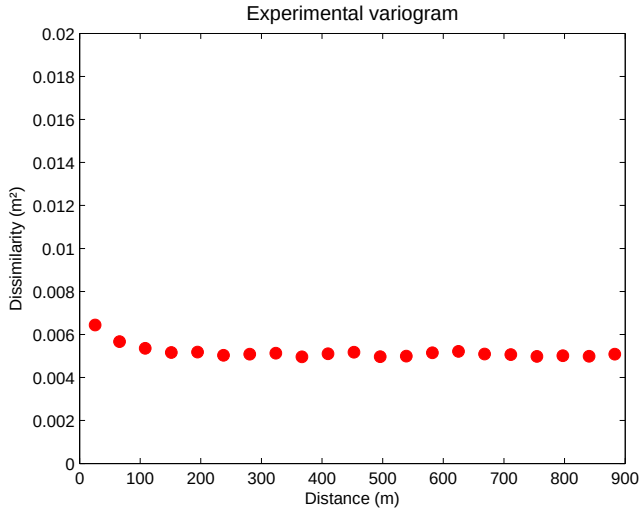

Figure 3.46: Experimental variogram for the Kriging residuals.

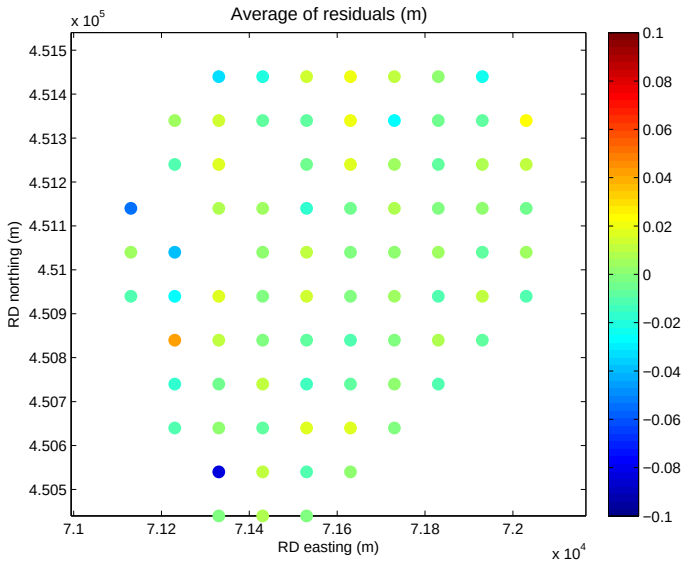

Figure 3.47: Kriging residuals averaged in a regular grid.

One major drawback of Kriging is though, that local observations do not influence the residual variance, thus high local variability in the water depth does not lead to a high local standard deviation for the bathymetry map obtained. More specifically, the standard deviation of the bathymetry map is found to be 7.3 cm everywhere, even when it is expected that there is a relation between this standard deviation and for example the water depth.

With this in mind, an attempt has been made to relate the standard deviation of the SBES measurements to several parameters, like the water depth, sailing speed, sailing direction and rate of turn. A big problem encountered with this assessment, is that the measurement conditions were not the same for the whole survey area. For example, there is a clear relation between the sailing speed and the water depth (i.e. over deeper water the jet ski sailed faster), hence the parameters of interest are correlated. Something similar holds for the sailing direction, because the cross-shore tracks are influenced by changing topography, while the along shore tracks are not.

Therefore, to find the relation between the survey parameters and the standard deviation, a different dataset is needed, i.e. one in which the same area is sailed many times and where only one parameter is changed at a time.

Error budget

Next to quantifying the precision of the SBES measurements and the bathymetry map, it is important to look at the possible causes of the standard deviations given before. This is because this information provides clues on how future surveys might be improved.

For this purpose, it is necessary to make a list of all sources contributing to an error in the depth value. All sources that have been identified are given in table 3.10.

Factor influencing uncertainty	Order of magnitude	Possible correction methods	Resulting (vertical) uncertainty
Platform attitude	Dependent on bathymetry, < 20 cm	Use orientation sensor with some assumptions about terrain	cm
Opening angle or footprint size	Dependent on bathymetry, < 15 cm	Make the opening angle smaller	cm
GPS accuracy with 7 km baseline (1σ)	3.4 cm	Use a smaller baseline	2 cm
Obstructions/objects at seafloor	Dependent on error nature	Filter outliers	cm
Sound speed in the water column	< 10 cm	Measure the sound speed (e.g. indirectly via pressure, temperature and salinity)	mm
Vertical offset between the SBES and GPS antenna	113.6 cm	Measure the offset	mm

Table 3.10: Error budget for single beam echo sounding.

From table 3.10, it becomes clear that the opening angle of the SBES transducer and the platform attitude contribute significantly to the standard deviation, because they can both not be corrected for. This is mainly due to the fact that the jet ski is not equipped with an attitude or orientation sensor.

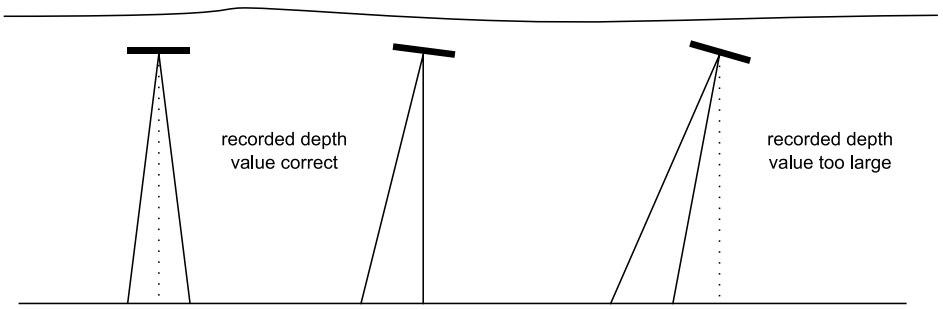

Figure 3.48: Recorded depth value for different platform orientations.

A further explanation of this error is provided in figure 3.48. In this figure, it can be seen that when the attitude angle of the jet ski exceeds half the opening angle, the depth of the water will be overestimated. Otherwise, the first signal return from the seafloor will still correspond to the correct water depth, i.e. for the depth error Δd it holds:

$$\Delta d = \begin{cases} 0 & \text{for } \phi \leq 0.5\theta \\ \frac{d}{cos(\phi - 0.5\theta)} - d & \text{otherwise} \end{cases} \tag{3.4}$$

where d is the water depth, θ the opening angle and ϕ the attitude angle.

For a water depth of 5 m, an opening angle of 8° and a tilt of 10°, equation 3.4 results in an error of 2.8 cm. For comparison, an attitude angle of 15 degrees in 10 m deep water results in an error of 19 cm, which is about the maximum expected error.

Note that in equation 3.4 the assumption is made that the seafloor is flat. When the seafloor has a slope, the resulting error gets either larger or smaller, depending on to which side the jet ski tilts. Apart from this, a very small part of the error (< 1 cm) will be compensated for by the tilt of the GPS antenna.

What is even more important though, is that all attitude angles larger than half the opening angle result in overestimating the water depth. Hence, it is expected the water depth gets biased when the jet ski is not always close to horizontal in the water.

As a side note, solving for this specific problem might favour using a transducer with a larger opening angle. This is however not considered to be a solution, because then the error induced by the real sea floor not being flat gets larger, and the net error will stay the same.

Apart from the opening angle and platform attitude, a third contributor to the standard deviation is the accuracy of the GPS measurements or the georeferencing in general. In table 3.10 it was already

listed that the expected standard deviation for the GPS measurements is 3.4 cm for the known baseline length.

Some additional information can be gathered by plotting (part of) the SBES measurements against time, see figure 3.49. The red line in the figure gives the moving average of 50 measurements, indicating the bathymetry. When subtracting this moving average from the data and zooming in a bit, the signal shown in figure 3.50 results.

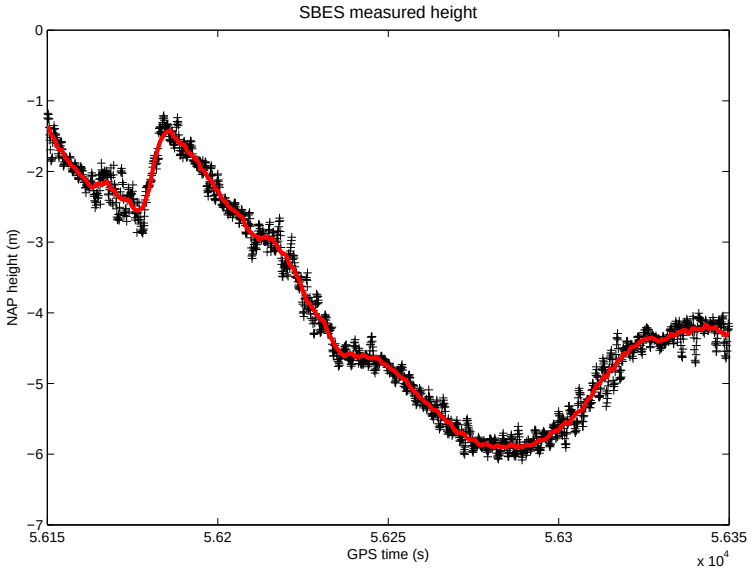

Figure 3.49: SBES measurements versus time.

In figure 3.50, it is clear that there is some periodic signal left, with a period of 3 to 4 seconds. Both this period and the amplitude correspond with the surface waves on the water, as measured by Rijkswaterstaat [3]. Although the surface waves appear to be resolvable from the GPS measurements, it is likely that with only measuring the height once a second, it is not possible to fully reconstruct the actual shape of the waves. Hence, an additional georeferencing error is expected. The exact size of this error is hard to assess though, without knowledge of the real height of the waves.

The fourth error source listed in table 3.10 is of a somewhat different nature, and is caused by objects at the seafloor. For example, when a brick is present at the sea floor, this momentarily reduces the measured depth and therefore induces an error with respect to the surface of interest. This is purely theoretic though, since in reality there won't be much objects present at the bottom, and indeed none of these outliers have been detected in the dataset.

The rest of the error sources mentioned in the table are not so much related to the standard deviation of the measurements, but more to the systematic error or bias. It was already said that an attitude angle of the jet ski can only increase the measured water depth, thus resulting in a bias. Other factors that can cause a bias in the measured water depth are the sound speed in the water column and insufficient knowledge about the vertical offset between the transducer and GPS antenna.

For example, suppose that no correction was made for the sound speed, i.e. all depth values are calculated for a sound speed of 1500 m/s instead of 1515 m/s (assuming the latter is correct). Then for a water depth of 10 m, this results in a bias of

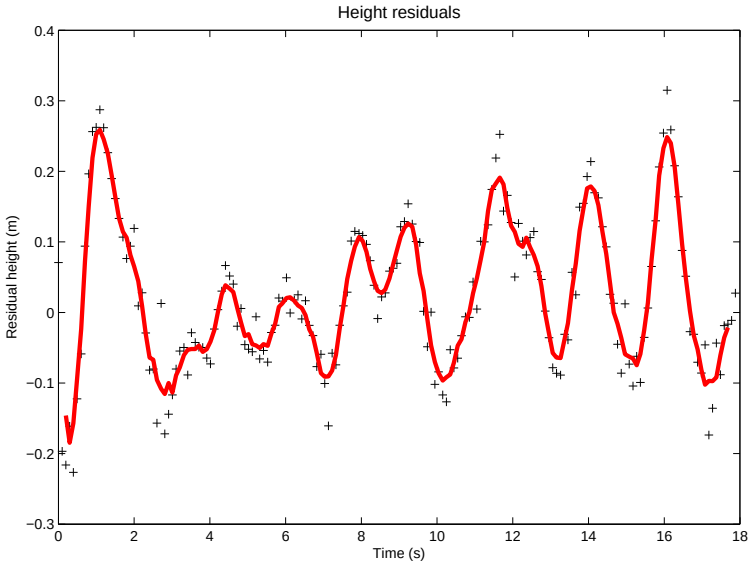

Figure 3.50: Residuals of SBES measurements.

$$10 - 10 \cdot \frac{1515}{1500} = -0.10 \text{ m}$$

Thus in this case, the water depth would be underestimated by 10 cm. This underlines the importance of having a reliable sound speed profile for the time of measurement, especially when producing a bathymetry map.

Anyhow, it is hard to give an estimate of the bias for the acquired data set, because no sufficient data on the true bathymetry is available. Some attempt has been made to assess the systematic error by comparing the SBES measurements to the JARKUS profiles [15] and a GPS 'backpack walk' performed by the jet ski drivers, but so far without any meaningful result.

Moreover, in the end there is not so much interest in the bathymetry itself, but more in the change of bathymetric features over time. In that case, only the variability of the bias is important, because if the bias would always be the same this would not influence the difference between datasets acquired at a different time instance. Nevertheless, some variation in the bias is expected, for example because of a variation in sound speed that cannot perfectly be corrected for.

3.5 GPS

The last measurement technique used in this project is GPS. As has been hinted at in the previous paragraphs, the main objective of having GPS measurements in this project is to allow georeferencing of the measurements of other survey platforms.

Beside the main objective, GPS measurements are also used to measure the profile of some parts of the beach and dunes. The purpose is to give an additional dataset and fill the gaps of the other measurement techniques, since not all parts of the planned survey area can be covered. For instance, some

parts of the beach remain wet during low tide, and are therefore not accessible with photogrammetry or terrestrial laser scanning. However, these areas are accessible with GPS.

3.5.1 Working principle

The main principle behind positioning with GPS is triangulation in space, based on the measurement of ranges between the receiver and the satellites. By simultaneously measuring ranges to three different satellites (of which the positions are known), the position of the receiver can be derived from the intersection between the three distances. The fundamental GPS observable is signal travel time between satellite and receiver. However, the receiver clock may introduce error, and this error must be estimated. Therefore a range to a fourth satellite must be observed to provide a unique solution.

GPS provides two types of measurements, code phase and carrier phase. Code phase measurement basically measures the difference between signal reception time, as determined by the receiver clock, and the transmission time at the satellite, as marked on the signal. Carrier phase measurement basically measures the difference between the phase of the receiver-generated carrier signal and the carrier received from a satellite at the instant of the measurement. The carrier phase observable contains the ambiguity of the number of full phase cycles between the receiver and the satellite at the starting epoch, known as the integer ambiguity.

There are two GPS positioning methods used during this project, differential GPS (DGPS) and real time kinematic GPS (RTK-GPS). Both DGPS and RTK-GPS require simultaneous observations at two locations. The receiver with its antenna at the reference point (i.e. a point with known position) is usually referred to as the reference receiver or base station. The second receiver, whose antenna position is to be determined, is called the mobile receiver or rover. Using these methods, the position of the rover is acquired in real time.

The basic idea behind DGPS is to take advantage of the fact that the errors associated with GPS positioning (i.e. satellite clock, ephemeris and atmospheric propagation) are similar for users separated up to several hundreds of kilometers, and these errors vary slowly with time. If the position of a GPS receiver is known, the combined effect of the errors can be estimated for each satellite. Then these error estimates can be made available to the GPS users in the area (i.e. the rover receivers) to mitigate errors and improve the quality of the position estimates. Such correction can be made in real time using a radio link [72]. While this approach is usable for both code and carrier phase measurement, DGPS is commonly used for code measurements, which require a minimum of four satellites to be tracked.

RTK-GPS, on the other hand, uses carrier phase observations. In RTK mode, the measurements at the reference receiver are transmitted to the rover via a radio link. A key feature required by RTK is the ability to estimate the integer ambiguities while the rover is in motion [72]. This method allows the rover receiver to initialize and resolve the ambiguity integers without static initialization. RTK requires the use of dual frequency L1 & L2 GPS observations [56]. A minimum of five satellites should be tracked with this method.

3.5.2 Acquisition platform

For the single beam echo sounding, the jet ski is equipped with a GPS receiver. The GPS receiver is a Septentrio PolaRx2e high-end dual frequency receiver [33], which tracks the GPS L1 & L2 carrier

frequencies. The receiver on its own does not have a display unit, but all monitoring (and logging) is done with the on-board computer. For positioning, the RTK positioning method is used. The position corrections are received via the Internet, with access provided by a 3G High-Speed Downlink Packet Access (HSDPA) data card from KPN installed in the computer. The corrections are downloaded in RTCM 2.1 standard message format, from a reference station in Hoek van Holland, which is approximately 7 km from the survey site [18]. The raw GPS data is also logged in the receiver, to allow post processing if needed.

For the Medusa radioactivity probe, both the onshore and offshore measurement platforms are equipped with GPS receivers. Georeferencing is done using the DGPS method. For the offshore measurements corrections are received from EGNOS satellites, while the onshore measurements received corrections from a reference station in Hoek van Holland.

For the land measurements (i.e. terrestrial laser scanning and photogrammetry), georeferencing of the reference points has been done with GPS measurements using the RTK method. The equipment used are two Leica SR530 receivers [29]. These are dual frequency geodetic GPS receivers with RTK capability, with detachable radio modems to allow data communication between a base station and rover.

The remainder of this paragraph will only discuss the GPS measurements for the land measurements and the beach profiling.

3.5.3 Measurement campaign

During the measurement week (15 to 19 September 2008), the base station was set at the bungalow at the camping site approximately 800 m from the survey area. To maintain the same base station position throughout the campaign, it was decided to place the antenna on the bungalow's roof, mounted on a horizontal platform (figure 3.51a). The receiver itself is placed inside the bungalow. This set-up was meant to avoid risks of external disturbance, as well as allowing the GPS receiver to have continuous electrical supply, which increases the measurement duration. During the additional measurement campaign (29 September 2008), the bungalow was no longer in use. Instead the base station was placed on top of one of the dunes at the survey area.

For the rover, the GPS antenna is mounted on a 2 m pole, connected to the receiver in a backpack, allowing full mobility during the survey (figure 3.51b).

To have a quality check of the measured positions, a reference point was measured with the rover. This is the *kernnetpunt* in Kijkduin, which is a reference point maintained by the Dutch Cadastre.

As mentioned earlier, control points for photogrammetry and terrestrial laser scanning have been measured. For photogrammetry, the ground control points have been measured, while for terrestrial laser scanning, the positions of the reference spheres have been measured.

Next to this, profiles of parts of the survey area have been measured. Two cross section profiles extending from the beach, over the dunes, ending at the edge of the grass area have been measured, as can be seen in figure 3.52. Distances between each point are between 1 and 3 m, depending on the variability of the terrain. Over the grass area the measurements are sparser as the area is much more flat. Measurements with denser grid have been done over the groyne and the wet area of the beach during low tide, as can be seen in figure 3.53.

(a) GPS base station. (b) GPS rover.

Figure 3.51: GPS base station and rover.

The RTK method used in this project requires the rover to stop for a few seconds to measure the position of the point of interest, hence the data stored are positions per point, not per epoch. With this method measurements of control points are done fast, i.e. each point can be measured in few seconds. More time is spent on moving between the points and waiting for the control points to be set up. Beach profiling, on the other hand, takes far more time. One profile from the beach to the edge of the grass area takes about one hour. Based on the beach area that was measured with GPS, it is estimated that it takes about 2.5 hours to measure a 7200 m^2 area with a 4 by 4 m grid.

3.5.4 Data processing

Since the base station position is not known, it has to be calculated in post processing. This is done by differencing between the base station and a reference point with known coordinates and logged observations. The reference point used here is the Delft reference point, which is a permanent GNSS reference station, maintained by DEOS - TU Delft [11]. Coordinates of these reference points are given in table 3.11.

Reference point	Coordinates in ETRS89 (latitude, longitude, height)	Coordinates in RD/NAP (X, Y, h)
Delft [2]	N51° 59’ 10.02219" E4° 23’ 15.30302" 74.369 m	86334.425 m 444663.460 m 30.836 m
Kijkduin	N52° 03’ 38.7696” E4° 12’ 43.5042” 46.69 m	74414.10 m 453148.77 m 3.29 m

Table 3.11: Reference point coordinates.

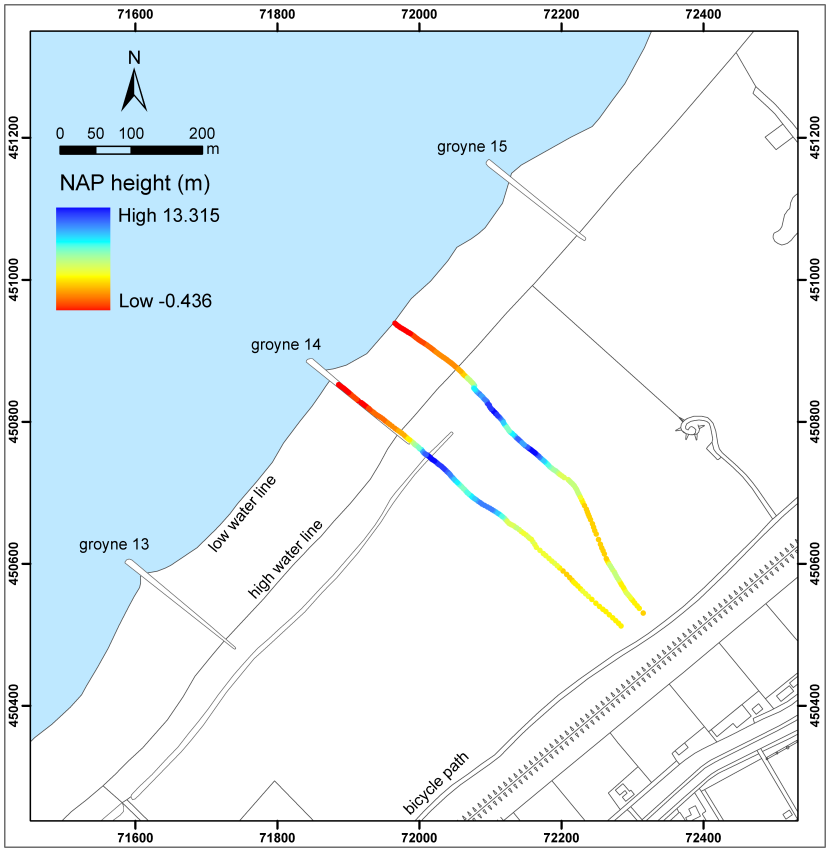

Figure 3.52: Cross section profiles.

The software used for data processing is Trimble Geomatics Office [28]. Since this is not the default software for Leica receivers, all data must first be converted to RINEX format before processing. This was done with a program called teqc.exe, which is a freeware converter [27].

As mentioned earlier, post processing is required to calculate the position of base station, by differencing between the base station and a reference point. For this purpose, logged observations of both stations are needed. During the campaign, the base station logged 4 to 6 hours of observations everyday, with 10 s update rate. Observation data of the Delft reference station are available from [11] and for this purpose a 10 s update rate data was downloaded and used.

Once all data are converted to RINEX format, the base station position is calculated for each day. This is done due to the uncertainty whether the base station antenna position shifted during the five observation days, since the custom made platform used to mount the antenna was not fixed to the roof. Furthermore, there is enough data for each day to calculate a daily solution.

After the daily solutions of the base station are acquired, the differences with the logged base station coordinate in the rover are calculated. This is necessary since the logged rover coordinates are referred to the base station coordinates, which at the time of survey were simply the navigation solution, and thus an offset with the real position is expected. The calculated differences are then used to correct the rover coordinates.

Note that at this point the coordinates for both base station and rover positions are in ETRS89, an

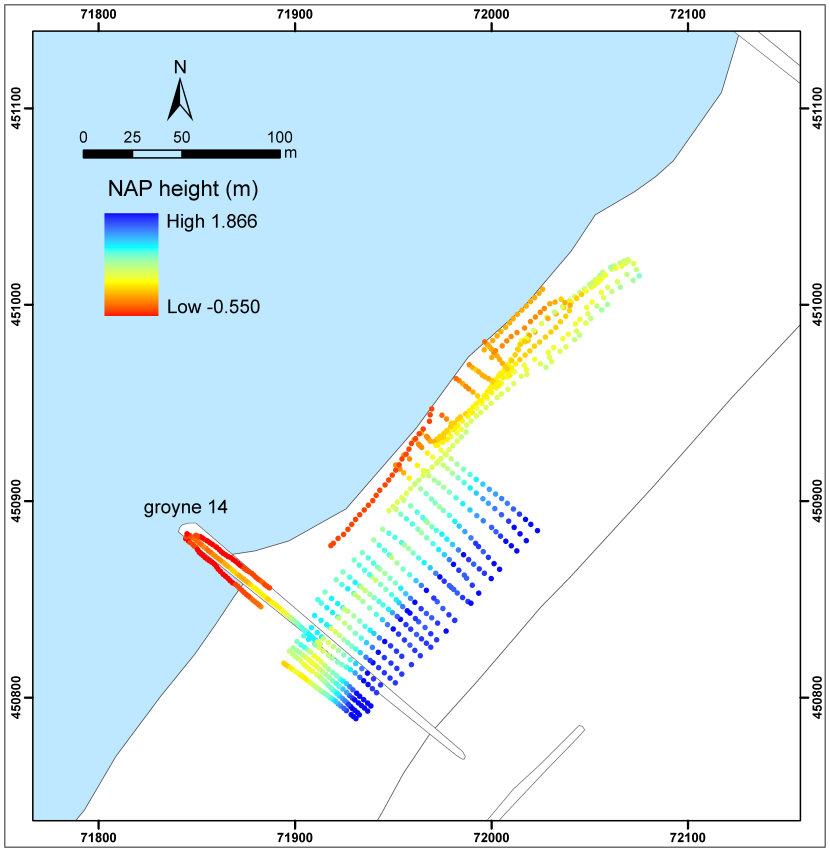

Figure 3.53: GPS measurements over the groyne and the wet area of the beach.

Earth fixed reference system. For further data presentation and data fusion, they are transformed into RD/NAP, the Dutch coordinate system. This is done using Coordinate Calculator v.4.1, freeware software from the Dutch Cadastre [7].

3.5.5 Results

The results of the GPS measurements are horizontal and vertical positions of the control points of the photogrammetry and terrestrial laser scanning measurements. Next, the positions of the profile points are also acquired, as previously shown in figure 3.52 and 3.53. All these positions are given in the Dutch RD/NAP coordinate system.

3.5.6 Quality assessment

Resolution

The spatial resolution of the GPS measurements done in this project is completely dependent on the distance between the measured points. For instance for the cross section profiles the distance between two consecutive points is between 1 and 3 m, while for the wet area, the distances are between 1 and 4 meter.

Accuracy

Using the RTK method, the baseline accuracy that can be expected is 1 cm + 1 ppm for horizontal position and 2 cm + 2 ppm for height [29].

The accuracy of the rover positions is also dependent on the accuracy of the base station position. As mentioned earlier, the base station position is calculated in post processing by relative positioning to the Delft reference station. A typical accuracy for such static survey with 10-50 km baseline is 0.5 cm + 1 ppm for horizontal position [56] and 1 cm + 2 ppm for height.

Error budget

A problem which became apparent after post processing the base station data is that the antenna on the bungalow roof is not very stable. The computed daily solution for the five days shows some differences in the order of a few cm, as shown in table 3.12.

Day	X (m)	Y (m)	Z (m)
15 September	3921647.397	286168.864	5005120.139
16 September	3921647.386	286168.862	5005120.126
17 September	3921647.382	286168.863	5005120.123
18 September	3921647.400	286168.866	5005120.140
19 September	3921647.391	286168.863	5005120.136

Table 3.12: Daily base station solutions in ETRS89.

Next to this the variability over the observation period can be seen in figure 3.54. There is no clear trend over the five observation days. However, a slight change is visible in the vertical direction, particularly on the fifth day.

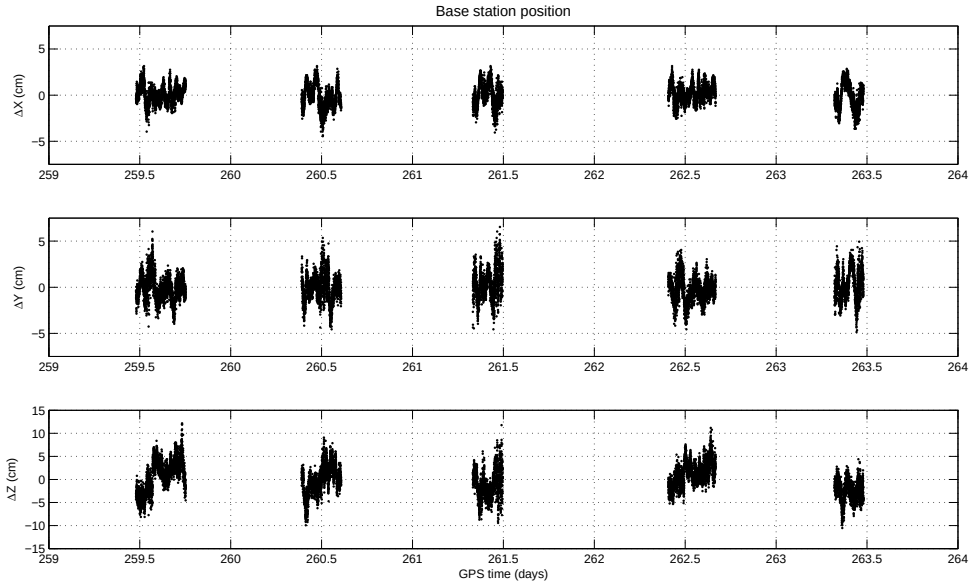

Figure 3.54: Base station observation variability.

4 Data merging and comparison

The results of the individual data acquisition methods have been shown in the previous chapter. However for the coastal monitoring purpose, it is important to have one dataset which represents the whole area rather then separate datasets. With this in mind, an attempt has been made to combine the collected datasets. Due to the lack of overlap between the on shore and offshore measurements, the data merging has been done separately for the onshore and offshore datasets.

Next to this, a comparison has been made between the onshore datasets with an existing dataset of the survey area, which is the airborne laser scanning data collected by Rijkswaterstaat between March and July 2008. Further, another potential use of the collected photogrammetry dataset is described.

4.1 Onshore datasets

The two main techniques of land measurements in the project are the terrestrial laser scanning (TLS) and the kite aerial photogrammetry (KAP). An overlap between the measurement area of the two techniques exists on the beach part of the survey area. Datasets from the Leica laser scanner and the high resolution kite aerial photogrammetry (KAP) over this area are used for the data merging.

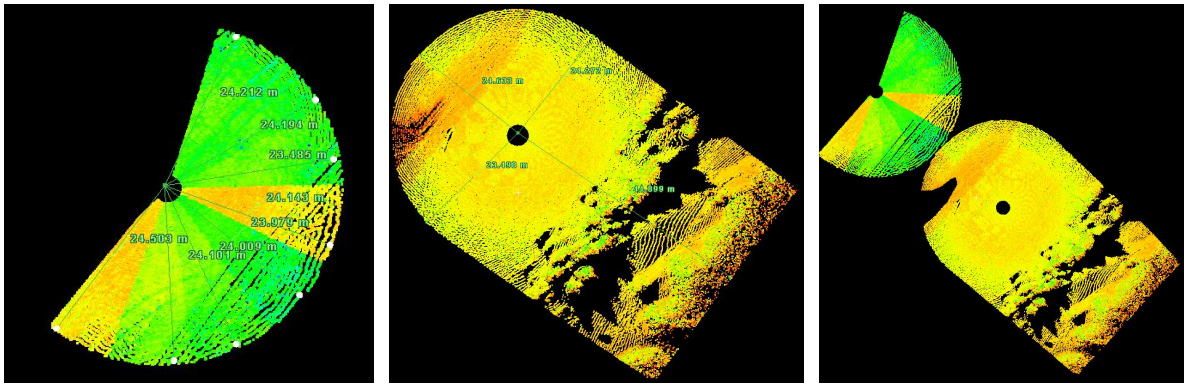

(a) First scan. (b) Second scan. (c) Combination of two scans.

Figure 4.1: Laser scan datasets.

Two measurements using the Leica scanner have been performed within the survey area; the locations and area of the two scans are shown in figure 4.1. The edges of the point clouds have been cut to obtain better comparison with a higher accuracy. The range of the first part scan (the green part) is about 24 m. The yellow part represents the results of the second scan, with the radius of 24 m as well. The distance between the scanner and the middle of the straight edge is about 45 m.

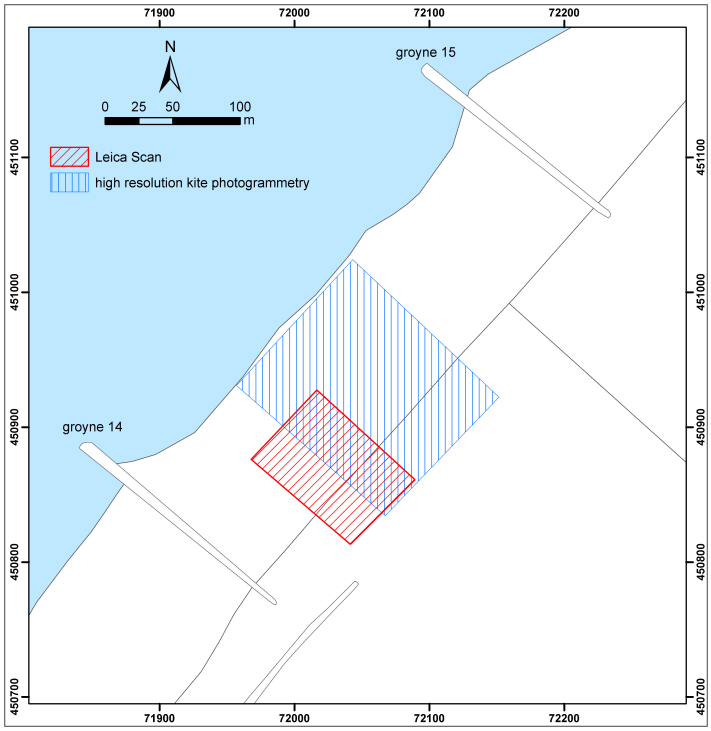

Figure 4.2: Area covered by kite aerial photogrammetry and terrestrial laser scanning.

After registration, georeferencing and removing noise, the coordinates of the points are exported into MATLAB for comparison with the KAP data.

Figure 4.2 shows the areas of the two different acquisition platforms, in which the overlapping area can be seen clearly. A decision about which data is best used has to be made in this overlapping area. Therefore the difference between the two datasets in this overlapping area is evaluated.

Figure 4.3 shows that there are some bigger differences (about 30 to 40 cm) between TLS and KAP data at the part before the dunes. The bad registration and georeferencing (with about 20 cm error) of both the TLS data and the KAP data is one of the reasons for the large differences. Furthermore, the line of sight of the scanners to the terrain surface is partly blocked. Due to these obstructions, the terrain lying behind is not visible in the dataset. Of course, the noise in the KAP model also caused the big difference. The differences seem too smooth to be caused by inaccuracies, therefore a systematical error in one of the two datasets is expected.

To asses data quality of both datasets, values of both datasets are compared with a GPS point in the area where the big difference occurs. In figure 4.3, two photogrammetry ground control points are visible in the overlapping area. The ground control point in the blue area lies in the area with the biggest difference between TLS and KAP data. The height of this ground control point is checked in the GPS data. The difference between the GPS height and the laser scanning height is about three cm, while the height difference between the GPS height and the photogrammetry height is about 30 cm, thus the TLS data seems more accurate in this area. This is probably due to the fact that this overlapping area is near the edge of the photogrammetry block, where distortions are more common. Therefore it is recommended that when a large area of beach is to be measured, aerial photogrammetry is used, but the area near the edges of the photogrammetry block can also be measured with a laser scanner to eliminate these distortions.

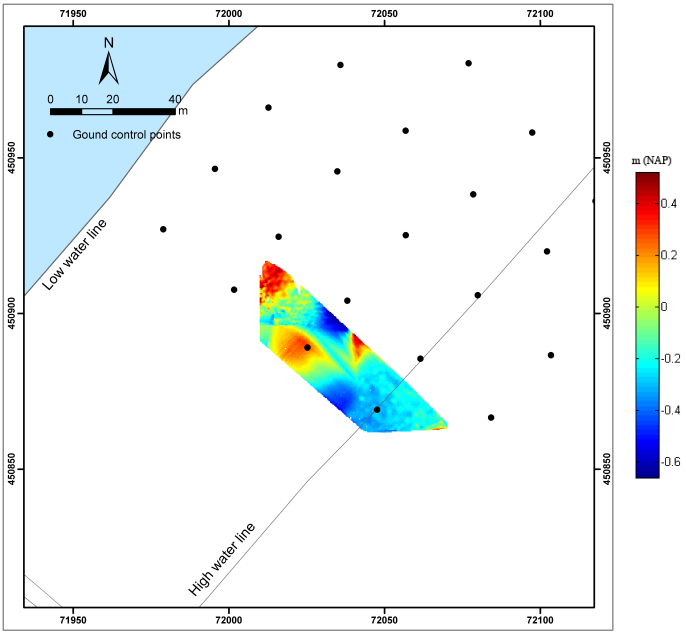

Figure 4.3: Differences between the datasets created with KAP and TLS. The black stars are photogrammetry ground control points.

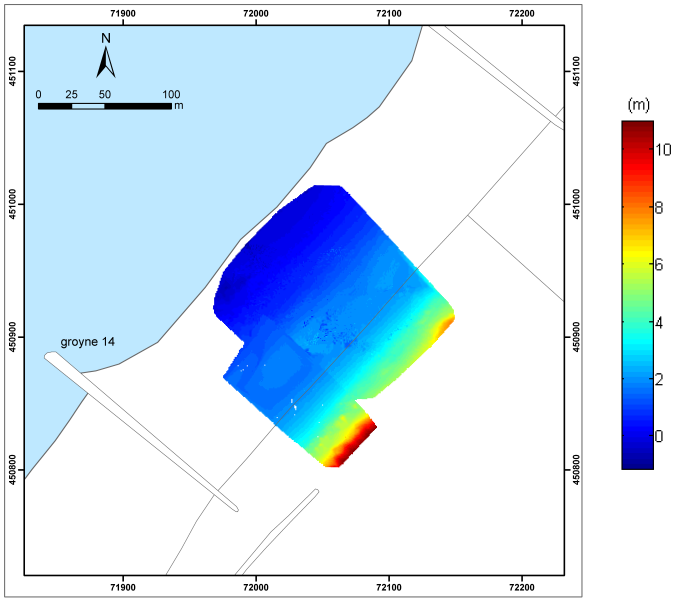

Figure 4.4: Result of kite aerial photogrammetry and terrestrial laser scanning data merging.

The result of the merging of the two datasets is shown in figure 4.4. The merging is done by making one large grid that covers both the photogrammetry and the laser scanning data. The actual data is interpolated over this grid. In the area with overlap between the two datasets, the data of the terrestrial laser scanning was chosen, since the data seems more accurate.

The merging shows that both the photogrammetry and the TLS data show the same trend. On the edge

between the photogrammetry data and laser scanning data a slight jump in height is visible, which is probably due to inaccuracies, primarily caused by the photogrammetry data.

4.1.1 Data comparison

A couple of months prior to the project, an airborne laser scanning campaign was done by Rijkswaterstaat. The resulting dataset of the Monster-Ter Heijde area has been used to make a comparison with both the KAP dataset and the TLS scanning dataset.

The difference between the KAP data and the airborne laser scanning data is shown in figure 4.5. In the left figure of figure 4.5, the whole kite aerial photogrammetry area is visible, and in the right the picture is zoomed in to the area also covered by the Leica laser scanner. This is done for a comparison.

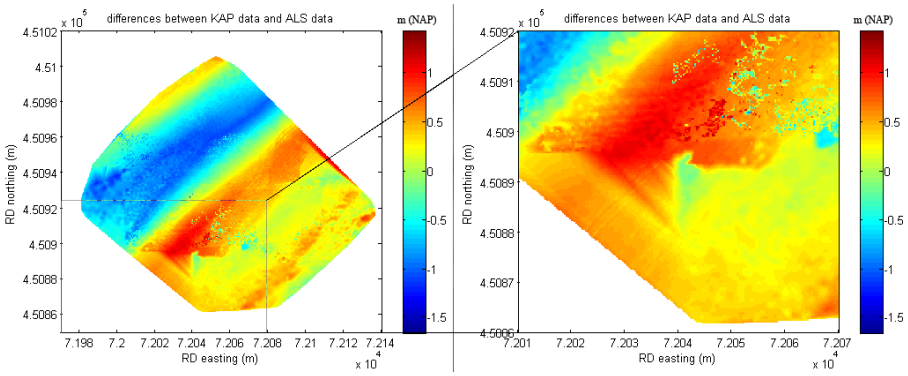

Figure 4.5: Differences between the kite aerial photogrammetry data and the airborne laser scanning data.

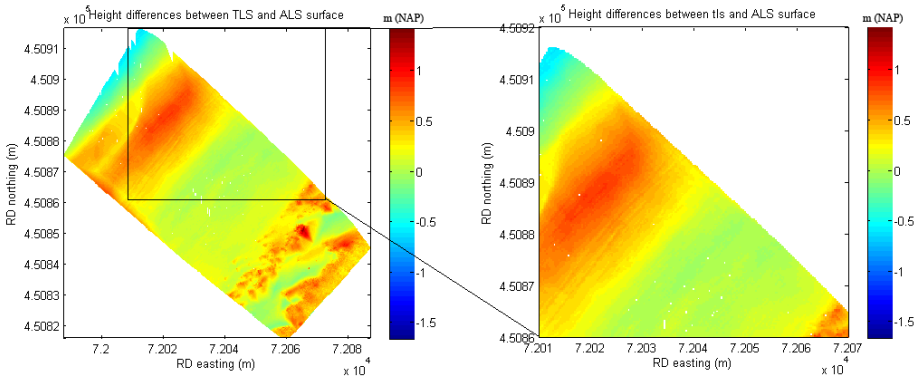

Figure 4.6: Differences between the terrestrial laser scanning data and the airborne laser scanning data.

In figure 4.6 the differences between the TLS data and the airborne laser scanning (ALS) data are shown. Again, to the left the whole TLS area is visible, while the right picture is zoomed in to the area which is also covered by the aerial photogrammetry data.

When these figures are compared, it becomes clear that the differences between the KAP data and the ALS data show the same deformation as the differences between the TLS data and the ALS data. In the area near the sea, the ALS data is higher than the measurements made during the project, while at the higher beach the ALS data is lower. In the dune area there is not much difference. This can be seen even better when the height profiles of the airborne and terrestrial laser scanning data are visualized (see figure 4.7.

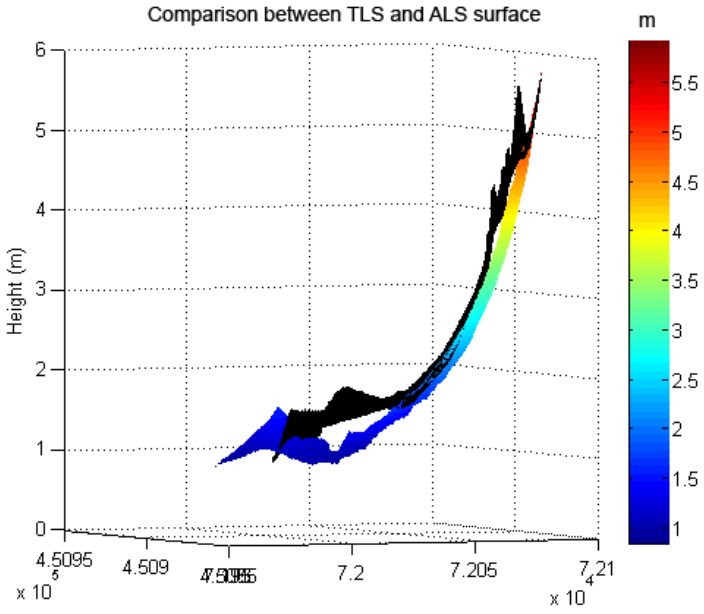

Figure 4.7: Comparison between the TLS and ALS data. The black surface is the surface of TLS.

This would suggest that in the period between the two measurements, sand has moved from the coastline to the higher beach. This may have been caused by tidal movement of the sea (i.e. sand is transported to the back of the beach at high tide) and by the wind. The prevailing wind direction in the Netherlands is south-west (see chapter 2.1.1).

This shows that comparing height models acquired over a period over a couple of months can give an insight in the changes at the beach site.

4.1.2 Other use of data

Next to extracting the topography of the survey area, it is also possible to extract other geographical information from the collected datasets. For example a simple classification can be used to analyze the aerial images acquired with the kite aerial photogrammetry technique. If the photogrammetric properties of the objects in each image are distinct, a segmentation and classification can be achieved.

To show this possibility, a simple classification has been performed over an image from the low resolution campaign. Some sample sets have been selected which represents different types of land cover (in this case, sand, grass, and soil). Using these sample sets, a simple supervised classification

Class	R	G	B
Sand	148 (29, 0)	158 (26, 0)	172 (25, 4)
Grass	71 (11, 8)	118 (14, 9)	120 (15, 3)
Bushes	31 (10, 9)	56 (14, 5)	46 (14, 5)
Soil	24 (9, 9)	57 (9, 7)	67 (11, 3)

Table 4.1: RGB values of the classes in the image.

is done by using a sample of image elements for each land cover class to estimate parameters for input to the classifier. The sample sets are based on the RGB value of each pixel.

Table 4.1 illustrates RGB mean and standard deviation values for the various objects of an example image of the low-resolution acquisition campaign (Figure 4.8a). In the RGB space, objects that have an average intensity of (148, 158, 172) are sand cells, objects with an average intensity of (71, 118, 120) are grass cells,objects with an average intensity of (31, 56, 46) are bushes cells and objects with an average intensity of (24, 57, 67) are soil cells. The standard deviation of the pixels found in these objects is large enough that classification on an individual pixel basis will not yield ideal results.

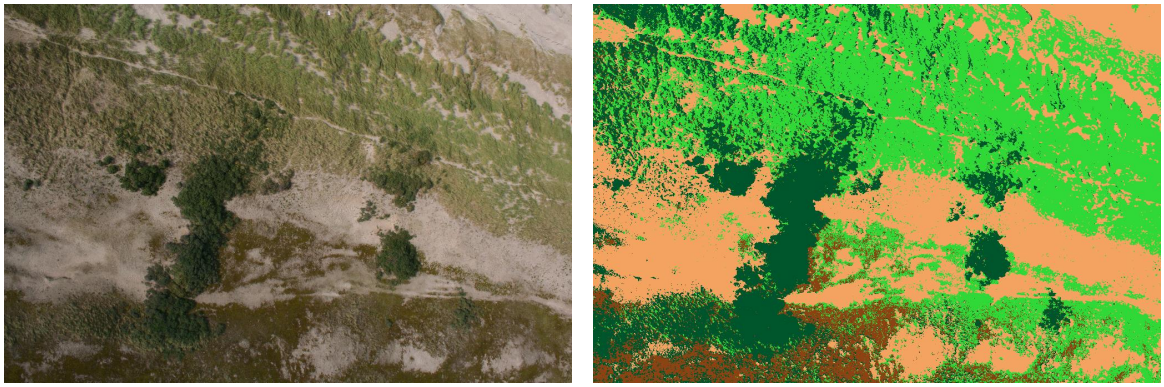

(a) Sample figure. (b) Classification result.

Figure 4.8: Sample image and classification result.

Classification based on RGB value is sometimes disputable due to the large colour variations in different situation. In other words, the RGB value is very much dependent on different factors such as sunlight, image contrast and shadow. For example during a sunny day, the colour of the objects will be different from the colour of the same objects during a cloudy day.

Class	Pixels	Pixel (%)	Area (m^2)
Sand	2715608	34.10	429.95
Grass	3084736	38.74	488.45
Bushes	1594405	20.02	252.42
Soil	567875	7.13	89.90

Table 4.2: Information of the selected classes.

From this simple RGB classification (figure4.8b), we have extracted information from an image that represent an area of about 1261 m^2as shown in table 4.2. Although the method used in this example

is not advance, this at least gives the idea that it is possible to perform classification over the acquired images.

4.2 Offshore datasets

The data merging of the Medusa with the other measurement techniques is straight forward. The data from Medusa and the bathymetry are overlaid in order to get more insight in the spatial distribution. The result of this data merging gives the opportunity to make nice visualizations of the spread of the K-concentration. On the other hand is it also possible to try to look for possible correlation between the two parameters. The resulting overlay is depicted in figure 4.9. In this figure is the earlier performed suppletion nicely visible in the bathymetry as well as the local variations of the K-concentration.

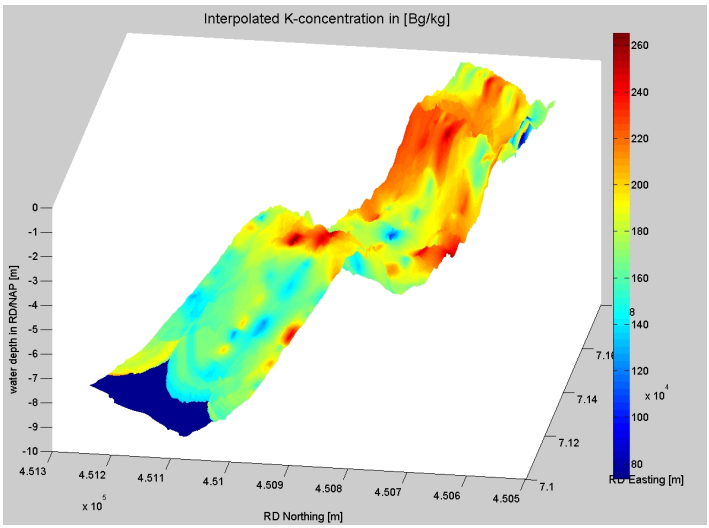

Figure 4.9: Bathymetry data (surface) with the K-concentration overlay (colors) .

The next aspect that might be important is the correlation between the water depth and the grain size. The general trend is that the grain size decreases with the water depth; more mud in deeper water. But it is very difficult to validate this in our dataset since this general trend is applicable on a much larger scale. The grainsize in the region of interest might also be much more influences by local disturbances than by this weak correlation between depth and grain size (see figure 4.10).

In order to get a better insight into the correlation between the grain size and the topography two aspects were checked for their relation. In the first place the K-concentration measurements are sorted. After this sorting 30 K-concentration bins are defined in which the corresponding water depth is averaged. The result of this sorting procedure is depicted in the left graph in figure 4.11. It is hard to derive a clean trend from this data but there is no discussion on the fact that is a residual signal in this relation. One would expect, as mentioned before, an increasing K-concentration in deeper water. This behaviour seems to be present in the data but there is a sudden inverse relation visible between 6 m and 3 m water depth. One possible cause for this disturbance might be the sand bar present in this depth interval which is the result from beach nourishment. Beach nourishments are often performed with sand that originates far from the suppletion area which can therefor disturb the trend analysis.

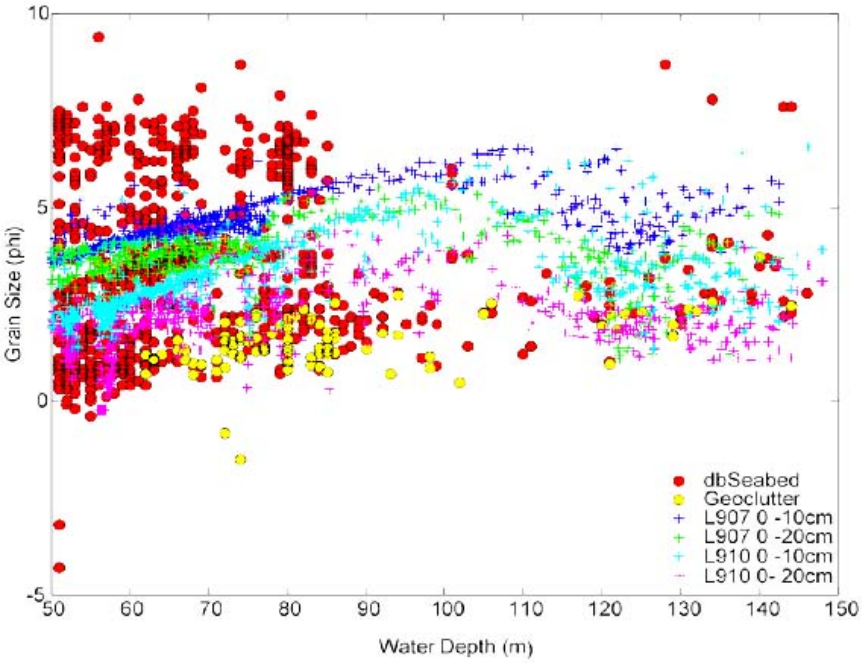

Figure 4.10: Grain size trend with depth, as defined by [14].

One way to investigate this hypothesis is to eliminate the nourished region from a larger dataset and perform the same processing steps again.

The other thing that might influence the grain size distribution is the gradient in the topography. Sand and mud have differing characteristics with respect to their cohesion and shape. Furthermore the gradient has effect on the local hydraulics by inducing reduction or acceleration of water current. In order to investigate the correlation between the gradient and the water depth is the first order derivative of the topography determined in two directions. The absolute value from this derivative is averaged for the earlier defined 30 intervals of the K-concentration. The result from this is depicted in the rightmost graph in figure 4.11.

From this data it can be concluded that there is a relation between the two parameters. Nevertheless there is a residual signal in the dataset, which may also be the result from the foreign sand of the sand bar. This factor, as with the depth-concentration relation, can be cancelled out by eliminating the sandbar from the dataset. These hypotheses could be analyzed when a larger dataset is available in order to increase the certainty and make the correlation stronger.

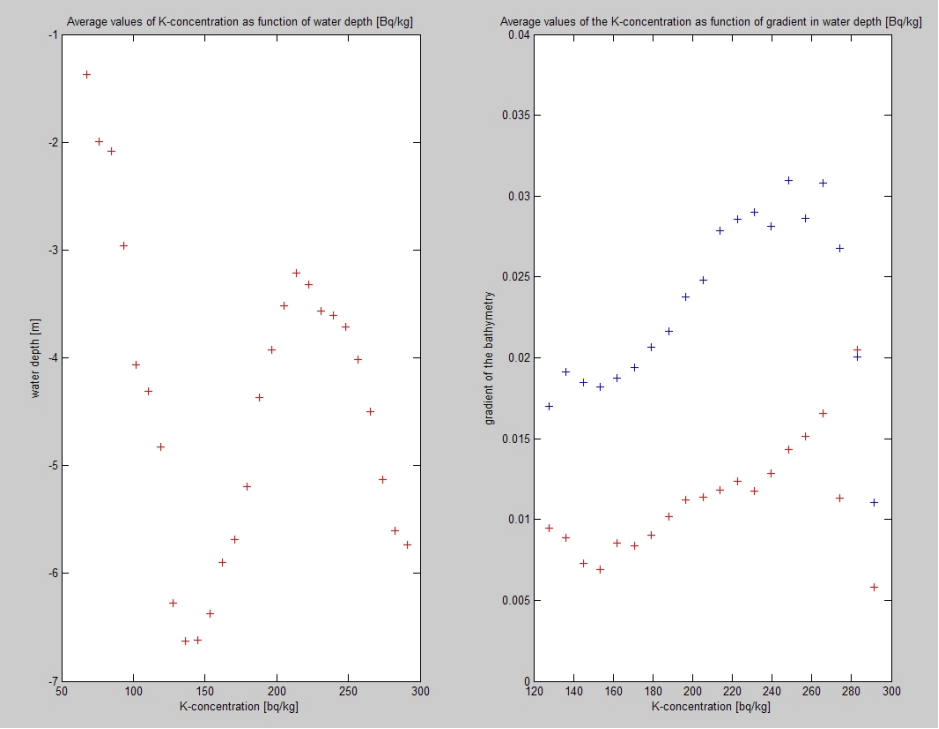

Figure 4.11: Correlation between K-concentration and water depth and between K-concentration and the first order derivative of the bathymetry.

5 Monitoring strategy

So far this report has described how the measurements using the five acquisition platforms have been conducted and the results have also been shown. One thing to keep in mind is that the measurements done in this project are on a smaller scale compared to the actual monitoring program which will be done by Boskalis. Therefore it is important to see whether the methods used in the project can be used on a much larger scale. Further it is also necessary to look into other potential methods for coastal monitoring.

5.1 Operational aspects

5.1.1 Photogrammetry

Costs

Kite Aerial Photogrammetry (KAP) is a relatively cheap technique which is able to cover a large survey area in a short time. In principle, the equipment needed is a kite, a camera and a cradle to mount the camera to the kite (or the kite rope). Furthermore ground control points are needed. These can easily be made using wooden plates with a paper showing a ground control point pattern glued on it. To keep them in place temporarily on the beach, a few nails would suffice.

The kite used in this project was developed specially to be used for kite aerial photogrammetry by Frank Krijnen [4], and costs about €100. For the camera of this project, a Canon EOS 350 has been used and that costs about €600. More advanced cameras will be more expensive.

The camera cradle costs about €20 and the ground control points of wood cost about €40. Paper, glue and nails have marginal costs, since these are standard office supplies. The total cost was about €800, mostly depending on the price of the camera. The main advantage is that most equipment (e.g. kite and camera) needs to be purchased once because they can be used again. This means that a second campaign will be much cheaper.

Duration

The area that can be covered is limited by the camera characteristics. First of all, the battery of the camera needs to be reloaded every now and then, but most cameras have a battery which should lasts at least one day, so that is not a limiting factor. Furthermore, the storage room on the data chip in the camera is limited, but on most modern chips one could save up to 2 GB. With an average size of 2.5 MB per pixel, one could capture about 800 pictures in one data chip, which should be more than enough for one day of kite aerial photogrammetry.

Acquisition time

Both the acquisition and the processing can be done rather quickly. During the project, the high-resolution acquisition campaign was done in three hours. This included setting up the ground control points, flying the kite to take the photos and measuring the ground control points with GPS. The area was about 200 by 100 meters. Of course, for a larger area more ground control points are needed, thus the acquisition will take longer. However, it should be possible to acquire data over an area of a couple of hundreds of meters within a day.

Limitations

Airborne photogrammetry is severely limited by the weather. Especially the wind speed is a limiting factor. If the wind speed is below 8 knots, the kite can't fly in the air good enough to ensure a more or less stable flight. When the wind speed gets above 24 knots, it is becomes too difficult. The kite will not go high enough because the angle between the kite rope and the beach will become too small. Rain in itself is not a limitation (i.e. the camera will work in the rain), but the quality of the pictures may become less, and flying the kite in the rain is not preferable. Furthermore, during rainy weather, the wind is usually stronger.

On good days (i.e. wind up to 12 knots and dry, sunny weather) it may be possible that the beach is crowded, especially during hot days in summer. Of course, it is possible to temporarily close down the beach where the measurements will be taken, but this may be a limiting factor when larger areas are to be surveyed.

Another limitation is the flying height of the kite, which is limited by the length of the flying line. This can simply be solved by using a longer line for higher flights, however kites are not allowed to go higher than 150 m (500 feet) due to air traffic control restrictions. This limitation should be taken into account when a large area is to be measured, because it affects the coverage of the measurement.

5.1.2 Terrestrial laser scanning

Costs

If the pulsed laser scanner Leica ScanStation 2 is taken into consideration, as it was used for trial scans in the project and proved to be successful, the costs for multitemporal monitoring of the coastal area are high just at the beginning. The initial investment cost of this system is rather high, since buying a TLS system that includes laser scanner, laptop and high-reflective targets would cost around €170,000. To compare surveys from different time domains, GPS measurements are needed, what adds to the initial cost for the equipment and also increases the cost of the measurement process itself. The measurement campaign can be done with at least 4 people (i.e to carry the equipment, set the targets and measure the GPS coordinates).

Duration

Duration of a measurement campaign is limited according to battery capabilities, which differ with the TLS system used, i.e the Faro LS880 has a maximum duration of 3 hours and the Leica ScanStation 2 has a maximum duration of 6 hours. However this problem can simply be solved by using a power generator of about €1,000. Unlike the rest of the techniques used in this project, TLS can be used to measure during the night.

Acquisition time

Measuring the topography of sites up to 0.4 km^2 would take approximately a week of field work. This time is estimated according to the number of scans that have an overlap of 30% and can cover the area of approximately 500 by 500 m, duration of a single scan that depends on the settings for the resolution and finally the battery duration, which lasts for six hours [17].

Limitations

As it can be concluded from the TLS measurement results in this project and also from other study [65], only time-of-flight systems that emit pulses are suited for long-range applications.

Nevertheless the TLS accuracies are comparable with typical quoted accuracies for ALS [48]. However, the area covered with the TLS is much smaller. It follows that the TLS can be efficiently used for DEM generation when local detailed surveys are required. On the other hand it is possible to acquire bigger area in shorter time with the TLS, if a mobile mapping system (MMS) is used. At least on the beach a 4*x*4 vehicle or an all terrain vehicle equipped with a laser scanner could be used (see paragraph 5.4.4).

Another limitation of the TLS is also bad scanning geometry in case of flat terrain, where the vertical accuracy decreases very fast when the incidence angle exceeds 84 degrees, which implies with a scanning height of 2.5 m and a flat terrain a maximal range of 24 m. (see paragraph 3.2.6).

After relatively quick acquisition, considering the size of the area measured with very high spatial resolution and very high vertical accuracy [48], the processing of the data can take a few weeks or more. The processing time depends on the requirements for the final results (e.g. DTM, comparison of DTMs, vegetation extraction and analysis).

An important property of the TLS is that there are no first or last returns, so also non-topographical features (e.g. trees, shrubs and dense ground vegetation) are included in point-cloud. The question for the further processing is how to remove erroneous points and which point filtering method to employ.

5.1.3 Medusa radioactivity probing

Costs

The Medusa radioactivity acquisition platform can be subdivided into onshore and offshore. There is no solid estimate for the cost associated with both acquisition platforms. Nevertheless, it is feasible

enough to illustrate the acquisition hours needed for every platform and hence it can be converted to a cost estimation. Besides the man power, the initial costs associated with the offshore platform is mainly dependent on the costs of a boat, a crystal sensor, a GPS receiver and fuel. While for the onshore platfrom the costs are dominated by investments in the sensor and GPS receiver.

Acquisition time

The area that can be covered depends on the required spatial resolution. The offshore acquisition at Monster-Ter Heijde presented a high spatial resolution of 1.5 m, with a line spacing of 30 m. This covered an area of 1 km^2, which took approximately 7 hours including the equipment setup. The onshore area of 2.4 km^2 was covered with a higher spatial resolution than necessary. This is due to the fact that the high resolution survey (i.e. 20 cm along track and across track 5 m) does not improve the final interpolations because the measurement error will increase and become dominant (see paragraph 3.3.6). Instead a spatial resolution of 1 m along track and 5 m across track is feasible enough for an acceptable interpolation. In this case the acquisition will take about 32 hours.

Limitations

The correlation coefficient of mean grain size and the corresponding concentration has to be calculated. The significance of correlation is related to the number of independent measurements of both variables. If there are only few points, there will be a substantial uncertainty in any correlation. Thus there will be uncertainty in the final product. This also calls for additional time needed to retrieve additional sampling.

Another limitation is the bathymetry; it is not possible to survey shallow waters due to safety issues. Furthermore the groynes could damage the sensor since it is being dragged on the sea bottom.

5.1.4 Single beam echo sounding

The working principles of the single beam echo sounding together with the implementation as done in this project has been described in paragraph 3.4. From here, the operationability of this method can be derived.

Costs

In terms of acquisition platform, there is not a typical figure of the costs of such platform, since the cost is entirely dependent on the type of platform and sensors, e.g. type of jet ski, GPS receiver, single beam echo sounder, etc. However for the system used in this project, the cost is estimated to be no less then €30,000. Next to this there are also some additional costs for maintenance and upgrades.

In terms of man power, a survey requires at least two experienced people, one being the jet ski driver, the other one for surveillance, public communication and for registering occurring events. If the jet ski can not be launched from a boat ramp, at least 4 strong people are required to carry the 300 kg weighing jet ski over a distance.

Duration

With the current system, the maximum survey duration is 5 hours. This limitation is due to the limitation of the computer batteries as well as physical endurance of the surveyors.

Acquisition time

A survey covering an area of 1 km^2 can be conducted in 3 to 4 hours. However some more time is needed for preparation before the survey and wrapping up after the survey (see table 5.1), therefore the whole survey can cost about a full working day (9 to 10 hours). This also relates to the operational costs, e.g. man power and fuel.

Activity	Time
Packing / transport arrangements / transport / installation / preparation	3 hours
Survey of 1 km2 area	3 to 4 hours
Packing / cleaning / transport after survey	3 hours
Total time	9 to 10 hours

Table 5.1: Acquisition time breakdown.

Limitations

Apart from the limited survey time per day, there are some other constrains to the usage of this method for coastal measurements.

In terms of survey planning, it is possible to plan a survey a week prior to the survey day. However in practice the final decision is taken one or two days in advance. Weather reports with wind and wave predictions have to be closely followed in order to survey in acceptable conditions. This means that flexibility of the surveying crew is required. In principle it is possible to conduct a survey during rain, since the onboard equipment is waterproof. However the survey will be more difficult then on a normal day. Another consideration is the lowest possible temperature for sailing. Naturally it is not possible to sail during frost, but at a temperature lower than 10 ºC, a (long) survey will be uncomfortable for the jet ski driver. The quality of the protective clothing like a proper dry suit determines the minimum allowable water and air temperatures.

The tide is another thing to take into consideration. As the measurements have to be made as near to the shore as possible, a high water level is needed for the survey. This means that it is preferable to sail during high tide. The time of high tide shifts from day to day. If for example in autumn or winter time, this high tide is between 7.00-9.00 or 19.00-21.00, then it is not possible to conduct a survey, since sailing in the dark is not an option. This limits the surveying time possibilities, especially in the autumn and winter when the days are shorter.

Next, there is a minimum depth of 1 m for the single beam echo sounder. During neap tide, even at the highest water level, it is not possible to come close enough to the shore to measure the coastal processes there, since there is not enough water depth. Thus it is preferable to sail during spring tide.

Some other important considerations for the survey are the wave height and wave period. While the maximum sailing wave height is not known quantitatively, it can be said that steep and breaking waves occurring in the surf zone, caused by a long swell (i.e. progressive movement up and down outside the surf zone), can be dangerous for the jet ski and its driver and disturbs the measurements. Next to this, short waves in the same order of the jet ski length cause the most pitch and roll motion, which influence the measurements. That being said, it is preferable to avoid these conditions during surveying.

5.1.5 GPS

Costs

The cost of conducting GPS measurements as done during this project is generally dependent on two things, the equipment and the man power used. The more rovers used, the higher the daily cost, but on the other hand using more rovers leads to a faster surveying time since a larger area can be covered in the same time. A trade-off between the number of rovers and the survey time can give a good estimate of the optimal costs.

Duration

The duration of a GPS survey is mainly dependent on the battery duration of the receivers. Within the setting of this project, there is no problem with the GPS base station at the bungalow, since it had continuous electrical supply. For the rover, the standard battery has a duration of about 5 to 6 hours. Obviously having extra batteries can extend the survey time.

Acquisition time

As mentioned in paragraph 3.5.6, with the RTK-GPS method used in this project (i.e. positions are recorded per point), the rover has to stop for a few seconds at each point. This means that the more points measured (i.e. denser grid), the longer acquisition time is needed. It is estimated that it takes 2.5 hours to measure a 7200 m^2 area with a 4 by 4 m grid.

Limitations

As discussed in previous paragraph, one of the limitations of using RTK-GPS for profiling is the acquisition time with respect to the area covered. This is the major drawback of using this method in a large scale monitoring program.

Another limitation is the range of the radio link between the base station and rover. According to the specifications of the used GPS receiver [29], the maximum range of the low power radio as used in the project is 10 km. But this requires a clear line of sight, and as discovered during the measurement campaign, without a clear line of sight the maximum range is 4 km, whereas at this point the signal drops repeatedly.

5.2 Overview of used methods

In the table 5.2 an overview of all techniques which have been used in the project is given, highlighting the important parameters for choosing and using a certain technique. Not all parameters are relevant to every technique, and for some techniques not all the parameters are known. The first four techniques can be directly compared, since they all measure topography. The single beam echo sounder is the only technique used in this project which measures bathymetry.

Sensor	Photogrammetry		Laser scanning	RTK-GPS	Radioactivity probing		SBES
Method/platform	close range	kite aerial	terrestrial	rover & base station	backpack	boat	jet ski
Measurement area	onshore		onshore	onshore; limited offshore	onshore	offshore	offshore
Measured area/time (- small; + large)	0	+	0	-	0		0
Measurement type	image		points	points	points		points
Spatial resolution (- low; + high)	+		++	-/0	0		0
Height accuracy as evaluated	-	15-20 cm	15 cm	3-4 cm	-		-
Theoretical height accuracy	2 cm	2-6 cm	5 cm	2.2 cm	-		5 cm
Product	DTM, land cover classification		DTM, possibly land cover classification	DTM	grain size map		DTM, possibly grain size map
Time of measurements	day		day/night	day/night	day/night	day	day
Weather/sailing conditions	no rain	no rain; needs wind	no/little wind	-	-	small waves	small waves
Costs (- low; + high)	-		+	0	0		0

Table 5.2: Overview of the acquisition methods used in the project.

Since elevation data is the most important variable to be measured, the accuracy assessment should be done for all techniques (i.e. the practical height accuracy). The RTK-GPS has a typical vertical accuracy around 2 cm and can therefore serve as a reference dataset for all three land topography methods and possibly also for the bathymetry method. The accuracy check was done for the kite photogrammetry, but not for the TLS and SBES, since there was no overlap between TLS and SBES measurement and GPS measurements. The height accuracy gained from actual measurements (practical) in case of TLS, is therefore obtained from the report on the georeferencing step in the Cyclone software.

5.3 Recommendations

5.3.1 General recommendations

A source of inefficiency and difficulty during the measurement campaign of this project, particularly for the land measurements, is the use of different ground control points, i.e. at each measurement campaign the control points needs to be placed and measured again in different positions. This was mainly due to the restriction of the measurement permit, which did not allow any equipment whatsoever to be left at the survey area during the night. However in the actual coastal monitoring project, it is likely that different condition applies, which allows the usage of common fixed control points over some period of time.

Measuring some common points or objects will also allow comparison between different measurement techniques and helps in the data merging process. A recommendation is to use objects such as beach poles as the common benchmark for all techniques.

5.3.2 Photogrammetry

The main problem with kite aerial photogrammetry is the stability of the platform. Due to the kite being unstable, the chance of capturing blurry pictures is rather high. The kite used during the measurement campaign is rather stable when the wind has the right strength, but the suspension used causes the main instability.

A cross beam suspension with a single axis has been used, which has oscillation problems in the direction perpendicular to the axis. To resolve this problem a Picavet suspension could be used, which involves a rigid cross suspended below the kite line with each of the cross four ends connected to two attachments on the kite line. The line providing these connections is a continuous loop. Its attachment to the kite line and Picavet cross sometimes involves pulleys. The result is a nominally self-leveling platform that resists a turning moment, as in the camera cradle rotating below it [47].

Another issue is the visibility of the ground control points. In the photos, the ground control points should be at least 20 to 25 pixels to allow accurate measurement. Bigger ground control points than the ones used during the measurement campaign should be considered.

During the post processing of the kite images, it was found that although the images covered the whole area, the images could not be processed in one block when the relative orientation is used. This was because a picture with a fundamental combination of ground control points was missing. Problems like this are difficult to prevent, because the exact locations of the images can not be controlled due to the instability of the platform. A way to prevent this problem is to use a higher frequency on capturing images.

5.3.3 Terrestrial laser scanning

Due to the bad scan geometry, as already discussed, it is suggested to lift the scanner up on a higher platform for at least 3 m.

To measure unobstructed terrain and have less work later with the filtering of the data, it is advised to scan the area when there are less people around. Sensor-wise it is possible to measure also during the night or during cloudy but not rainy days. In the further research, it should be tested how the wind influences the measurement accuracy, especially if the scanner is placed on a higher platform.

In case of measuring the dunes, which are densely vegetated with grass and bushes, it is more difficult to obtain terrain points. Therefore a pulse laser scanner with an ability to record more echoes or a full-wave laser scanner is advised. Using this kind of data the filtering of points to ground and non-ground one is easier and additionally more information about the vegetation can be exacted (e.g. the density and the type of vegetation).

5.3.4 Medusa radioactivity probing

Regarding to the results of the processing section of the Medusa dataset, to minimize the interpolation error, it is recommended to have a line spacing of 30 m for offshore and 5 m for onshore. This is important for the sake of an acceptable spatial continuity of the data in order to have feasible geostatistical interpolations.

The on shore surveying duration can be shortened by mounting the sensor on an all terrain vehicle (see paragraph 5.4.4). For the offshore platform it is advised to support navigation equipment such as hand held GPS or electronic chart map in order to have homogeneous tracks.

5.3.5 Single beam echo sounding

After evaluating the results of the single beam echo sounding measurements and data processing, some recommendations can be given to improve the future measurements.

In the current measurement setup, it is apparent that there are data gaps in the survey tracks as a result of the jet ski sailing too fast for the HydroBox to record the returned signal. Therefore, it is recommended for the jet ski driver to try to maintain a somewhat lower speed while taking measurements, to make sure that the returned signal is recorded.

To create a bathymetry map, it is important to have measurement data which covers the whole survey area as equally as possible. In the evaluated survey, there are fewer tracks over the deeper area, thus the interpolation result for this area is less reliable. For future measurements, it is recommended to survey in equally spaced tracks over the whole area.

Further, now that there is knowledge of how the bathymetry profile looks like and where the features of interest are, next time the jet ski can sail over those features more slowly to have more measurements and make it easier to observe changes at those locations.

Some improvements can also be done on the survey platform itself. It is advisable to install an inertial measurement unit (IMU) device on board of the jet ski, that can measure the heave, pitch and roll angles. By integrating the output of the IMU with the other measurements in HYPACK, depth errors due to platform attitude can at least be partially corrected for.

To correct for the sound speed better, it is recommended to measure the sound speed profile at least a few times during the survey. This can be done with equipment such as conductivity, depth and temperature (CTD) profiler or a sound velocity profiler. The costs of such equipment vary between €3000 to €6000.

An obstacle encountered during the data processing is finding the relation between different survey parameters (i.e. the water depth, sailing speed, sailing direction and rate of turn) and the standard deviation. Therefore a different dataset is needed, in which data the same area is sailed many times and where only one parameter is changed at a time. Having this dataset will allow a better assessment of the data quality.

5.3.6 GPS

After reviewing the problems encountered during this project, some recommendations can be given to improve the usage of the RTK-GPS method in the future.

First, a problem during this project is the instability of the base station (see also paragraph 3.5). For future work it is recommended to carefully choose a base station position which is stable and have minimum external disturbance (e.g. ground movement from heavy traffic). Since the coastal monitoring is planned to be a continuous project, it may be worthwhile to establish a permanent reference point to be used as base station. This reference point can be constructed nearby the survey area, in the form of a monument such of those of the Cadastre reference points. The position of the point should be measured with high accuracy. By doing so, the exact coordinates of the point are known and this eliminates the need to do post processing of the base station position each time.

Another problem as mentioned in paragraph 5.1.5 is the range of radio link. This range can be extended by using a high power radio or a GSM phone, with a maximum range of 30 km in favorable condition according to the manual [29]. It must be noted though, that having such a long baseline between base station and rover will reduce the accuracy of the rover positions.

An alternative solution is to use GPS receivers which are able to receive corrections from one of the nearby commercial stations, i.e. a GPS receiver equipped with a radio or wireless internet modem. This alternative excludes the necessity of setting up a base station, and also the radio link range issue.

Another issue encountered during the measurement campaign is the limited number of GPS rover receivers. Having only one rover, it is not possible to do measurements of control points and profiling simultaneously. This gives a problem of logistics, since the rover has to go back and forth from the land measurements (i.e. terrestrial laser scanning and photogrammetry) locations to the profiling locations, which obviously cost time. In this sense, it is advisable to use more than one GPS rover receivers.

Acquisition time is a drawback of this method, as mentioned in 5.1.5. An option to increase the measurement time is to record positions per epoch, i.e. the rover can keep moving and the positions are recorded in certain time interval. This way the surveying time will correspond to the walking speed of the surveyor. An average human walking speed is 4 km/hour. Note that using this method normally translates to mounting the GPS antenna on a backpack, which introduce an extra error from the surveyor's movement and from the surveyor not standing straight, although this error is within few cm. Another option is to mount the GPS receiver on a moving platform (see paragraph 5.4.4).

5.4 Other acquisition methods

To survey the coastal areas is often more difficult and challenging due to dynamic processes that occur here at different spatial and temporal scales. Furthermore the area of interest in the coastal environment combines the land and off-land measurements, which requires different measurement strategies and platforms for thr land and sea part. The non-contact techniques are in favour for hazardous environments and hard accessible areas as could be the case of the coast immediately after a storm.

Several surveying methodologies can be used to measure the terrain and bathymetry in the coastal environment and to investigate surface morphology changes over time. Beside techniques which were described or used already in this project, some other techniques can be also considered. Each methodology has different specifications as spatial resolution, costs and acquisition time. For this reason a research has been done for other acquisition methods that would be suitable for the project area and would solve some problems discussed already above or add some value to the final results.

5.4.1 Photogrammetry

In this project, kite aerial photogrammetry and close-range photogrammetry have been chosen as the acquisition method, since the other remote sensing and photogrammetry techniques are principally far too expensive and thus not feasible. Apart from this aspect, the coverage of each alternative acquisition techniques and the spatial resolution have been taken into consideration (see table 5.3).

Technique	Costs	Spatial coverage	Spatial resolution
Satellite photogrammetry	+	++	–
Airborne photogrammetry	+	+	+
Helicopter photogrammetry	+	o	+
UAV photogrammetry	-	o	o
Kite photogrammetry	–	o	o
Balloon photogrammetry	–	–	o
Terrestrial photogrammetry	–	– –	+

Table 5.3: Criteria of evaluation of the photogrammetric techniques.

The costs of satellite photogrammetry are high and the same holds for the standard aerial photogrammetry. An airplane needs to be arranged as well as a camera system suitable for airborne photogrammetry. This results to very high costs, therefore aerial photogrammetry using standard airplanes or helicopters is only feasible when a large strips of land needs to be measured in a relatively short time. However, there are possibilities of using balloons or kites to take aerial images of small projects with a low coverage.

The spatial resolution of a photogrammetric image is depends on the scale of the image. This scale is in turn dependent on the distance between the object and the projection centre of the camera and the focal length of the camera. When aerial photogrammetry is used, this distance is usually equal to the flying height. For close-range photogrammetry, the scales become bigger, giving a better resolution of the image.

Due to the natural difficulties associated with dynamic processes of the coastal zones, monitoring techniques based on videogrammetry have been successfully developed. In this different acquisition method, a video camera from an aerial platform is used to record land imagery or differently, an advanced and automated terrestrial video station is used to collect long-term and high-resolution data sets, which offer enhanced opportunities for the prediction of coastal processes [34].

Figure 5.1: Argus video cameras in Noordwijk aan Zee, The Netherlands [9].

An example of videogrammetry applied on monitoring coastal changes is the Argus video monitoring system which has been improved since 1992. Nowadays it features a fully digital video technology, which provides high image quality in combination with detailed pixel resolution. A continuous (typically every daylight hour) collections of image data are extended along regions of hundreds of meters to several kilometers. Currently, 30 Argus stations and 120 cameras are operating daily in eight countries. The greatest acceptance has been in Europe where Argus technologies are at the heart of the three-year EU coastal view program, and in Australia, where 10 stations are now operating [9].

The system typically consists of four to five video cameras, spanning a 180º view, and allowing full coverage of about four to six kilometers of beach (see figure 5.1).

Cameras are mounted on a high location along the coast and connected to an ordinary PC on site, which in turn communicates to the outside using ISDN, DSL or wireless LAN. Data sampling is usually hourly and continues during rough weather conditions. As the process of data collection is fully automated, the marginal operating costs are virtually zero.

5.4.2 Mobile mapping system

The terrestrial laser scanning method is getting more and more attention and is developing very fast in recent years. Just in three years from 2004 the number of terrestrial laser scanners sold has doubled [65]. Beside high-precision measurements and detailed 3D reconstruction of industrial objects such as cars and measurement of outdoor scenes featuring objects of complicated shape, the upcoming application of TLS is the land survey. This type of application can be developed now, while the

maximum measurement range of the new laser scanners has enlarged. In comparison with methods as photogrammetry and airborne laser scanning, which already proved their use for terrain mapping, the TLS offers some new possibilities.

Figure 5.2: An example of the mobile mapping system [1].

One of the solutions to measure the coastal topography with a TLS system is a mobile mapping system (MMS). Data captured by MMS is used for a variety of applications where precise measurements of the built or natural environment are required. MMS represent the next generation in the rapid collection of 3D data. MMS integrates the positioning system, high resolution cameras to make a simultaneous photography and a laser scanner. With post processing methods the results are georeferenced imagery and a point cloud that can be used in most GIS and CAD systems. There are already many MMS on the market [41] and one of them is shown in figure 5.2.

Mobile Mapping surveying is designed for collecting survey lidar data over large areas that are impractical with static lidar sensors but require an accuracy and resolution that exceeds airborne technologies. With a high system accuracy and resolution, MMS offers unprecedented 3D detail from a moving vehicle. It aims at acquisition of precise information of buildings and objects on the beach, vegetation, poles and etc from a moving vehicle. Point density of the laser depends on the speed of the vehicle but ranges from several hundred to several thousand per square meter [41].

5.4.3 Amphibious vehicle

A possible alternative for coastal measurement is the usage of amphibious vehicle as the measurement platform. An example of such a system which has been used in the Dutch coast is the water and beach profiler called WESP (Water En Strand Profiler), developed by the laboratory of physical geography of the Utrecht University [8]. The WESP is a large multi-purpose vehicle which can operate from the beach and drive into the sea (see figure 5.3). A GPS receiver with a radio link is mounted on the WESP, as well as a tilt and compass system to correct for the difference between the GPS antenna position and the actual bottom, which is about 15 m below. The advantage of using the WESP is the ability to measure continuous tracks from the foot of the dunes to as far as water depths of about 8 meters, which eliminates the problem of combining onshore and offshore measurements.

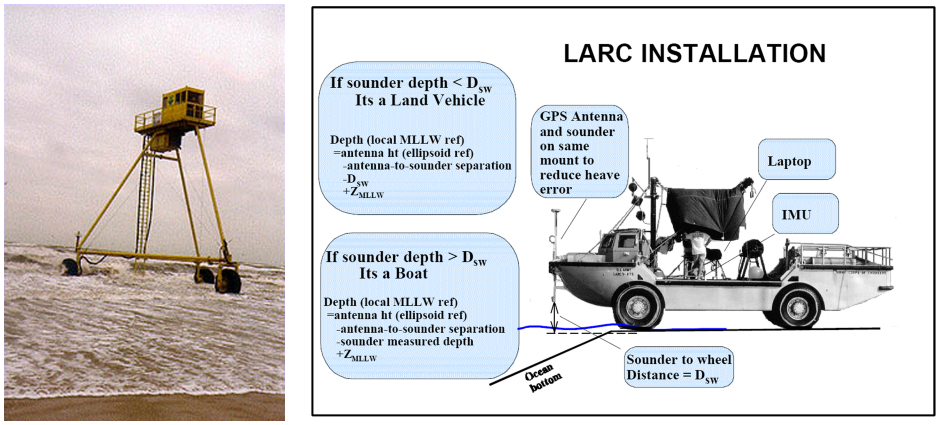

(a) WESP. (b) LARC.

Figure 5.3: The WESP [8] and LARC [51].

Another system using an amphibious vehicle, but of a much smaller size is a platform called LARC (Lighter Amphibious Resupply Cargo). The system is owned by the U.S. Army Corps of Engineers [51]. On the vehicle, a GPS receiver, a single beam echo sounder, an IMU and a computer is installed for the measurements (see figure 5.3). The LARC enables surveys across the shoreline with a single vehicle and also enables complete coverage of shoals. The topographic surface value is chosen in a simple logical software decision to be either the depth as indicated above or the distance to the bottom of the wheels depending on whether the vehicle is floating or is supported on its wheels.

Theses platforms are usable to measure the tidal area and fills the data gap as experienced in this synthesis project. However they are not usable for other parts of the coast, such as the dunes, and in case of the WESP, it is not suitable to measure deeper waters (i.e deeper than 8 m).

5.4.4 All terrain vehicle

An all terrain vehicle (ATV, also known as quad-bike) has been used in other coastal monitoring projects (for example see [44]). The typical construction is mounting a GPS receiver on the ATV, and then the ATV is used to measure grids of beach profiles, using RTK-GPS method and recording positions per epoch. Using ATV can decrease the acquisition time and increase the size of the surveyed area compared to the traditional walking survey. In addition, other sensors can also be mounted on the ATV, for instance the Medusa radioactivity probe. This way multiple acquisition method can be done on the same time. It should be noted that the usage of ATV is only possible over the beach, since over the dunes and the grass area the use of any vehicle is not allowed.

5.5 Advise on monitoring

Coastal change occur temporally from seconds (e.g. individual waves) to decades (e.g. climate variability) and spatially from centimeters (e.g. ripples) to hundreds of kilometers (e.g. littoral cells). Figure 5.4 illustrates the temporal and spatial components of beach change.

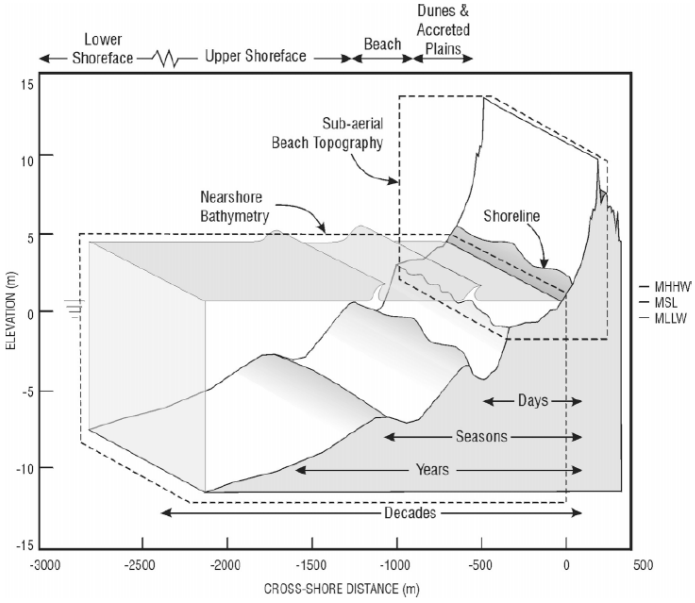

Figure 5.4: Conceptual diagram illustrating the motivation for a nested sampling scheme for monitoring beach change. The horizontal arrows represent approximate timescales for cross-shore morphological change [78].

There are 3 objectives for this monitoring program; monitoring storm-induced morphological change (1), monitoring beach nourishment (2), monitoring the annual changes of the morphology (3). The storm-induced changes and the beach nourishment related changes are event-based. The idea is that the frequency and location of measurement are determined as such that the 3 objectives can be reached in the most efficient way. For all 3 objectives the affected area, the frequency of the factors/events of influence and the monitoring strategy is discussed.

Conceptual diagram illustrating the motivation for a nested sampling scheme for monitoring beach change. The horizontal arrows represent approximate timescales for cross-shore morphological change.

5.5.1 Storms

Storms events cause significant changes to the coastal topography. In the first place storms cause an exponential increase in aeolian sediment transport with respect to moderate weather conditions. This sediment transport might cause migration and deformation of dunes and could thereby affect the vegetation present on the dunes. Another important consequence from storm conditions is the exponential increase of the wave energy with respect to moderate weather conditions. This explains the great importance of the storm events with respect to the overall morphodynamic changes; the storms have a relatively large impact on the morphodynamics for the wind transport as well as the wave energy.

One side-effect of storm winds is the storm surge effect. Storm surge is the rise in water-level on an open coast as a result of the combined impact of the wind stress on the water surface, the atmospheric pressure reduction. The storm surge at a location is inversely proportional with the water depth in the offshore area off the shoreline. This means that shores out to deep oceans will only be exposed to

relatively small surge where as shores out to shallow seas can be exposed to high surge. These forces can cause significant changes might also masks the local morphological behavior of the beach and the near shore.

Affected area

Storm surge allow the water to reach areas that are not affected by waves during normal tide. Thereby, with the higher water levels, waves cause erosion of the frontal dune systems, and finer sediments being redistributed along the beach profile.

The storm active zone can change hundreds of meters of the shore line profile in a just a few hours; coastal components are affected intensively on the temporal scale (wash over, erosion, sedimentation, etc). The expected deformation can not be easily predicted; for example storm surges caused by winds can be highly erosive and dune retreat at rate of order of tens of cubic meters per meter. The degree of deformation can be highly variable and depends on many factors, such as wind and wave direction with respect to the sediment type, profile slope, and dune face, etc.

For example, during a 1 in 100 year high magnitude storm, waves may erode several meters into the fore dune that sits well behind the normally active zone of accretion and erosion. Also, several lower-magnitude storms that occur in quick succession can produce a similar degree of erosion because the intervening periods are too short for constructive swell waves to push a significant amount of sediment back to the shoreline.

Frequency of event

The occurrence of storms is dependant on the season. During the summer, there is on average one storm every month while during winter there are on average 5 storms every month (refer to 2.1.1). In total there is 500 hrs/year of storm conditions which represents only 5% of the year.

Monitoring

The monitoring of the coast related to storm events is of interest for beach protection. Directly after the storm the coast should be measured in order to analyze the direct consequences and impact of the storm. Some weeks after the storm, the storm related features and damage to them, has reached again a state of equilibrium which is of interest and should also be modeled. The model that is acquired some weeks after the storm is in turn the initial situation before the next storm. As a result, the storm related beach monitoring programs can focus on measuring the visible beach and the foreshore and offshore area which are all affected by storms one day after and three weeks after each storm.

5.5.2 Sand suppletion

Nourishment process is usually used to protect and support shore line erosions, since this process is man made, the natural behavior will be out of balance and will start to take different behavior in

order to reach the balanced state. Consequently, the nourished area will transport according to the dynamical forces (e.g. currents, waves, etc). This transportation is very important to monitor and will be one of the concerns in order to understand the dynamical behavior of that area (e.g. where the sand goes).

Affected area

There are different sand supplement settings, therefore the affected area can vary according to the used setting. Since the beach profile is dynamic during the course of the year and seeks to establish the equilibrium state, the following scenarios can be illustrated:

- Placement as an extension of natural berm "at fairly steep slope". The physical changes are more pronounced near the shore line. Physical changes to the seafloor will decrease with the distance offshore because the wave action in deeper water is diminished near the bottom and less sand is suspended in the water column (see figure 5.5).

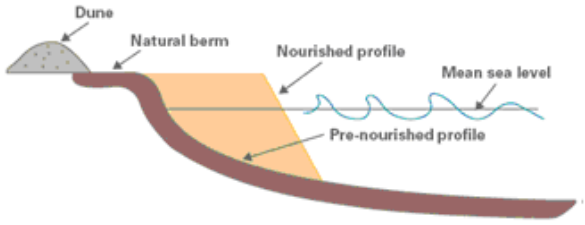

Figure 5.5: Natural berm nourishment [32].

- Subaqueous placement in an offshore mound. The use of mound relies in the expectation that the material will provide wave height reduction and eventually move ashore and widen the beach. The sediment in the nourished area can become finer and can attain the same grain size as in the pre-nourished situation (see figure 5.6).

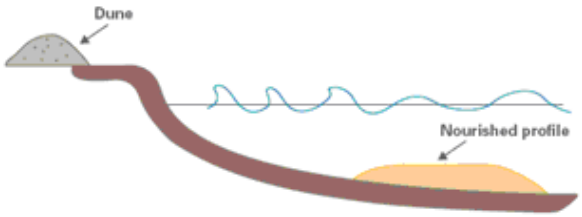

Figure 5.6: Subaqueous nourishment [32].

Frequency of event

Coastal nourishment is one of the options as response for shoreline erosion. However, coastal nourishment has a finite life time and re-nourishment is almost always required. Thus the frequency of of nourishment or sand suppletion depends typically on coastal policy and protection schemes. As consequent, the monitoring projects should estimate and predict this frequency.

Monitoring

For such projects the analysis of the sediment character and dynamics is very important before and after nourishment in order to evaluate the impact of the of the nourishment morphological behaviour. Therefore, it is recommended that the monitoring should be subdivided into different parts related to the project phases: pre-construction monitoring, construction monitoring, and post-construction monitoring.

Preconstruction monitoring involves collection of data that describe regional baseline and site specific process. One initial measurement campaign not long before start of the project should suffice for project planning.

Construction monitoring involves collecting data on how much sand was actually placed and where, and on the materials that were actually used. The project progress should indicate the frequency of measurements.

Post construction monitoring involves the systematic collection of data after construction is completed to study the project's performance. Consequently, it is important to take into account the economic aspect; too frequent monitoring will not be helpful for the analysis and will be rather overwhelming on the project budget. In first instance the morphological rate of change will be the largest; gradually the rate of change will decrease and the coast will find its equilibrium. Measurements should be taken at increasing intervals, first every week and after a month every 2 months.

5.5.3 Annual changes

The Dutch coast consists mostly of sand, which serves as the foundation of the coast. The coastal foundation zone is dynamic and constantly changing in terms of location and shape. Approximately 12 million m^3 of sand is transferred annually from the North Sea to the Wadden Sea as a result of rising sea level and coastal erosion. Sandy beaches are dynamic sedimentary systems that naturally experience phases of erosion and accretion that operate over a range of time intervals. These morphological changes affect the whole coastal system features. The dimension of these features and changing rate determines the number of sample points and the sampling pattern needed to accurately represent the landform.

Affected area

When monitoring annual changes, the main features of interest are the large scale and global features. The monitoring includes determination of long term coastal evolution. To develop reliable understanding and predictive capabilities of coastal change, knowledge of the subaqueous beach and upper shore face, beach, dunes vegetation variability is necessary. The rate of change related to the long term coastal evolution is small. This results in a monitoring strategy that aims at monitoring once in every season. The campaign has a large coverage (the entire coastal system) and is done at a low resolution which is sufficient to model the gradual changes on a large scale.

Frequency of event

The dynamic interaction between environmental forcing and coastal morphology occurs over a wide range of time and space scales; temporal responses range from tens of seconds (wave cycles) to interannual or decadal climatic variations (storms), whereas spatial scales range from centimeters (ripples) to hundreds of kilometers (littoral cells). The main features of interest are the large scale features and global coastal changes like dune migration and intertidal bar migration. The migration of these intertidal bars is usually 100 to 300 m every year which.

Monitoring

To develop reliable understanding and predictive capabilities of coastal change, knowledge of the subaqueous beach and upper shore face, beach, dunes vegetation variability is necessary. The rate of change related to the long term coastal evolution is small. This results in a monitoring strategy that aims at monitoring once in every season. The campaign has a large coverage (the entire coastal system) and is done at a low resolution which is sufficient to model the gradual changes on a large scale. Therefore acquisition methods such as videogrammetry, airborne techniques are very efficient especially for seasonal and long term monitoring. After some years, trend analysis should make 4 campaigns every year redundant which allows to do less surveying and thereby reduce the costs.

To conclude, monitoring programs need to be evaluated periodically and adjusted to meet the need of the project or coastal behavior. For example, the sand erosion of a specific area may show significant changes only following major storms; consequently, surveys need to be conducted only after such storm. Similarly, after a period of years, seasonal variations in beach profiles may be known, so frequent beach surveys become unnecessary.

Table 5.4 summarizes the monitoring strategy and parameters.

	Storms	Beach nourishment	Gradual changes
Dunes	Kite aerial and UAV photogrammetry	Kite aerial photogrammetry	ALS, photogrammetry, remote sensing
Vegetation	Kite aerial photogrammetry	Kite aerial photogrammetry	ALS, photogrammetry, remote sensing
Inter-tidal	Videogrammetry	Videogrammetry	Videogrammetry
Offshore	SBES	SBES	SBES
Sediment	Radio active, soil samples	Radio active, soil samples	Radio active, soil samples
Beach	Mobile mapping system, close range and kite aerial photogrammetry	Mobile mapping system	Mobile mapping system, close range and kite aerial photogrammetry
Event frequency	On average one per month	Dependent on protection scheme	Continuous
Measurement campaign	1 day and 3 weeks after storm	Zero measurement, every week (first month), every 2 months (first year)	Continuous and seasonal

Table 5.4: Monitoring plan.

6 Conclusions

During this synthesis project, five different acquisition methods have been investigated with respect to their usage in coastal monitoring, which contributes to the Building with Nature project by providing some basis for the monitoring project. The five techniques are photogrammetry, terrestrial laser scanning, Medusa radioactivity probing, single beam echo sounding and GPS. To further study how these techniques can be applied for coastal monitoring, measurements using the techniques have been conducted at an area of the coast of Monster-Ter Heijde. With these measurements, information about the coastal topography, bathymetry and grain size distribution has been gathered.

The photogrammetry method which has been used is kite aerial photogrammetry, from which the results has been processed using specific photogrammetry software, leading to two results, an orthophoto and a digital terrain model. These first results of the kite aerial photogrammetry are promising, but the achieved accuracy is not high enough for precise monitoring. Therefore both the acquisition and the processing method should be improved.

From the terrestrial laser scanning, the results of the Leica ScanStation 2 scans have been used to produce a digital terrain model of a part of the survey area. Having problems with the data acquisition, at this point it is not possible to have a fair validation of the results of terrestrial laser scanning, therefore further study is recommended.

Grain size distribution information over the entire area has been gathered with the Medusa radioactivity probing method, on both the onshore and offshore part. Due to a problem with the laboratory result for grain size determination, it was decided to work with the K (potassium) concentration that has a negative correlation with the grain size. As the result, K-concentration maps for the offshore and onshore survey area have been produced. These maps can give valuable information about the development of the coast.

The single beam echo sounding method has been used to measure the near shore bathymetry of the area. As a result, a bathymetric map has been produced. In this map, interesting features are visible, such as the groynes and their scour holes. The results show that the jet ski single beam echo sounding method is nearly operational, however some improvements in terms of platform and surveying is still needed to achieve a higher quality dataset.

Next to the individual results, data merging has been done for the onshore and offshore datasets. For the onshore datasets, the results of terrestrial laser scanning and kite aerial photogrammetry have been merged into a topographic map of the beach. On the offshore side, the K-concentration map has been overlaid with the bathymetric map, which gives a good visualization of the spread of the K-concentration and shows the correlation between the water depth and the grain size.

What are still missing in this project are information on the intertidal area, since there is no overlap between the onshore and offshore datasets. During the project it was found that the jet ski was unable take valid measurements past the low water line, which means there is no sounding data

available for the intertidal area. Therefore another method to measure is needed for this area, such as videogrammetry.

Looking at the datasets retrieved and the geographical information which have been extracted during this project, there are still some other uses of the data which are still open for further study. From the kite aerial photogrammetry, a simple classification of the acquired images based on RGB value has been demonstrated. The first result is promising and indicates future potential. From the terrestrial laser scanning, it can be recommended to study the use of the data to extract vegetation density information, and to use the intensity for land cover classification. For the single beam echo sounding method, there is a possibility to use the echo energies to derive the sediment grain size, therefore a further study is recommended.

Noting the problems encountered during the project, some recommendations to improve the usage of the five acquisition method for the actual monitoring project have been made. Next to it some alternative methods which are considered to be useful for coastal monitoring are suggested.

At the end, a monitoring plan has been suggested for the future coastal monitoring within the Building with Nature project. The suggested monitoring plan is presented for different zones and features of the coastal area where different changes of morphology are expected, taking into consideration the capabilities and specifications of the different acquisition techniques. According to the parameters of each zone, the most suitable acquisition method is described, together with its spatial and temporal resolution, and the approaches for data analysis.

While there is not a single optimum acquisition method to monitor the various events affecting the coastal morphology, it is possible to adapt different types of measurements plan to every event. Therefore the frequency and locations of measurements are relative to the different events, namely storm, beach nourishment, and annual changes.

Bibliography

[1] 3D Laser Mapping. http://www.3dlasermapping.com. Last visited: 17 Oct. 2008.

[2] Actief GPS Referentie Systeem Nederland. http://www.agrs.nl. Last visited: 1 Oct. 2008.

[3] Actuele waterdata. http://www.actuelewaterdata.nl. Last visited: 30 Sep. 2008.

[4] Aircatcher.com: a fresh look at aerial photography. http://www.aircatcher.com. Last visited: 13 Oct. 2008.

[5] American Society for Photogrammetry and Remote Sensing. http://www.asprs.org. Last visited: 13 Oct. 2008.

[6] Canon. http://www.canon.com. Last visited: 13 Oct. 2008.

[7] Coordinate Calculator v.4.1. http://www.rdnap.nl/download/download.html. Last visited: 1 Oct. 2008.

[8] De Water En Strand Profiler - WESP. http://www.geog.uu.nl/fg/wesp.html. Last visited: 13 Oct. 2008.

[9] ENCORA Coastal Plan. http://www.encora.eu. Last visited: 17 Oct. 2008.

[10] FARO. http://www.faro.com. Last visited: 13 Oct. 2008.

[11] GNSS Laboratory of the Delft University of Technology - Site Information for Delft. http://gnss1.lr.tudelft.nl/dpga/station/Delft.html. Last visited: 2 Oct. 2008.

[12] The HydroBox Hydrographic Echo Sounder. http://www.syqwestinc.com/hydrobox/index.htm. Last visited: 5 Sep. 2008.

[13] HYPACK Hydrographic Survey Software. http://www.hypack.com. Last visited: 13 Oct. 2008.

[14] INSTAAR - Institute of Arctic and Alpine Research. http://instaar.colorado.edu. Last visited: 16 Oct. 2008.

[15] JAaRlijkse KUStmetingen. http://public.deltares.nl/display/MCTDOC/JARKUS+Data. Last visited: 16 Oct. 2008.

[16] Leica Photogrammetry Suite. http://gi.leica-geosystems.com/LGISub1x12x0.aspx. Last visited: 30 Sep. 2008.

[17] Leica ScanStation 2. http://www.leica-geosystems.com/hds/en/lgs_62189.htm. Last visited: 13 Oct. 2008.

[18] LNR Globalcom GPS Reference Stations - Hoek van Holland. http://www.lnrglobalcom.com/site/gpsspot/11.html. Last visited: 4 Sep. 2008.

[19] MATLAB. http://www.mathworks.com/products/matlab. Last visited: 30 Sep. 2008.

[20] MUMM | North Sea facts. http://www.mumm.ac.be/EN/NorthSea/facts.php. Last visited: 29 Sep. 2008.

[21] NWS Rip Current Awareness Home Page. http://ripcurrents.noaa.gov. Last visited: 16 Oct. 2008.

[22] Oceans and their Margins. http://earthsci.org/education/teacher/basicgeol/ ocean/ocean.html. Last visited: 29 Sep. 2008.

[23] Oil glossary of Schlumberger. http://www.schlumberger.com. Last visited: 30 Sep. 2008.

[24] PhotoModeler. http://www.photomodeler.com. Last visited: 30 Sep. 2008.

[25] Projectbureau Delflandse Kust. http://www.delflandsekust.nl. Last visited: 13 Oct. 2008.

[26] Python Programming Language. http://www.python.org. Last visited: 13 Oct. 2008.

[27] TEQC - The Toolkit for GPS/GLONASS/Galileo/SBAS Data | UNAVCO Facility. http://www.unavco.org/facility/software/teqc/teqc.html. Last visited: 30 Sep. 2008.

[28] Trimble Geomatics Office. http://www.trimble.com/geomaticsoffice.shtml. Last visited: 13 Oct. 2008.

[29] Leica SR530 Geodetic RTK Receiver Brochure. Leica Geosystems, 2001.

[30] Engineering and Design - Hydrographic Surveying. Chapter 18, Coastal Engineering Surveys. Publication EM 1110-2-1003, USACE, 2002.

[31] Leica Photogrammetry Suite User Guide. Leica Geosystems, 2003.

[32] Beach nourishment - How beach nourishment projects work. Coastal and Hydraulics Laboratory, Engineer Research and Development Center (ERDC), U.S. Army Corps of Engineers, 2007.

[33] PolaRx2/2e User Manual 3.2.0. Septentrio Satellite Navigation, 2007.

[34] S. Aarninkhof. *Nearshore bathymetry derived from video imagery*. PhD thesis, Delft University Press, 2003.

[35] A. Adami, F. Guerra, and P. Vernier. Laser scanner and architectural accuracy text. In *Proc. XXI International CIPA Symposium*. CIPA, 2007.

[36] M.J. Adriani and J.H.J. Terwindt. Sand stabilisation and dune building. Communications 19, Rijkswaterstaat.

[37] J. van Alpen and M.A. Damoisseaux. Geomofologische kaart van de Nederlandse kustwateren, schaal 1:125.000. *KNAG Geografisch Tijdschrift*, 22: 161–167, 1988.

[38] S.M. Arens, Q. Slings, and C.N. de Vries. Mobility of a remobilised parabolic dune in Kennemerland, The Netherlands. *Geomorphology*, 59(1-4): 175–188, 2004.

[39] B. Augustijn and B. Zwart. Stormenkalender; chronologisch overzicht van alle stormen (windkracht 8 en hoger) langs de Nederlandse kust voor het tijdvak 1990-1996. Publication 176, KNMI.

[40] R.A. Bagnold. *The Physics of Blown Sand and Desert Dunes*. Menthuen, 1941.

[41] D. Barbera, J. Millsa, and S. Smith-Voyseyb. Geometric validation of a ground-based mobile laser scanning system. *Journal of Photogrammetry and Remote sensing*, 63: 128–141, 2008.

[42] R.A. Beach and R.W. Sternberg. Infragravity driven suspended sediment transport in the swash, inner and outer-surf zone. In *Proc. Coastal Sediments '91*, pp. 114–128. ASCE, 1991.

[43] C.C. Benton. Notes on Kite Aerial Photography. http://arch.ced.berkeley.edu/kap. Last visited: 13 Oct. 2008.

[44] D.F. Bernstein, C. Freeman, M.F. Forte, P.T. Gayes, J Park, and H. Mitasova. Survey design analysis for three-dimensional mapping of beach and nearshore morphology. In *Proc. Coastal Sediments '03*. ASCE, 2003.

[45] M. Boers. Zandgolven langs de Noord-hollandse kust. Een bijdrage aan meerjarige suppletie-planning. Technical report, RIKZ/OS/2002.117X, 2002.

[46] L. Bornaz and F. Rinaudo. Terrestrial laser scanner data processing. http://www.isprs.org/istanbul2004/comm5/papers/608.pdf. Last visited: 2 Oct. 2008.

[47] A. Casalboni. Kite Aerial Photohraphy and Historical Kite. http://www.kapcasalboni.it. Last visited: 13 Oct. 2008.

[48] S. Coveney. Terrestrial laser scanning for the generation of a local high accuracy digital elevation model. In *Presentation on Earth Observation Reseach in Ireland*, 2007.

[49] H.M. van den Dool, R.E. Kistler, S. Saha, and J.F. den Tonkelaar. Reanalysis and Reforecast of the Jan 31 - Feb 1 1953 North Sea Gale. Technical report, Climate Prediction Center, 2001.

[50] P. Doornenbal and S. van Heteren. Bathymetric range map of the Dutch Continental Shelf (NCP). Technical report, TNO Built Environment and Geosciences, 2008.

[51] J.P. Dugan, K.C. Vierra, W.D. Morris, G.J. Farruggia, and D.C. Campion. Uniqe vehicles used for bathymetry surveys in exposed coastal regions. Conference paper, The Hydrographic Society of America.

[52] B. Elfrink and T. Baldock. Hydrodynamics and sediment transport in the swash zone: a review and perspectives. *Coastal Engineering*, 45(3-4): 149–167, 2002.

[53] I.M.J. van Enckevort. *Daily to yearly nearshore bar behaviour*. PhD thesis, Utrecht University, 2001.

[54] M.E. Field, C.H. Nelson, D.A. Cacchione, and D.E. Drake. Sand waves on an epicontinental shelf: Northern Bering Sea. *Marine Geology*, 42(1-4): 233–258, 1981.

[55] S. Gao and M. Collins. The use of grain size trends in marine sediment dynamics: a review. *Chinese Journal of Oceanology and Limnology*, 19(3): 265–271, 2001.

[56] S. Gopi. *Global Positioning System: Principles and Applications*. McGraw-Hill, 2005.

[57] M. Goto and K. Tazaki. Clay Mineralogical Analysis of the Paleo-Environment: Sedimentary Environment of the Kuruma Group. *Journal of the Clay Science Society of Japan*, 38(2): 91–102, 1998.

[58] P.H.G.M. Hendriks, J. Limburg, and J. de Meijer. Full-spectrum analysis of natural γ-ray spectra. *Journal of Environmental Radioactivity*, 53(3): 365–380, 2000.

[59] R.J. Huggett. *Fundamentals of Geomorphology*. Routledge, 2002.

[60] F. Khalaf. Textural characteristics and genesis of the aeolian sediments in the Kuwaiti desert. *Sedimentology*, 36(1): 253–271, 1989.

[61] G.F. Knoll. *Radiation Detection and Measurement*. J. Wiley & Sons, 2000.

[62] K. Kraus. *Photogrammetry. Vol. 1 & 2*. RICS Books, 1993.

[63] K. Kraus, I. Harley, and S. Kyle. *Photogrammetry: geometry from images and laser scans*. De Gruyter, 2007.

[64] T. Kusterle. Surf Zone Hydrodynamics. Seminar paper, Faculty of Mathematics and Physics, University of Ljubljana.

[65] M. Lemmens. Terrestrial Laser Scanners. *GIM International Magazine*, August 2007.

[66] T. Luhmann. *Close range photogrammetry: principles, methods and applications*. Whittles, 2006.

[67] K.V. Mackenzie. Nine-term equation for sound speed in the oceans. *Journal of the Acoustical Society of America*, 70(3): 807–812, 1981.

[68] G. Masselink, A. Kroon, and R.G.D. Davidson-Arnott. Morphodynamics of intertidal bars in wave-dominated coastal settings - A review. *Geomorphology*, 73(1-2): 33–49, 2006.

[69] S.B. McArdle and A. McLachlan. Sand beach ecology swash features relevant to the macrofauna. *Journal of Coastal Research*, 8(2): 398–407, 1992.

[70] J.W.H. van de Meene. The shoreface-connected ridges along the central Dutch coast - part 1: field observations. *Continental Shelf Research*, 20(17): 2295–2323, 2000.

[71] J.W.H. van de Meene and L.C. van Rijn. Tide- and stormdriven sediment transport on the inner-shelf along the Dutch coast. In *Proc. Coastal Dynamics '94*, pp. 822–836. ASCE, 1994.

[72] P. Misra and P. Enge. *Global Positioning System: Signals, Measurements and Performance*. Ganga-Jamuna Press, 2006.

[73] G. Nagle. *Advanced Geography*. OUP Oxford, 2000.

[74] P. Nielsen. Groundwater dynamics and salinity in coastal barriers. *Journal of Coastal Research*, 15(3): 732–740, 1999.

[75] C. Ollier. *Weathering*. Oliver & Boyd, 1984.

[76] P.D. Osborne and G.A. Rooker. Sand re-suspension events in a high energy infragravity swash zone. *Journal of Coastal Research*, 15(1): 74–86, 1999.

[77] S. Passchier and M.G. Kleinhans. Observations of sand waves, megaripples, and hummocks in the Dutch coastal area and their relation to currents and combined flow conditions: marine sandware and river dune dynamics. *Journal of Geophysical Research*, 110(F04S15): 1–15, 2005.

[78] P. Peter Ruggiero, G.M. Kaminsky, G. Gelfenbaum, and B. Voigt. Seasonal to Interannual Morphodynamics along a High-Energy Dissipative Littoral Cell. *Journal of Coastal Research*, 21(3): 553–578, 2005.

[79] F. Press and R. Siever. *Understanding Earth*. W.H. Freeman & Co., 2003.

[80] L.C. van Rijn. Sand budget and coastline change of the central Dutch Coast between Den Helder and Hoek van Holland. Report H2129, Project Kustgenese, Delft Hydraulics, 1995.

[81] A. Robert. *River Processes: An Introduction to Fluvial Dynamics*. Hodder Arnold, 2003.

[82] T. Schulz and H. Ingensand. Influencing Variables, Precision and Accuracy of Terrestrial Laser Scanners. In *Proc. Ingeo 2004*, 2004.

[83] M. Schwartz, editor. *Encyclopedia of Coastal Science*. Springer Netherlands, 2005.

[84] P. Sistermans and O. Nieuwenhuis. Case Study: Holland Coast (The Netherlands). Technical report, EUROSION, 2007.

[85] R.M. Sorensen. *Basic Coastal Engineering*. J. Wiley & Sons, 1978.

[86] A. Stolk. Zandsysteem kust - een morfologische karakterisering. Kustverdediging na 1990. Report GEOPRO 1989-02, Department of Physical Geography, Utrecht University, 1989.

[87] J.H.J. Terwindt. Sand waves in the Southern Bight of the North Sea. *Marine Geology*, 10(1): 51–67, 1971.

[88] W.S.J. Uijttewaal. The Flow in Groyne Fields: Patterns and Exchange Processes. In *Water Quality Hazards and Dispersion of Pollutants*, pp. 231–246. Springer Netherlands, 2005.

[89] M. Visser. *On the transport of fine marine sediment in the Netherlands coastal zone*. PhD thesis, Utrecht University, 1993.

[90] H. Wackernagel. *Multivariate Geostatistics*. Springer, 2003.

[91] D. van der Wal. Modelling aeolian sand transport and morphological development in two beach nourishment areas. *Earth Surface Processes and Landforms*, 25(1): 77–92, 2000.

[92] T.F. Wever. Bedforms and Bedform Migration - A Data Review. In *Proc. International Workshop Marine Sandwave and River Dune Dynamics II*. University of Twente, 2004.

[93] K.M. Wijnberg. Extracting decadal morphological behaviour from high-resolution, long-term bathymetric surveys along the Holland coast using eigenfunction analysis. *Marine Geology*, 126: 301–330, 1995.

[94] K.M. Wijnberg. On the systematic offshore decay of breaker bars. In *Proc. 25th International Conference on Coastal Engineering*, pp. 3600–3613. ASCE, 1997.

[95] M. Wijngaarden, L.B. Venema, R.J. de Meijer, J.J.G. Zowlsman, B. van Os, and J.M.J. Gieske. Radiometric sand-mud characterisation in the Rhine-Meuse estuary - Part A. Fingerprinting. *Geomorphology*, 43(1): 87–101, 2002.